



Search for resonant leptoquark production via lepton–jet signatures in pp collisions at $\sqrt{s} = 13$ TeV and $\sqrt{s} = 13.6$ TeV with the ATLAS detector

The ATLAS Collaboration

This paper presents a search for physics beyond the Standard Model targeting a heavy resonance visible in the invariant mass of the lepton–jet system. The analysis focuses on final states with a high-energy lepton and jet, and is optimised for the resonant production of leptoquarks—a novel production mode mediated by the lepton content of the proton originating from quantum fluctuations. Four distinct and orthogonal final states are considered: e +light jet, μ +light jet, $e+b$ -jet, and $\mu+b$ -jet, constituting the first search at the Large Hadron Collider for resonantly produced leptoquarks with couplings to electrons and muons. Events with an additional same-flavour lepton, as expected from higher-order diagrams in the signal process, are also included in each channel. The search uses proton–proton collision data from the full Run 2, corresponding to an integrated luminosity of 140 fb^{-1} at a centre-of-mass energy of $\sqrt{s} = 13$ TeV, and from a part of Run 3 (2022–2023), corresponding to 55 fb^{-1} at $\sqrt{s} = 13.6$ TeV. No significant excess over Standard Model predictions is observed. The results are interpreted as exclusion limits on scalar leptoquark (\tilde{S}_1) production, substantially improving upon previous ATLAS constraints from leptoquark pair production for large coupling values. The excluded \tilde{S}_1 mass ranges depend on the coupling strength, reaching up to 3.4 TeV for quark–lepton couplings $y_{de} = 1.0$, and up to 4.3 TeV, 3.1 TeV, and 2.8 TeV for $y_{s\mu}$, y_{be} , and $y_{b\mu}$ couplings set to 3.5, respectively.

Contents

1	Introduction	2
2	ATLAS detector	5
3	Data and simulated event samples	6
4	Object reconstruction	7
5	Event selection	9
6	Background estimation	12
	6.1 Reducible backgrounds	13
	6.2 Irreducible backgrounds	15
7	Systematic uncertainties	19
8	Results	21
	8.1 Results for control and validation regions	22
	8.2 Results for signal regions	25
	8.3 Interpretations	25
9	Conclusion	34

1 Introduction

While the discovery of the Higgs boson [1, 2] and subsequent precision measurements of its properties [3, 4] remain landmark achievements, an equally fundamental scientific motivation for the Large Hadron Collider (LHC) [5] is the search for physics beyond the Standard Model (BSM). Numerous BSM theories predict the existence of new massive states that could be produced resonantly in proton–proton (pp) collisions at the TeV scale, provided their masses lie within the experimentally accessible range of the LHC. When produced through resonant mechanisms, these states would manifest as localised excesses in the invariant mass spectra of their decay products. Such distinctive peaks superimposed on the smoothly falling background predicted by the Standard Model (SM) would constitute an unambiguous signature of new physics. Consequently, resonance searches constitute a cornerstone of the research programs for both the ATLAS and CMS experiments.

Leptoquarks (LQs) represent a prominent category of hypothetical heavy states predicted by various grand unified theories featuring extended gauge groups [6–8]. These colour-charged particles carry both baryon and lepton numbers, naturally reflecting the underlying symmetry between the two sectors as predicted by unifying theories and suggested by observed patterns in nature. Characterised by fractional electric charges and postulated in either scalar or vector forms, LQs decay into distinctive lepton–quark pairs whose flavour composition depends on the LQs’ coupling parameters.

Extensive investigations of LQ signatures were conducted using the datasets collected during the LHC Run 1 and Run 2 data-taking periods. Previous LHC searches have primarily focused on two production

mechanisms: pair production (PP) [9] mediated by quantum chromodynamics (QCD) and coupling-dependent single production (SP) in association with a lepton [10], as illustrated in Figure 1 (a) and (b), respectively. While PP cross-sections depend predominantly on the strong coupling constant and remain largely independent of LQ coupling parameters, production via SP becomes more and more relevant with increasing coupling values due to its direct dependence on these parameters. Additional LQ sensitivity also arises from non-resonant contributions to dilepton production via t -channel processes (Drell–Yan, DY) seen in Figure 1 (c).

This paper introduces a novel probe of s -channel resonant LQ production shown in Figure 1 (d) and (e), enabled by recent advancements in understanding the proton’s lepton content that arises from quantum fluctuations. State-of-the-art next-to-leading-order (NLO) calculations of lepton parton distribution functions (PDFs) [11] show that, despite the relative scarcity of leptonic constituents of the proton compared to quarks and gluons, this previously unexplored production channel offers competitive sensitivity relative to established search strategies [12]. The resonant production mechanism yields a relatively clean final state comprising a lepton–jet system whose invariant mass distribution could reveal a characteristic resonance peak, similar to single LQ production. This distinctive signature motivates the development of dedicated search algorithms within the ATLAS experimental programme.

The analysis employs a \tilde{S}_1 LQ with absolute electric charge $\frac{4}{3}e$ as a benchmark signal. This LQ is a singlet under the $SU(2)$ SM gauge group, with purely right-handed Yukawa couplings to down-type quarks and leptons. Therefore, it is characterised by a simple, exclusive decay topology into a down-type quark and a charged lepton, with no additional competing decay channels into neutral leptons. Four distinct coupling scenarios are investigated where the LQ exclusively interacts through single non-zero coupling parameters: $y_{de}, y_{s\mu}, y_{be}$ and $y_{b\mu}$, corresponding to first/second-generation lepton (e, μ) couplings with d/s - or b -quark partners. Alternative models featuring couplings to u/c -quark flavours show detector-level signatures kinematically indistinguishable with the studied scenarios, permitting phenomenological re-interpretation through coupling parameter rotation in the quark flavour space. The ATLAS Collaboration has performed a pair-production search focusing on scalar LQ decays into quark–lepton ($q\ell$) final states with $\ell = e, \mu$, establishing mass exclusion limits up to 1.8 TeV (electron channel) and 1.7 TeV (muon channel) assuming a branching ratio into a charged lepton and a quark of 100%, with minimal dependence on the quark flavour [13]. These results also served as input for a statistical combination of LQ searches [14] to enhance sensitivity across different decay modes. Searches for LQ pair-production from the CMS Collaboration constrain scalar LQ masses up to 1.4 TeV and 1.5 TeV for couplings to electrons and muons, respectively [15, 16]. For couplings to muons and b -quarks, these constraints extend up to 1.8 TeV [17]. A recent search by the CMS Collaboration for t -channel LQ exchange strengthens the constraints on large couplings involving up- and down-type quarks and electrons or muons, probing LQ masses up to 5 TeV [18]. The CMS Collaboration also conducted a search for resonant LQs with couplings to a τ -lepton and a $u/d/s/b$ quark using data collected in 2016–2018 [19].

The present analysis introduces the first dedicated exploration of resonant LQ production mechanisms coupling to first- and second-generation leptons (e/μ). It is conducted using $\sqrt{s} = 13$ TeV and $\sqrt{s} = 13.6$ TeV pp collision data collected with the ATLAS experiment from 2015 to 2018 in LHC Run 2 (140 fb^{-1}) and from 2022 to 2023 in Run 3 (55 fb^{-1}), respectively.

The analysis incorporates four mutually exclusive detection channels: $e + \text{light-jet}$, $\mu + \text{light-jet}$, $e + b\text{-jet}$, and $\mu + b\text{-jet}$, where light-jet refers to jets that are not tagged as containing a b -hadron decay. To ensure methodological consistency, a similar analysis strategy is implemented across all channels while preserving channel-specific optimisations. Each channel features dedicated 1-lepton (1L) and 2-lepton (2L) signal regions (SRs), where the 2L topology is specifically designed to account for the NLO diagram shown

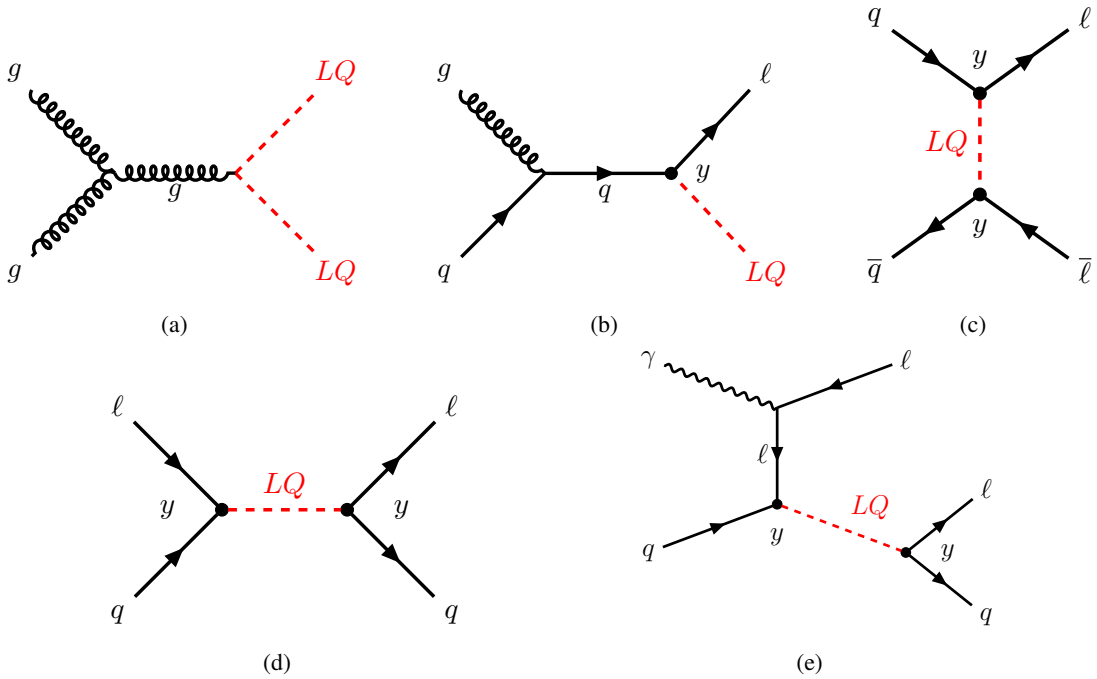


Figure 1: Example Feynman diagrams for the (a) pair, (b) single, (c) Drell–Yan, as well as (d) leading-order and (e) next-to-leading-order resonant LQ production modes. The symbol y marks interactions mediated by a LQ Yukawa coupling to quarks and leptons.

in Figure 1 (e). These diagrams are mediated via the photon constituent of the proton which is less suppressed than the lepton content and therefore their contributions are approximately on equal footing with the ones from the s -channel LQ production. Signal extraction employs a shape-based discrimination strategy through a multi-bin template likelihood analysis of the lepton–jet invariant mass ($m_{\ell j}$) spectrum. This approach combines channel-specific background modelling, kinematic selection thresholds, and independent treatments of systematic uncertainties, enabling simultaneous constraints on potential signals across the full $m_{\ell j}$ phase space covered in this analysis. Backgrounds with prompt, genuine leptons are constrained using dedicated control regions (CRs), complemented with data-driven techniques to estimate contributions from misidentified (“fake”) or non-prompt (FNP) leptons. An individual analysis selection is developed for each channel and is applied separately on the Run-2 and Run-3 datasets, enabling cross-validation between the two data-taking periods. For the interpretation of results, the observed $m_{\ell j}$ spectra from Run 2 and Run 3 are fitted simultaneously to maximise the sensitivity to the benchmark signal.

The rest of this paper is organised as follows. A brief description of the ATLAS detector is given in Section 2, and the data and simulation samples used are discussed in Section 3. Overviews of the reconstruction of physics objects and the event selection are presented in Sections 4 and 5, respectively. The background estimation strategy is described in Section 6. The systematic uncertainties related to this search are described in Sections 7. The results of the search are given in Section 8. Finally, Section 9 presents the conclusions.

2 ATLAS detector

The ATLAS detector [20, 21] at the LHC covers nearly the entire solid angle around the collision point.¹ It consists of an inner tracking detector surrounded by a thin superconducting solenoid, electromagnetic and hadronic calorimeters, and a muon spectrometer incorporating three large superconducting air-core toroidal magnets.

The inner-detector system (ID) is immersed in a 2 T axial magnetic field and provides charged-particle tracking in the range $|\eta| < 2.5$. The high-granularity silicon pixel detector covers the vertex region and typically provides four measurements per track, the first hit generally being in the insertable B-layer (IBL). It is followed by the SemiConductor Tracker (SCT), which usually provides eight measurements per track. These silicon detectors are complemented by the transition radiation tracker (TRT), which enables radially extended track reconstruction up to $|\eta| = 2.0$. The TRT also provides electron identification information based on the fraction of hits (typically 30 in total) above a higher energy-deposit threshold corresponding to transition radiation.

The calorimeter system covers the pseudorapidity range $|\eta| < 4.9$. Within the region $|\eta| < 3.2$, electromagnetic calorimetry is provided by barrel and endcap high-granularity lead/liquid-argon (LAr) calorimeters, with an additional thin LAr presampler covering $|\eta| < 1.8$ to correct for energy loss in material upstream of the calorimeters. Hadronic calorimetry is provided by the steel/scintillator-tile calorimeter, segmented into three barrel structures within $|\eta| < 1.7$, and two copper/LAr hadronic endcap calorimeters. The solid angle coverage is completed with forward copper/LAr and tungsten/LAr calorimeter modules optimised for electromagnetic and hadronic energy measurements, respectively.

The muon spectrometer (MS) comprises separate trigger and high-precision tracking chambers measuring the deflection of muons in a magnetic field generated by the superconducting air-core toroidal magnets. The field integral of the toroids ranges between 2.0 and 6.0 T m across most of the detector. Three layers of precision chambers, each consisting of layers of monitored drift tubes, cover the region $|\eta| < 2.7$. These were complemented in the innermost layer of the endcap region by cathode-strip chambers in Run 2, which were replaced in Run 3 by layers of small-strip thin-gap chambers and Micromegas chambers, both providing precision tracking in the region $1.3 < |\eta| < 2.7$. The muon trigger system covers the range $|\eta| < 2.4$ with resistive-plate chambers in the barrel region, thin-gap chambers in the endcap regions, and, in Run 3, the aforementioned small-strip thin-gap chambers and Micromegas chambers in the innermost layer of the endcap.

The luminosity is measured mainly by the LUCID-2 detector that records Cherenkov light produced in the quartz windows of photomultipliers located close to the beampipe.

Events were selected by the first-level trigger system implemented in custom hardware, followed by selections made by algorithms implemented in software in the high-level trigger [22, 23]. The first-level trigger accepted events from the 40 MHz bunch crossings at a rate close to 100 kHz, which the high-level trigger further reduced in order to record complete events to disk at about 1.25 kHz and 3 kHz in Run 2 and Run 3, respectively.

¹ ATLAS uses a right-handed coordinate system with its origin at the nominal interaction point (IP) in the centre of the detector and the z -axis along the beam pipe. The x -axis points from the IP to the centre of the LHC ring, and the y -axis points upwards. Polar coordinates (r, ϕ) are used in the transverse plane, ϕ being the azimuthal angle around the z -axis. The pseudorapidity is defined in terms of the polar angle θ as $\eta = -\ln \tan(\theta/2)$ and is equal to the rapidity $y = \frac{1}{2} \ln \left(\frac{E+p_z}{E-p_z} \right)$ in the relativistic limit. Angular distance is measured in units of $\Delta R \equiv \sqrt{(\Delta y)^2 + (\Delta \phi)^2}$.

The Run-3 detector configuration benefits from several upgrades compared with that of Run 2 to maintain high detector performance at the higher pile-up levels of Run 3. The improvements include a new innermost layer of the muon spectrometer in the endcap region, which provides higher redundancy and a large reduction in fake muon triggers. The trigger system also benefits from new digital electronics readout of the LAr calorimeters with significantly increased granularity. Other updates and further details are provided in Ref. [21].

A software suite [24] is used in data simulation, in the reconstruction and analysis of real and simulated data, in detector operations, and in the trigger and data acquisition systems of the experiment.

3 Data and simulated event samples

The data used in this analysis were collected using a set of single-electron and single-muon triggers [25, 26]. The transverse momentum thresholds of the online leptons vary across data-taking periods and depend on whether isolation requirements are applied at the trigger level. For electrons (muons), the p_T thresholds range from 24–26 (20–24) GeV for triggers with isolation, and increase up to 120–140 (50) GeV for those without isolation requirements. Application of data-quality requirements [27] results in data samples corresponding to integrated luminosities of 140 fb^{-1} and 55 fb^{-1} for Run 2 and Run 3, respectively.

While background contributions from misidentified or non-prompt leptons are mainly estimated by using data-driven techniques, Monte Carlo (MC) simulations are used to estimate the event yields and systematic uncertainties for both the signal processes and SM backgrounds featuring prompt-lepton production. These simulated event samples include the effect of multiple pp interactions in the same or neighbouring bunch crossings (pile-up), as well as the effect on the detector response due to interactions from bunch crossings before or after the one containing the hard interaction. All MC events were then re-weighted to match the pile-up distribution observed in the data. To simulate the detector response, background and signal MC samples were processed through the ATLAS simulation framework [28] in GEANT4 [29].

Simulated signal samples of resonant LQ production are used to optimise the event selection and interpret the results. Events are generated with an implementation of this process in POWHEG BOX RES at NLO [30] with the LUXlep-NNPDF3.1_{NLO} PDF set² [11] and are interfaced with HERWIG 7.2.3 for parton shower, hadronisation, and underlying event using the H7.2-Default set of tuned parameters [31]. This implementation models both the LQ production and subsequent decay. Decays of bottom and charm hadrons are performed by EVTGEN 2.1.1 [32].

The 2L selections of the analysis are sensitive to the photon-induced diagrams of resonant LQ production but also to other LQ production modes that feature a second lepton in the final state such as DY and single production. Therefore, dedicated combined DY+SP LQ samples are generated with a POWHEG BOX implementation at NLO [33] and used additionally in the interpretation of the results. These samples use the same PDF set as the resonant LQ samples and are similarly interfaced to HERWIG 7.2.3 for the parton shower. These samples also take the interference from DY LQ production with SM DY $Z/\gamma^* \rightarrow \ell\ell$ into account. As the latter is estimated from dedicated samples, the LQ signal samples only include the interference but not the SM contribution. The DY+SP samples include a $m_{\ell\ell} > 100 \text{ GeV}$ requirement at matrix-element level to increase the acceptance of the generated events for the signal selections in this analysis.

² This PDF set includes both leptons and photons in the proton content.

The \tilde{S}_1 LQ is used as benchmark and four different types of minimal LQ scenarios are considered. Only one LQ coupling is considered at a time while all other couplings are set to zero. The couplings considered are y_{de} , $y_{s\mu}$, y_{be} and $y_{b\mu}$ that result in an $e + \text{light-jet}$, $\mu + \text{light-jet}$, $e + b\text{-jet}$ and $\mu + b\text{-jet}$ signature, respectively. For the scenarios with y_{de} and $y_{s\mu}$ couplings, samples with LQ masses between 1 and 5 TeV are generated. Models with couplings to b -quarks have lower production cross-sections due to the smaller b -quark PDF, hence the generated samples cover LQ masses between 1 and 3.5 TeV. The signal samples cover the LQ coupling range from 0.1–1.0 for y_{de} and from 0.5–3.5 for the other scenarios. The ranges of the signal parameters are motivated by the expected sensitivity of the search, taking into account existing constraints from collider and low-energy (for y_{de}) experiments, and restricting to the perturbative regime of the theory [8]. The signal production cross-sections and uncertainties are taken from the POWHEG BOX RES implementations and evaluated according to prescriptions from Ref. [34]. As an example, the production cross-section for a 2 TeV LQ at $\sqrt{s} = 13$ TeV for y_{de} couplings between 0.1 and 1.0 range from 0.024 fb to 2.5 fb. At $\sqrt{s} = 13.6$ TeV these cross-sections increase by approximately 16%.

A variety of MC generators is utilised to model the SM backgrounds involving the production of prompt leptons. The event generator configurations for SM processes are mostly identical between the Run 2 and Run 3 MC samples, except that more recent generator versions are used for some of the latter. Table 1 provides a comprehensive overview of the SM background samples utilised in the analysis. Additional information regarding ATLAS simulations of $W + \text{jets}$, $Z + \text{jets}$, $t\bar{t}$, single-top (Wt , t -channel, s -channel), and diboson processes is available in Refs. [35–38]. The decays of bottom and charm hadrons are performed by EVTGEN versions 1.2.0, 1.6.0 and 2.1.1 [32], except for the backgrounds modelled using SHERPA, for which the decays are performed internally.

In addition to the hypothesized resonant LQ production, taking into account the lepton PDF in the proton also predicts a SM ℓj scattering process at the LHC. Such a process has not been observed yet but features the same lepton–jet signature as the targeted LQ model. To take this contribution into account, an ℓj scattering sample is generated at leading-order using MADGRAPH 3.3.4 [39] and interfaced with HERWIG 7.2.3 and the LUXlep-NNPDF3.1NLO PDF set. To enrich the sample in events with large $m_{\ell j}$, the transverse momentum (p_T) of the lepton is required to be greater than 50 GeV and the generation is performed in bins of lepton p_T .

4 Object reconstruction

Events are required to contain a primary vertex built from at least two associated tracks with $p_T > 0.5$ GeV. The primary vertex with the highest sum of squared transverse momenta $\sum p_T^2$ of its associated tracks [67] is identified as the hard-scatter vertex of interest in each event. A set of basic data-quality requirements is applied to ensure a fully operating detector and to suppress contributions from detector noise or non-collision backgrounds [68].

Two categories of analysis objects are defined and utilised to define the search regions. Leptons and jets are first “preselected” using loose selection criteria; those that satisfy additional, tighter requirements are designated as “signal” objects. For electrons, also an intermediate category—falling between the preselected and signal definitions—is introduced which is employed in the data-driven estimate of the FNP electron background, as detailed in Section 6.

Preselected electrons are reconstructed using ID tracks matched to energy clusters in the electromagnetic calorimeter. These satisfy $p_T > 10$ GeV and $|\eta| < 2.47$ with a *LooseAndBLayerLLH* identification [69, 70].

Table 1: Simulated signal and background event samples with the corresponding matrix element and parton shower (PS) generators, cross-section order in α_s used to normalise the event yield, set of tuned parameters (tune) for the underlying-event and the generator PDF sets used. For diboson samples, $V \in \{W, Z\}$. “Default” refers to the default tune of the SHERPA generator. When different, the settings used for the simulation of samples compared with Run-3 data are mentioned in parentheses. Abbreviations used are defined as: leading-order (LO), next-to-leading-order (NLO), next-to-next-to-leading-order (NNLO), next-to-leading-logarithmic (NLL), next-to-next-to-leading-logarithmic (NNLL). The PDF set employed in the PS is generally the same as in the generator except for the $t\bar{t}$, single-top and the MG5_AMC@NLO $t\bar{t}+Z$ and $t\bar{t}+W$ samples where the NNPDF2.3LO [40] set is used.

Physics process	Generator	Parton shower	Normalisation	Tune	PDF (generator)
Resonant LQ signal	POWHEG Box RES [30]	HERWIG 7.2.3 [31]	NLO	H7.2-Default [31]	LUXlep-NNPDF3.1NLO [11]
DY+SP LQ signal	POWHEG Box v2 [33]	HERWIG 7.2.3	NLO	H7.2-Default	LUXlep-NNPDF3.1NLO
$Z/\gamma^*(\rightarrow \ell\ell)+\text{jets}$	SHERPA 2.2.11 [41, 42] (SHERPA 2.2.14)	SHERPA 2.2.11 [43] (SHERPA 2.2.14)	NNLO [44]	Default [38]	NNPDF3.0NNLO [45]
$Z/\gamma^*(\rightarrow \tau\tau)+\text{jets}$	SHERPA 2.2.14	SHERPA 2.2.14	NNLO [44]	Default	NNPDF3.0NNLO
$W(\rightarrow \ell\nu, \tau\nu)+\text{jets}$	SHERPA 2.2.11 [41] (SHERPA 2.2.14)	SHERPA 2.2.11 (SHERPA 2.2.14)	NNLO [44]	Default	NNPDF3.0NNLO
$t\bar{t}$	POWHEG Box v2 [46–49]	PYTHIA 8.230 [50]	NNLO+NNLL [51–57]	A14 [58]	NNPDF3.0NLO
Single-top	POWHEG Box v2 [47–49, 59]	PYTHIA 8.230	NLO+NNLL [60]	A14	NNPDF3.0NLO
Diboson VV	SHERPA 2.2.11, 2.2.12 (SHERPA 2.2.14, 2.2.16)	SHERPA 2.2.11, 2.2.12 (SHERPA 2.2.14, 2.2.16)	LO–NLO [61–64]	Default	NNPDF3.0NNLO
$t\bar{t}+Z$	MG5_AMC@NLO 2.3.3 [39, 65]	PYTHIA 8.210 [50]	NLO [39]	A14	NNPDF3.0NLO
$t\bar{t}+W$	MG5_AMC@NLO 2.3.3 (SHERPA 2.2.14)	PYTHIA 8.210 (SHERPA 2.2.14)	NLO	A14 (Default)	NNPDF3.0NLO
Multijet	PYTHIA 8.230 (PYTHIA 8.308)	PYTHIA 8.230 (PYTHIA 8.308)	LO [66]	A14	NNPDF2.3LO
ℓj scattering	MADGRAPH 3.3.4 [39]	HERWIG 7.2.3	LO	H7.2-Default	LUXlep-NNPDF3.1NLO

Electrons reconstructed in the calorimeter transition region, $1.37 < |\eta| < 1.52$, are not considered. The longitudinal impact parameter z_0 of preselected electron tracks is required to satisfy $|z_0 \sin \theta| < 0.5$ mm. Signal electrons must also satisfy $p_T > 25$ GeV, the *Tight* likelihood-based identification criteria and have a transverse impact parameter d_0 with uncertainty $\sigma(d_0)$ satisfying $|d_0/\sigma(d_0)| < 5$. To further reject FNP electrons, the *HighPtCaloOnly* isolation discriminant [70] is employed that is calculated from energy deposits in the calorimeter cells in a cone around the electron candidate.

Preselected muons are reconstructed by combining tracks from the ID and the muon spectrometer subsystems. These are required to have $p_T > 10$ GeV, $|\eta| < 2.5$, satisfy the *High- p_T* identification criteria [71] and $|z_0 \sin \theta| < 0.5$ mm. Signal muons must have $p_T > 25$ GeV, impact parameter significance $|d_0/\sigma(d_0)| < 3$ and must satisfy an isolation requirement with a similar performance to the *PflowTight* criterion described in Ref. [71].

Hadronic jets are reconstructed using the anti- k_t algorithm [72] as implemented in FastJet [73] with a jet radius parameter of $R = 0.4$. The inputs to this algorithm are particle-flow objects [74] that combine measurements from the ATLAS inner detector and calorimeters [75]. The jet energy scale and resolution are calibrated using simulations, with in situ corrections obtained from data [76]. Preselected jets are required to satisfy $p_T > 20$ GeV and $|\eta| < 4.5$. Signal jets are required to have $|\eta| < 2.5$ and must additionally satisfy a pile-up jet rejection criterion based on a neural-network variant of the jet vertex tagger [77] if they have $p_T < 60$ GeV. Signal jets that satisfy the 85% efficiency working point of the *GN2* algorithm [78] are considered to likely contain b -hadrons and are referred to as b -tagged jets.

The missing transverse momentum p_T^{miss} is calculated as the magnitude of the negative vector sum of the transverse momenta of all identified hard physics objects (preselected leptons and jets) calibrated to their respective energy scales, with a contribution from an additional soft term [79]. This soft term is constructed from ID tracks matched to the hard-scatter vertex but not associated with any of the hard reconstructed objects.

Since the object reconstruction algorithms are applied independently, lepton and jet candidates may share contributions from the same detector signals. To resolve such ambiguities, an overlap removal procedure is applied to the preselected leptons and signal jets in the following order. First, any electron sharing an ID track with a muon is removed. Next, jets are removed if they are within $\Delta R < 0.2$ from a remaining electron. After this, electrons are in turn rejected if they are within $\Delta R < 0.4$ of any remaining jet. Subsequently, jets with any ghost-associated [80] muon or within $\Delta R < 0.2$ are removed if the jet has fewer than three associated tracks with $p_T > 500$ MeV. Finally, any muon within $\Delta R < 0.4$ of a jet is removed. Only objects that satisfy this overlap removal procedure are retained for the event selection.

5 Event selection

A set of analysis variables is derived from the physics objects that satisfy the identification criteria and are used in the event selections. These are briefly summarised below, where the leading lepton (jet) refers to the lepton (jet) with the largest p_T in the event:

- $m_{\ell j}$: Invariant mass of the system built from the leading lepton and leading jet in the event to reconstruct the LQ mass.
- $p_T^\ell/m_{\ell j}$: Ratio of the p_T of the leading lepton and the invariant mass of the lepton–jet system $m_{\ell j}$.
- $\Delta R(\ell, j)$: Angular separation $\Delta R(\ell, j) = \sqrt{\Delta\phi(\ell, j)^2 + \Delta\eta(\ell, j)^2}$ between the leading lepton and leading jet .
- $\Delta\phi(\ell, p_T^{\text{miss}})$: Azimuthal angle between the leading lepton and p_T^{miss} .
- $m_{\ell\ell}$: Invariant mass of the lepton pair in the 2L selections.
- $\mathcal{S}(p_T^{\text{miss}})$: Object-based p_T^{miss} significance [79] that provides a measure for the likelihood of the reconstructed p_T^{miss} to originate from real invisible particles instead of from detector effects.

All four channels share a common preselection designed to enrich the selected events in the kinematic phase space of interest and to serve as basis to define signal, control, and validation regions. Each event must contain at least one signal lepton (electron or muon) and at least one jet, both with $p_T > 130$ GeV. The invariant mass of the lepton–jet system, $m_{\ell j}$, is required to exceed 700 GeV. Although the leptons and jets from the LQ decays of interest typically have transverse momenta of several hundreds of GeV, the p_T requirements at the preselection level are relaxed to retain a sufficiently large sample of events for reliable background estimation.

The 1L selection requires exactly one signal lepton, while the 2L selection requires exactly two same-flavour signal leptons (ee or $\mu\mu$). Events with additional preselected leptons beyond those satisfying the signal lepton criteria are vetoed. For the 2L selections, an additional requirement of $m_{\ell\ell} > 70$ GeV is imposed, as the signal of interest with a resonantly produced LQ does not contribute much at low $m_{\ell\ell}$.

Table 2: Definitions of the preselection together with the 1L and 2L SRs for the $e + \text{light-jet}$, $\mu + \text{light-jet}$, $e + b\text{-jet}$ and $\mu + b\text{-jet}$ channels. The lepton requirements indicate an additional veto of preselected leptons, e.g. $N_e = 1$ requires the presence of exactly one signal electron but no other preselected lepton in the event.

Preselection									
		$m_{\ell\ell} > 700 \text{ GeV}$		$p_{\text{T}}^{\ell_1} > 130 \text{ GeV}$		$p_{\text{T}}^{j_1} > 130 \text{ GeV}$		$m_{\ell\ell} > 70 \text{ GeV (if } N_\ell = 2)$	
Region	$e + \text{light-jet}$		$\mu + \text{light-jet}$		$e + b\text{-jet}$		$\mu + b\text{-jet}$		
	SR-1L- e_j	SR-2L- e_j	SR-1L- μ_j	SR-2L- μ_j	SR-1L- eb	SR-2L- eb	SR-1L- μb	SR-2L- μb	
$m_{\ell j} [\text{GeV}]$	≥ 950		≥ 900		≥ 900		≥ 900		
N_e	1	2	0		1	2	0		
N_μ	0		1	2	0		1	2	
$N_{b\text{-jets}}$	0		0		1		1		
$\mathcal{S}(p_{\text{T}}^{\text{miss}})$	< 3.5		< 3.5		< 3.0	< 5.0	< 3.0	< 5.0	
$\Delta R(\ell, j)$	< 3.7	–	[2.9, 3.6]	–	–		[2.4, 4.2]		
$p_{\text{T}}^\ell/m_{\ell j}$	> 0.4	> 0.3	> 0.4	> 0.3	> 0.3	> 0.25	> 0.3	> 0.2	
$m_{\ell\ell} [\text{GeV}]$	–	> 160	–	> 160	–	> 150	–	> 120	

To ensure that events are selected in the plateau region of the trigger efficiency, a reconstructed lepton is required to be matched to the trigger-level lepton and to have a sufficiently high p_{T} above the corresponding online threshold, as described in Section 3. For muons, the p_{T} requirement of the event preselection alone guarantees that the single-muon triggers operate within their efficiency plateau. For electrons, the required p_{T} reaches up to 141 GeV in events selected by single-electron triggers that employ only a loose identification and no isolation criteria at the trigger level.

Events satisfying this preselection are then assigned to one of four analysis channels based on the lepton flavour and the number of b -tagged jets $N_{b\text{-jets}}$. The electron-based (muon-based) channels are restricted to events with either one or two electrons (muons). The $e + \text{light-jet}$ and $\mu + \text{light-jet}$ channels require the absence of any b -tagged jet (b -veto) while the $e + b\text{-jet}$ and $\mu + b\text{-jet}$ channels require the leading jet to be b -tagged.

Building on the preselection, additional requirements are applied—individually optimised for each channel and for the 1L and 2L selections—to enhance the separation between signal and background events. The resulting signal regions are referred to as SR-1L and SR-2L, respectively.

A summary of the SR definitions for each channel is provided in Table 2. Since the LQ signal does not produce genuine missing transverse momentum, an upper requirement on $\mathcal{S}(p_{\text{T}}^{\text{miss}})$ is applied to efficiently suppress W +jets and top-related backgrounds while retaining most of the signal events. The lepton and jet originating from a LQ decay are typically produced back-to-back in the detector, motivating a selection on their angular separation $\Delta R(\ell, j)$. In addition, the LQ decay products are expected to share the parent particle’s energy approximately equally, resulting in similar lepton and jet momenta. Therefore, each channel imposes a lower bound on $p_{\text{T}}^\ell/m_{\ell j}$ to reject SM events with a large p_{T} imbalance between the leading lepton and jet. Finally, in the SR-2L selections, a lower requirement on $m_{\ell\ell}$ is applied to suppress Z +jets events.

To maximise sensitivity across a broad range of potential LQ masses, the SRs are further binned in $m_{\ell j}$,

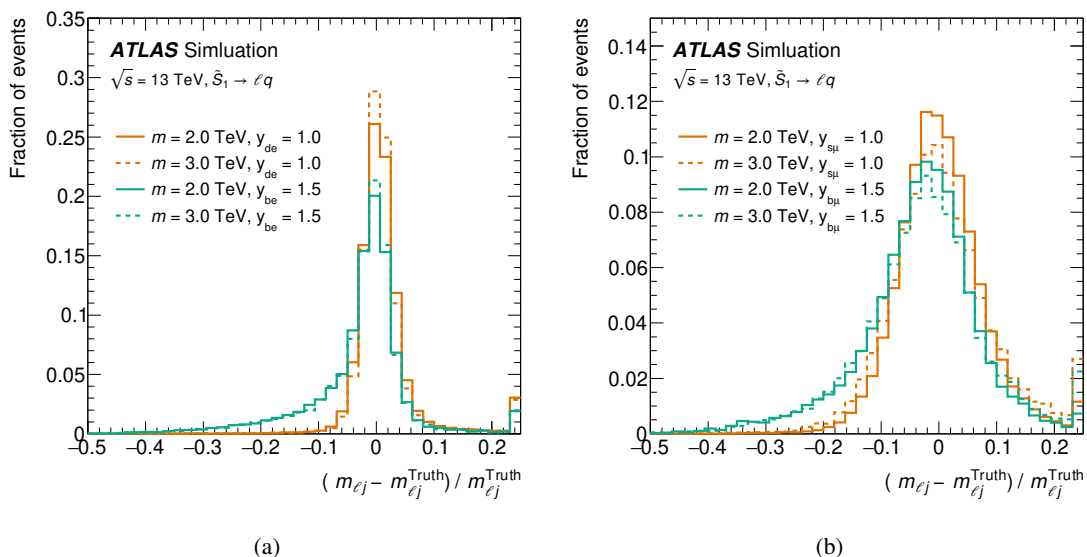


Figure 2: Relative difference between the reconstructed $m_{\ell j}$ and particle-level $m_{\ell j}^{\text{Truth}}$ invariant mass of the lepton–jet system for selected example LQ scenarios in the (a) $e + \text{light-jet}$ and $e + b\text{-jet}$, and (b) $\mu + \text{light-jet}$ and $\mu + b\text{-jet}$ channels using Run 2 MC simulation. The dashed lines correspond to an LQ scenario with a larger mass but the same coupling as the one shown by the solid lines. The particle-level invariant mass is calculated using the particle-level four-momenta of the reconstructed lepton and jet. The last bin contains the overflow.

targeting LQ masses of approximately 1 TeV and above. The binning choice is derived by the experimental resolution in $m_{\ell j}$, defined by the relative difference between the invariant mass of the lepton–jet system at reconstruction- and at particle-level. This resolution is evaluated using LQ signal samples and found to be largely independent of the LQ coupling, with only a mild dependence on the LQ mass. Figure 2 shows the relative difference between the reconstructed and the particle-level $m_{\ell j}$ for example LQ signals after application of the preselection requirements. Since the absolute $m_{\ell j}$ resolution worsens with increasing LQ mass, the $m_{\ell j}$ bin widths are gradually broadened across the spectrum. Binning continues until the SM background expectation falls below approximately one event, with the final bin in both SR-1L and SR-2L being inclusive and capturing all overflow events. No substantial difference between the $m_{\ell j}$ resolution between Run 2 and Run 3 is observed; therefore, the same binning strategy is applied to both data-taking periods.

Table 3 provides an overview of how the individual $m_{\ell j}$ SR bins are defined for each channel. In the $e + \text{light-jet}$ channel, the $m_{\ell j}$ resolution is found to be approximately 5%, motivating bin widths of 100 GeV for LQ masses around 1 TeV and 200 GeV for masses near 2 TeV. The first bin in the $e + \text{light-jet}$ SRs begins at $m_{\ell j} = 950$ GeV, while the final bin in SR-1L- $e j$ (SR-2L- $e j$) includes events with $m_{\ell j} \geq 3100$ (2300) GeV.

In the $\mu + \text{light-jet}$ channel, the $m_{\ell j}$ resolution is approximately 10%, due to the worsened momentum resolution for high- p_T muons compared with electrons. This suggests a bin width of 200 GeV for a LQ mass of 1 TeV and therefore the SRs in this channel begin at $m_{\ell j} = 900$ GeV with the final bin in both SR-1L- μj and SR-2L- μj includes events with $m_{\ell j} \geq 2300$ GeV.

In the b -tagged channels, the $m_{\ell j}$ resolution is slightly worse than in the corresponding light-jet channels due to the possible presence of neutrinos in b -hadron decays, and is determined to be approximately 8% in the $e + b\text{-jet}$ channel and 13% in the $\mu + b\text{-jet}$ channel. Both SR-1L- eb and SR-1L- μb begin at $m_{\ell j}$

Table 3: Binning of the $m_{\ell j}$ distribution used for SR-1L and SR-2L of the $e + \text{light-jet}$, $\mu + \text{light-jet}$, $e + b\text{-jet}$ and $\mu + b\text{-jet}$ channels, respectively.

	SR	Binning in $m_{\ell j}$ [GeV]
$e + \text{light-jet}$	SR-1L- ej	[950, 1050, 1150, 1250, 1350, 1450, 1600, 1750, 1900, 2100, 2300, 2550, 2800, 3100, ∞)
	SR-2L- ej	[950, 1050, 1150, 1250, 1350, 1450, 1600, 1750, 1900, 2100, 2300, ∞)
$\mu + \text{light-jet}$	SR-1L- μj	[900, 1100, 1300, 1600, 1900, 2300, ∞]
	SR-2L- μj	[900, 1100, 1300, 1600, 1900, 2300, ∞]
$e + b\text{-jet}$	SR-1L- eb	[900, 1100, 1300, 1550, 1850, 2200, ∞]
	SR-2L- eb	[900, 1100, 1300, 1550, ∞]
$\mu + b\text{-jet}$	SR-1L- μb	[900, 1175, 1550, 2025, ∞]
	SR-2L- μb	[900, 1175, 1550, ∞]

= 900 GeV, while the final bin in SR-1L- eb (SR-1L- μb) and SR-2L- eb (SR-2L- μb) includes events with $m_{\ell j} \geq 2200$ (2025) GeV and $m_{\ell j} \geq 1550$ (1550) GeV, respectively.

Therefore, the LQ decay width³ remains well below the experimental resolution for couplings up to about 1.5, corresponding to a width of approximately 80 GeV for a 2 TeV LQ. For the largest couplings considered, the effects of the intrinsic width and the detector resolution on the reconstructed LQ mass peak become comparable.

The signal composition in the SR-2L regions varies across the parameter space. For coupling values below 0.5, resonant LQ production accounts for approximately 70–80% of the total signal in these regions. As the coupling strength increases, the DY+SP production mode becomes increasingly relevant, reaching comparable levels to resonant production at couplings around 3.5. Within the DY+SP sample, the SP component, which also produces a peak in the $m_{\ell j}$ spectrum at the LQ mass, dominates for low couplings and LQ masses up to roughly 2 TeV. In contrast, the non-resonant DY contribution, which decreases steeply with $m_{\ell j}$ and thus has a comparable low selection efficiency in the SRs, gains in relative importance at larger couplings and LQ masses.

The overall signal efficiencies for resonant LQ production, including the detector acceptance, for the SR-1L and SR-2L selections in the $e + \text{light-jet}$ channel assuming a LQ with mass of 2 TeV and coupling of 1.0 are approximately 30% and 15%, respectively. In the $\mu + \text{light-jet}$ channel these selection efficiencies for a LQ of the same mass and a coupling of 1.5 are approximately 17% and 10%, respectively. The selection efficiencies in the b -tagged channels are smaller than in the light-jet channels and are 17% (12%) and 7% (7%) in the $e + b\text{-jet}$ ($\mu + b\text{-jet}$) channel, for a LQ signal with mass of 2 TeV and a coupling of 1.5.

6 Background estimation

The SM processes contributing to the phase space targeted by this analysis can be broadly classified into reducible and irreducible backgrounds. Reducible backgrounds include events containing at least one FNP lepton, originating from misidentified detector signatures such as jets, or from non-prompt leptons produced

³ The partial decay width Γ_{LQ} of a scalar LQ with mass m_{LQ} corresponding to coupling $y_{q\ell}$ is given at LO by $\Gamma_{\text{LQ}} = \frac{|y_{q\ell}|^2}{16\pi} m_{\text{LQ}}$ in the limit of large LQ masses [12].

in hadron decays involving heavy-flavour quarks. Irreducible backgrounds arise from processes with prompt, genuine leptons that produce final states resembling the target signal. The dominant irreducible contributions come from W + jets and Z + jets production, with top-quark processes providing an additional source in the b -tagged channels.

A combination of data-driven and MC-based techniques is used to estimate these SM backgrounds, as detailed in the following sections. The resulting predictions are validated in dedicated validation regions (VRs), which are typically enriched in specific background processes.

6.1 Reducible backgrounds

The particle-level information available in simulation samples enables a study of the origins of reconstructed leptons, allowing a distinction between genuine and misidentified objects. In the 1L selections of the e + light-jet and e + b -jet channels, a non-negligible fraction of the SM background is predicted to arise from FNP electrons. The most common origins of these misidentified electrons are prompt photons, arising from e.g. initial- and final-state radiation, and light-hadron decays. To estimate this contribution, a data-driven technique known as the fake-factor method [81] is employed in the 1L selections of the electron channels. In contrast, the selections requiring two electrons and all selections in the μ + light-jet and μ + b -jet channels receive only a small contribution from FNP leptons. In these cases, the FNP background is instead estimated directly from MC simulation.

In the fake-factor method, the number of FNP leptons entering an analysis region—i.e., those satisfying the “tight”, signal selection criteria for leptons, $N_{\text{signal}}^{\text{FNP}}$ —is estimated using a separate, independent data sample of “loose” leptons in the same region that meet a relaxed set of selection requirements. The ratio to extrapolate from the loose to the signal lepton sample is referred to as the “fake factor” (FF) and is derived from data, as described below. To isolate the FNP contribution, any contamination from real, genuine leptons in the loose lepton sample is estimated by using MC simulation and subtracted from the data. The resulting estimate of the number of signal FNP leptons $N_{\text{signal}}^{\text{FNP}}$ in a given region is computed as

$$N_{\text{signal}}^{\text{FNP}} = \text{FF} \cdot (N_{\text{loose}}^{\text{data}} - N_{\text{loose}}^{\text{MC, real}}).$$

Here, $N_{\text{loose}}^{\text{data}}$ and $N_{\text{loose}}^{\text{MC, real}}$ are the numbers of loose leptons observed in data and the estimated number of genuine loose leptons from simulation, respectively. The fake factor is typically parameterised in bins of relevant kinematic variables to account for dependencies in the extrapolation. These are derived as the ratio of signal to loose electrons in data, using a region enriched in FNP leptons and orthogonal to all other selections used in the analysis. The contamination from genuine leptons in both the loose and signal samples within the fake factor measurement region is estimated from MC simulation and again subtracted accordingly:

$$\text{FF} = \frac{N_{\text{signal}}^{\text{data}} - N_{\text{signal}}^{\text{MC, real}}}{N_{\text{loose}}^{\text{data}} - N_{\text{loose}}^{\text{MC, real}}}.$$

Loose electrons are defined as preselected electrons that fail to satisfy any of the signal electron selection criteria. They are further required to satisfy the *Medium* identification and *IsoLoose_VarRad* isolation working points [70] to match the associated online criteria and avoid any bias originating from the trigger

Table 4: Overview of the definitions for the regions employed to derive and validate the FNP electron estimate.

Region	FNP estimation		
	MR-fake	VR-fake	CR-W-fake
$m_{\ell j}$ [GeV]		> 700	
N_e		1	
N_μ		0	
$N_{b\text{-jets}}$		0	
$\Delta R(\ell, j)$		> 3.7	
$\mathcal{S}(p_T^{\text{miss}})$	< 3	3–5	> 5.0

requirements in the measured fake factors. Moreover, applying these requirements brings the loose electron definition closer to the signal one, reducing the size of the extrapolation between them while maintaining a sufficiently large number of events in the loose electron sample.

Fake factors are measured in events that satisfy the preselection described in Section 5. Such events must contain exactly either one loose or signal electron, no additional preselected leptons, and no b -tagged jets. To ensure orthogonality with the selections in the e + light-jet channel, a requirement of $\Delta R(\ell, j) > 3.7$ is imposed. An additional $\mathcal{S}(p_T^{\text{miss}}) < 3$ requirement suppresses contributions from W +jets events. This selection is referred to as fake factor measurement region, denoted by MR-fake. Events featuring $3 < \mathcal{S}(p_T^{\text{miss}}) < 5$ instead define the validation region VR-fake, which is used to assess the performance of the measured fake factors. While the loose electron samples in MR-fake and VR-fake are very pure in FNP leptons, the purity decreases to approximately 40% and 20% for signal electrons due to significant contamination from the W +jets process. To constrain the W +jets normalisation when validating the FNP estimate in VR-fake, events with $\mathcal{S}(p_T^{\text{miss}}) > 5$ are used to define a control region, CR-W-fake. A summary of the region definitions is provided in Table 4.

The fake factors are parameterised as a function of the electron p_T in three bins of $|\eta|$, and are shown separately for Run 2 and Run 3 in Figure 3. In Run 2, the fake factors range from 0.2 to 0.35 at $p_T \sim 130$ GeV, depending on $|\eta|$, and typically decrease to values between 0.05 and 0.1 for $p_T > 800$ GeV. In Run 3, higher values are observed, with fake factors ranging from approximately 0.35 to 0.5 at low p_T and from 0.05 to 0.25 at high p_T . This difference between Run 2 and Run 3 is consistently observed in both data and simulation. The $\Delta R(\ell, j) > 3.7$ requirement in the MR-fake region biases the selected electrons towards the more forward direction, limiting the available number of events in the central region and allowing only a coarser binning at high electron p_T . Although the fake factors are measured in events without b -tagged jets, they are applied in both the e + light-jet and e + b -jet channels. A b -tagged counterpart to MR-fake cannot be defined due to low FNP purity and limited number of events. Since MC simulation shows no strong dependence of the fake factors on the b -jet multiplicity, an additional uncertainty is assigned when applying them to events with b -tagged jets instead to cover this dependence, see Section 7.

Figure 4 shows the electron p_T distributions in VR-fake separately for Run 2 and Run 3, with the FNP background estimated by using the derived fake factors. The normalisation of W +jets in this region is constrained by performing a background-only fit (see Section 8) to the corresponding CR-W-fake region. The extracted normalisation factors for W +jets in the CR-W-fake regions are found to be compatible with unity. These fit results are used solely to validate the FNP estimate in VR-fake; the following section

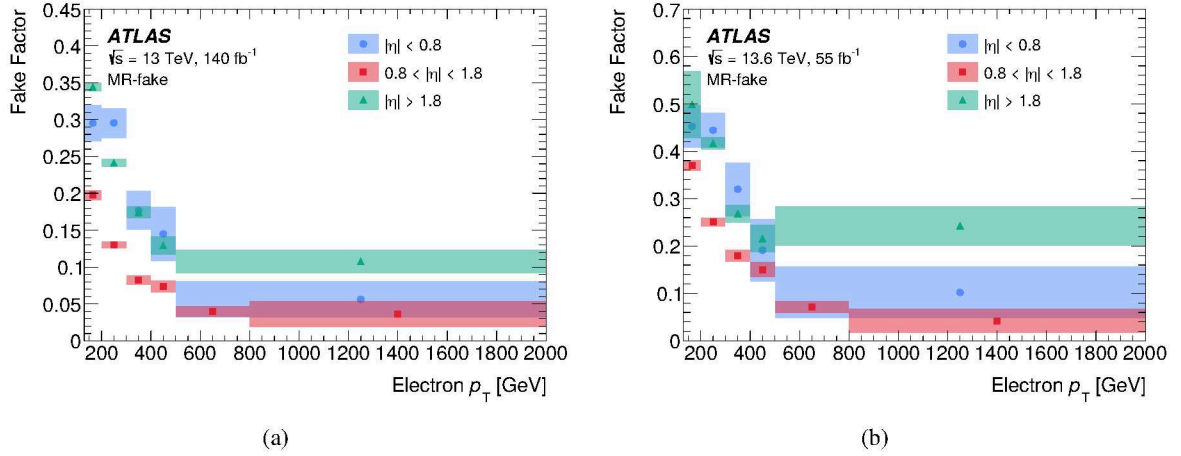


Figure 3: Measured electron fake factors in MR-fake for (a) Run 2 and (b) Run 3 with respect to p_T in the three $|\eta|$ bins. The uncertainty bands represent the statistical uncertainties in the fake factors. The last bin is inclusive in the electron p_T .

introduces the dedicated CRs used to constrain the $W+$ jets normalisation in the SRs. Good agreement between data and the SM predictions is observed across the p_T spectrum in both data-taking periods within systematic uncertainties (see Section 7), giving confidence in the procedure used to derive the fake factors.

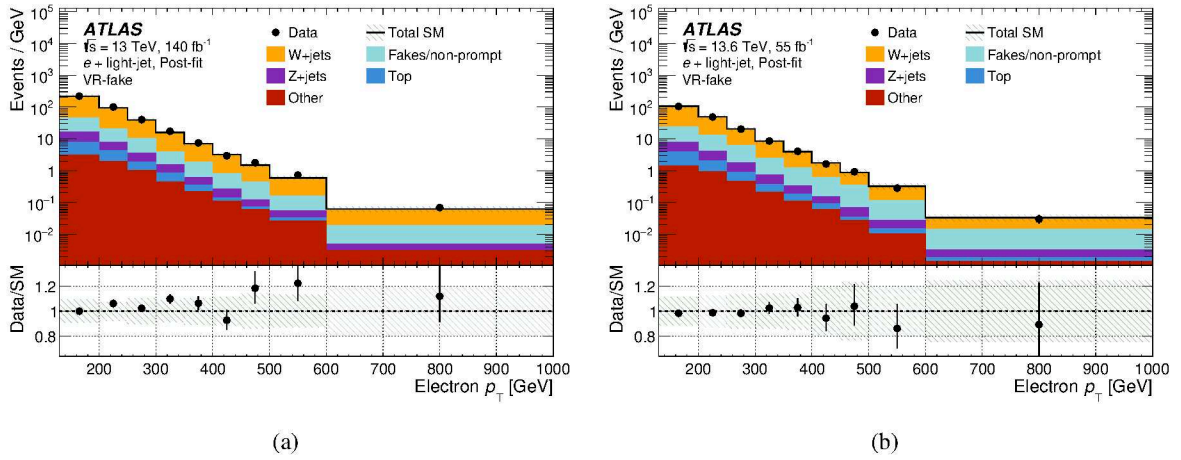


Figure 4: Post-fit distributions of the electron p_T in VR-fake for (a) Run 2 and (b) Run 3 using a background-only fit of CR-W-fake. The error bands include statistical and systematic uncertainties, with correlations between uncertainties taken into account. The last bin contains the overflow.

6.2 Irreducible backgrounds

Irreducible backgrounds are estimated from MC simulation, with the dominant processes being constrained to data through dedicated control regions. These CRs are individually optimised for each channel and enriched in a specific background process. The $W+$ jets and $Z+$ jets backgrounds are constrained in CR-W and CR-Z, respectively. The $e + b$ -jet and $\mu + b$ -jet channels define additional CR-T regions to normalise

Table 5: Definitions of the CRs and VRs for the $e + \text{light-jet}$ and $\mu + \text{light-jet}$ channels. The requirements listed are placed on top of the preselection introduced in the main text. The lepton requirements indicate an additional veto of preselected leptons, e.g. $N_e = 1$ requires the presence of exactly one signal electron but no other preselected lepton in the event. The VR-W and VR-Z regions follow the $m_{\ell j}$ binning of the associated SRs as described in the main text. The suffixes $-ej$ (e.g. in CR-W- ej) and $-\mu j$ of each region name are dropped in the table for brevity, respectively.

Region	$e + \text{light-jet}$						$\mu + \text{light-jet}$			
	CR-W	VR-W	VR- $S(p_T^{\text{miss}})$	CR-Z	VR-Z	VR- $m_{\ell\ell}$	CR-W	VR-W	CR-Z	VR-Z
$m_{\ell j}$ [GeV]	[700, 950]	> 950	[700, 950]	[700, 950]	> 950	[700,950]	[700, 900]	> 900	[700, 900]	> 900
N_e	1		1	2		2	0		0	
N_μ	0		0	0		0	1		2	
$N_{b\text{-jets}}$	0		0	0		0	0		0	
$\Delta R(\ell, j)$	< 3.7		< 3.7	–		–	[2.9, 3.6]		–	
$m_{\ell\ell}$ [GeV]	–		–	[70, 160]		[160, 250]	–		[70, 160]	
$S(p_T^{\text{miss}})$	> 3.5		< 3.5	< 3.5		< 3.5	> 3.5		< 3.5	
$p_T^\ell/m_{\ell j}$	> 0.4		> 0.4	> 0.3		> 0.3	> 0.4	> 0.2	> 0.3	

Table 6: Definitions of the CRs and VRs for the $e + b\text{-jet}$ channel. The requirements listed are placed on top of the preselection introduced in the main text. The lepton requirements indicate an additional veto of preselected leptons, e.g. $N_e = 1$ requires the presence of exactly one signal electron but no other preselected lepton in the event. The VR-W, VR-Z and VR-T-high regions follow the $m_{\ell j}$ binning of the associated SRs as described in the main text. The suffix $-eb$ (e.g. in CR-W- eb) of each region name is dropped in the table for brevity.

Region	$e + b\text{-jet}$							
	CR-W	VR-W	CR-Z	VR-Z	CR-T-high	VR-T-high	CR-T-low	VR- $S(p_T^{\text{miss}})$
$m_{\ell j}$ [GeV]	[700, 900]	> 900	[700, 900]	> 900	[900, 1300]	> 1300	[700, 900]	[700, 900]
N_e		1		2		1	1	1
N_μ		0		0		0	0	0
$N_{b\text{-jets}}$		1		1		≥ 2	≥ 2	1
$m_{\ell\ell}$ [GeV]		–		[70, 110]		–	–	–
$S(p_T^{\text{miss}})$		> 3.0		< 5.0		< 4.0	> 3.0	< 3.0
$p_T^\ell/m_{\ell j}$		> 0.3		> 0.25		> 0.3	> 0.3	> 0.3
$\Delta\phi(\ell, p_T^{\text{miss}})$		< 1.0		–		< 1.0	< 1.0	< 1.0

backgrounds containing top quarks. Events from $t\bar{t}$ and single-top production are therefore grouped into a common category labelled “Top” and constrained using a common normalisation factor. Other, rarer processes involving genuine leptons—such as diboson production, $t\bar{t}V$, and ℓj scattering—are estimated from MC simulation and grouped into a category labelled “Others”. MC events used to estimate the irreducible backgrounds are required to contain only genuine leptons to avoid double-counting with the FNP estimate described in the previous subsection. The extracted background normalisations are validated in the corresponding VRs which also adopt the $m_{\ell j}$ binning of the SRs. Summaries of the CR and VR definitions are provided in Table 5 for the light-jet and Tables 6 and 7 for the $e + b\text{-jet}$ and $\mu + b\text{-jet}$ channels, respectively.

All four channels follow a similar strategy to derive and validate the normalisations for $W + \text{jets}$ and $Z + \text{jets}$

Table 7: Definitions of the CRs and VRs for the $\mu + b$ -jet channel. The requirements listed are placed on top of the preselection introduced in the main text. The lepton requirements indicate an additional veto of preselected leptons, e.g. $N_e = 1$ requires the presence of exactly one signal electron but no other preselected lepton in the event. The VR-W, VR-Z and VR-T-high regions follow the $m_{\ell j}$ binning of the associated SRs as described in the main text. The suffix $-\mu b$ (e.g. in CR-W- μb) of each region name is dropped in the table for brevity.

Region	$\mu + b$ -jet								
	CR-W	VR-W	CR-Z	VR-Z	CR-T-high	VR-T-high	CR-T-low	VR-T-low	VR- $\mathcal{S}(p_T^{\text{miss}})$
$m_{\ell j}$ [GeV]	[700, 900]	> 900	[700, 900]	> 900	> 900	> 900	[700, 900]	[700, 900]	[700, 900]
N_e	0		0		0		0		0
N_μ	1		2		1		1		1
$N_{b\text{-jets}}$	1		1		≥ 2		≥ 2		1
$\Delta R(\ell, j)$	[2.4, 4.2]		[2.4, 4.2]		[2.4, 4.2]		[2.4, 4.2]		[2.4, 4.2]
$m_{\ell\ell}$ [GeV]	–		[70, 120]		–		–		–
$\mathcal{S}(p_T^{\text{miss}})$	> 3.0		< 5.0		> 4.0	[3.0, 4.0]	> 4.0	[3.0, 4.0]	< 3.0
$p_T^\ell/m_{\ell j}$	> 0.2		> 0.2		> 0.3		> 0.3		> 0.3

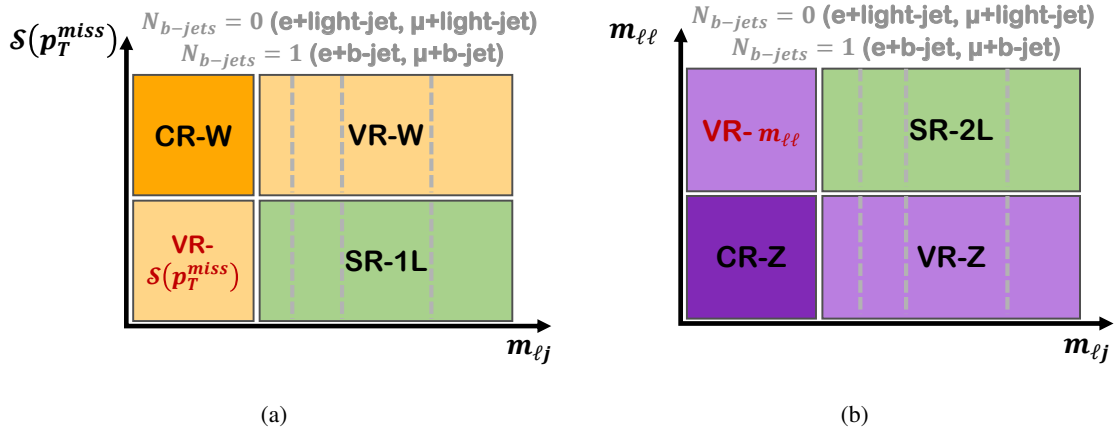


Figure 5: Illustrations of the CRs and VRs definitions for the (a) W +jets and (b) Z +jets backgrounds. The phase space of SR-1L and SR-2L is also indicated, respectively. Grey vertical dashed lines indicate that a region is binned in $m_{\ell j}$.

backgrounds. Both the CR-W and CR-Z are defined at lower $m_{\ell j}$ values than the SRs to ensure sufficiently large event counts in these regions. Illustrations showing the region layout of the CR-W and CR-Z are presented in Figure 5. These CRs span the $m_{\ell j}$ range from 700 GeV up to the start of the SRs, which begins at either 900 or 950 GeV depending on the channel. The VR-W and VR-Z regions apply the same selection as their respective CRs but cover the $m_{\ell j}$ range used in the SRs. To maintain kinematic similarity to the SRs, the CRs and VRs mirror the SR requirements on $\Delta R(\ell, j)$, $m_{\ell\ell}$, $\mathcal{S}(p_T^{\text{miss}})$, and $p_T^\ell/m_{\ell j}$ as closely as possible, with one selection inverted to ensure orthogonality. In some of these CRs and VRs, additional or relaxed requirements relative to the SRs are applied to ensure that the contamination from signals not already excluded by previous ATLAS searches remains below 10%. CR-W and VR-W replicate the SR-1L selection but invert the $\mathcal{S}(p_T^{\text{miss}})$ requirement to enrich W +jets events. Similarly, CR-Z and VR-Z mimic the SR-2L selection but require $m_{\ell\ell}$ to lie within a window around the Z boson mass. To facilitate a

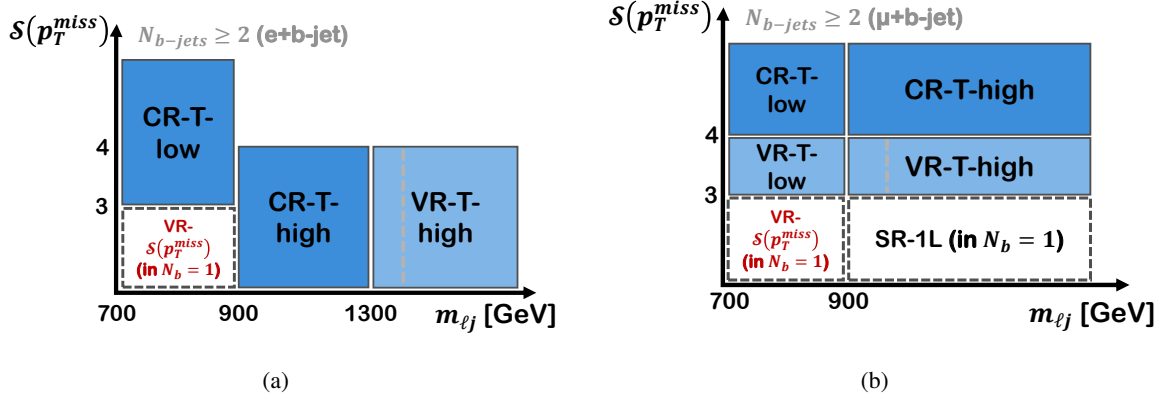


Figure 6: Illustrations of the CRs and VRs definitions for the top background in the (a) $e + b$ -jet and (b) $\mu + b$ -jet channel, respectively. The phase spaces of VR- $S(p_T^{\text{miss}})$ and SR-1L which select event with exactly one b -tagged jet are indicated as hatched boxes. The phase space SR-1L is only indicated in (b) as it overlaps with the phase space of CR/VR-T-high in (a) in the $m_{\ell j}$ - $S(p_T^{\text{miss}})$ plane. Grey vertical dashed lines indicate that a region is binned in $m_{\ell j}$.

validation of the background normalisations across $m_{\ell j}$, VR-W and VR-Z adopt the same $m_{\ell j}$ binning as SR-1L and SR-2L, respectively. If the expected number of events in a VR bin falls below approximately 10, the corresponding bin is made inclusive in $m_{\ell j}$ to ensure adequate event counts for validation.

The estimation strategy for the top background is adapted relative to that for the $V + \text{jets}$ processes, as its normalisation is found to depend on $m_{\ell j}$. The associated CR-T and VR-T regions select 1L events with two or more b -tagged jets, with the b -jet requirement ensuring orthogonality with the SRs. Both the $e + b$ -jet and $\mu + b$ -jet channels define a CR-T-high region at $m_{\ell j} > 900$ GeV to normalise top events in the high- $m_{\ell j}$ regime.

Since top-quark decays involving leptons yield genuine p_T^{miss} , CR-T-high- μb applies the same kinematic selections as SR-1L- μb but requires $S(p_T^{\text{miss}}) > 4.0$ to enhance the top fraction while suppressing signal contamination. Events with $3.0 < S(p_T^{\text{miss}}) < 4.0$ define VR-T-high- μb , which otherwise matches the CR selection and is binned in $m_{\ell j}$ for validation.

In contrast, CR-T-high- eb applies $S(p_T^{\text{miss}}) < 4.0$, i.e. an upper requirement on this variables similar as in the SRs, since the top normalisation also shows some dependence on $S(p_T^{\text{miss}})$ in the $e + \text{light-jet}$ channel. CR-T-high- eb extends up to $m_{\ell j} = 1300$ GeV, while higher- $m_{\ell j}$ events are covered by VR-T-high- eb , which otherwise mirrors the CR selection and is binned in $m_{\ell j}$.

The CR-W regions in both the $e + b$ -jet and $\mu + b$ -jet channels, which cover $m_{\ell j}$ values below 900 GeV, receive substantial contributions from top-quark backgrounds. To ensure proper normalisation of these events, dedicated CR-T-low regions are defined to normalise top events in the low- $m_{\ell j}$ regime. CR-T-low- eb adopts the same requirements as CR-W- eb , differing only in the b -jet multiplicity. CR-T-low- μb reflects the kinematic selections of SR-1L- μb but enforces $S(p_T^{\text{miss}}) > 4.0$. An illustration of the CRs and VRs definitions for the top background is shown in Figure 6.

A set of additional VRs is defined to test the robustness of the background normalisations when extrapolated over variables other than $m_{\ell j}$. The VR- $S(p_T^{\text{miss}})$ regions invert the $S(p_T^{\text{miss}})$ requirement of the corresponding CR-W selections to test the modelling of $W + \text{jets}$ at low $S(p_T^{\text{miss}})$. The extrapolation of the $Z + \text{jets}$ normalisation across $m_{\ell \ell}$ is validated with VR- $m_{\ell \ell}$. This validation region is defined only for the $e + \text{light-jet}$ channel, as the other three channels show significant signal contamination that precludes

its use. The $\mu + b$ -jet channel defines VR-T-low- μb , to validate the low- $m_{\ell j}$ top background normalisation across $\mathcal{S}(p_{\text{T}}^{\text{miss}})$ as the associated VR- $\mathcal{S}(p_{\text{T}}^{\text{miss}})$ receives a substantial contribution from this background.

7 Systematic uncertainties

While this search is predominantly limited by statistical constraints, experimental, theory, and modelling uncertainties have non-negligible contributions to the total uncertainty. These systematic effects are quantified and incorporated into the statistical model (see Section 8), with their key components detailed below. The overall effect of systematic uncertainties in the LQ mass sensitivity reach is found to be below 5%.

Figure 7 shows a decomposition into individual categories of the systematic uncertainties in the total SM predictions for the SRs in Run 2 of each channel, with a similar breakdown observed for the corresponding Run 3 regions. This decomposition is obtained by performing a series of fits in which the parameters associated with a given category are fixed to their best-fit values and held constant, effectively removing their contribution from the systematic model. The systematic uncertainty attributed to each category is then computed as the quadratic difference between the total background uncertainty in the nominal fit and that in the fit with the category fixed [82].

A detailed evaluation of detector-related systematic uncertainties is performed. These include uncertainties in lepton performance, covering trigger, reconstruction, identification, and isolation efficiencies for electrons [83] and muons [71], along with momentum calibration uncertainties for both lepton species. Jet energy calibration uncertainties are also considered, including those in the jet energy scale (JES) and jet energy resolution (JER) [76]. Additional jet-related uncertainties arise from efficiency corrections applied to pile-up jet tagging [77] and b -jet identification [84–86]. Missing transverse momentum uncertainties originate from the propagation of JES and JER uncertainties to the $p_{\text{T}}^{\text{miss}}$ calculation, supplemented by uncertainties related to tracks associated with the primary vertex but unmatched to reconstructed objects [79]. The uncertainties in the combined 2015–2018 and 2022–2023 integrated luminosities are 0.83% [87] and 2.0% [88, 89], respectively, obtained using the LUCID-2 detector [90] for the primary luminosity measurements, complemented by measurements using the inner detector and calorimeters. Additionally, a dedicated uncertainty accounts for discrepancies between data and simulation in pile-up profile modelling.

The treatment of FNP background employs distinct strategies across analysis channels. Simulated samples directly model these backgrounds in the $\mu + \text{jet}$ and $2e$ electron channels, with a conservative 80% normalisation uncertainty applied to account for potential mismodelling. In the $1e$ selections of the $e + \text{light-jet}$ and $e + b\text{-jet}$ channels, systematic uncertainties associated with the data-driven FNP estimate (Section 6) are characterised through multiple dedicated studies. The dominant uncertainty originates from the subtraction of the prompt-lepton contamination in the loose and tight electron samples, originating in particular from $W + \text{jets}$ events. Therefore, $\pm 15\%$ variations in the MC-derived real lepton fractions are propagated through the fake-factor calculation, with the variation magnitude chosen to cover the size of the $W + \text{jets}$ normalisation factors observed in the $e + \text{light-jet}$ channel, see Section 8. To account for the reduced binning granularity in p_{T} for central electrons with $p_{\text{T}} > 800$ GeV in the fake-factor measurements, an additional 70% uncertainty, based on the p_{T} dependence of the fake factors observed in MC simulation, is assigned on the FNP estimate from such electrons. A non-negligible dependence of the fake factors on $\Delta R(\ell, j)$ is observed. Comparing fake factors from MC simulation from events with $\Delta R(\ell, j)$ smaller and larger than 3.7, results in uncertainties of 50% ($p_{\text{T}} < 200$ GeV) and 25% ($p_{\text{T}} > 200$ GeV), respectively.

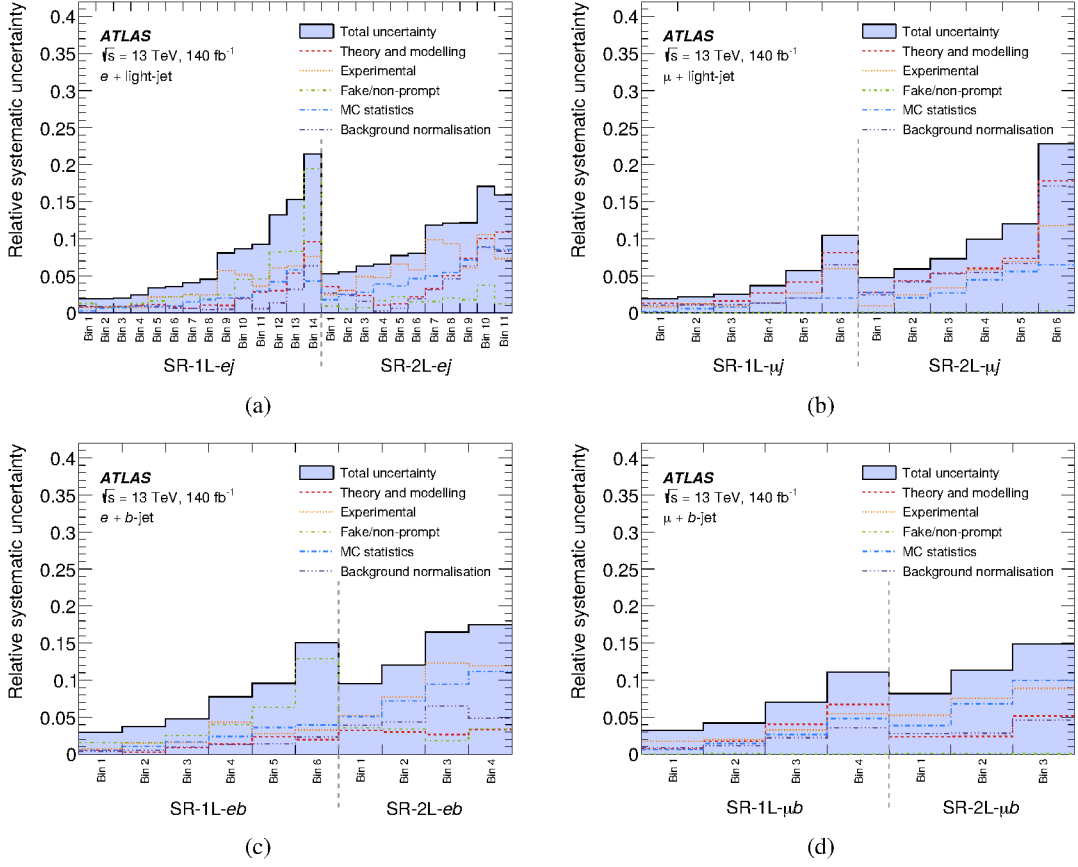


Figure 7: Relative systematic uncertainties in the post-fit SM background estimates in the (a) $e + \text{light-jet}$, (b) $\mu + \text{light-jet}$, (c) $e + b\text{-jet}$ and (d) $\mu + b\text{-jet}$ channels obtained from a background-only fit to the respective CRs and SRs. The “Fake/non-prompt” category reflects uncertainties impacting the FNP background estimate. Uncertainties originating from the limited size of the MC samples used to model the irreducible background contributions are contained in the “MC statistics” category. The “Background normalisation” category reflects uncertainty in normalisation factors for the $W + \text{jets}$, $Z + \text{jets}$ and top backgrounds extracted from the respective CR- W , CR- Z and CR- T regions. The “Theory and modelling” category includes the different sources of theory modelling uncertainties for the $W + \text{jets}$, $Z + \text{jets}$ and top backgrounds. The “Experimental” category covers detector related uncertainties from the reconstruction and selection of objects in the analysis. The individual uncertainties are correlated and do not necessarily add up in quadrature to the total uncertainty.

Differences between the FNP composition between the fake-factor measurement and application domains are evaluated using MC simulation and translated into an additional 50% uncertainty in the FNP estimate. Furthermore, potential $b\text{-jet}$ induced modifications to the fake factors were investigated through dedicated simulation studies comparing $b\text{-jet}$ enriched and depleted phase spaces in the $e + b\text{-jet}$ channel. The observed weak correlation between fake factor magnitudes and $b\text{-jet}$ presence was conservatively accommodated through an additional 25% uncertainty component in the FNP estimates derived for the $e + b\text{-jet}$ channel.

The background composition exhibits a strong channel dependence, with $W + \text{jets}$ production constituting the dominant contribution in SR-1L and $Z + \text{jets}$ prevailing in SR-2L. Systematic uncertainties in these $V + \text{jets}$ processes incorporate three principal components: variations of the QCD renormalisation μ_R and factorisation μ_F scales by a factor two evaluated through the envelope of seven $\mu_R - \mu_F$ combinations, PDF eigenvector variations using the NNPDF3.1 NNLO set, and α_S variations. Additional uncertainties are

applied to take into account electroweak corrections on the V + jets samples [91].

Top-quark backgrounds, while small in b -vetoed regions, are subleading contributions in the $e + b$ -jet and $\mu + b$ -jet channels. Their theory uncertainties mirror the V + jets framework in scale and PDF treatment, augmented by process-specific considerations including parton shower modelling differences quantified via PYTHIA 8.230 versus HERWIG 7.2.1 (for $t\bar{t}$) or HERWIG 7.1.6 (for single top) generator comparisons. Uncertainties associated with the level of initial- (ISR) and final-state radiation (FSR) are estimated by variations of α_S in the A14 tune [58] and variations of the renormalization scale for FSR branchings, respectively. The matrix element-parton shower interface uncertainty is assessed through a variation of the p_T^{hard} parameter that regulates how the radiation phase space of the parton shower is determined, following the prescription in Ref. [92]. Interference effects between $t\bar{t}$ and Wt processes are evaluated through diagram subtraction/removal scheme comparisons [93].

Similarly, uncertainties in the signal predictions from scale and PDF variations were evaluated using generator-level reweighting, focusing on $m_{\ell j}$ spectrum distortions in both the SR-1L and SR-2L regions. These uncertainties were found to have a negligible impact on the results and were therefore neglected.

As seen in Figure 7, the dominant sources of systematic uncertainties vary depending on the channel and signal region. In the SR-1L selections of the $e + \text{light-jet}$ and $e + b$ -jet channels, the leading uncertainty arises from the estimate of backgrounds with FNP electrons. Other major experimental uncertainties are associated with the jet energy scale and resolution, as well as the b -jet identification efficiency in the $e + b$ -jet and $\mu + b$ -jet channels. Among the modelling uncertainties, the most significant contributions come from QCD scale variations and electroweak corrections to the V + jets backgrounds.

8 Results

Observed data in the CRs, VRs, and SRs are compared with the SM predictions using a profile likelihood method [94]. The statistical model is constructed using the `cabinetry` [95] package, which interfaces with `pyhf` [96], a Python-based implementation of the `HISTFACTORY` [97] template. Parameters of interest, such as the signal strength, along with other floating parameters like normalisation factors, are determined via a maximum-likelihood fit to data. In each region, the expected event yield is modelled as the sum of contributions from the individual physics processes (samples). The predicted rate for each sample may depend on a set of free parameters ψ such as normalisation factors and the signal strength, and a set of constrained nuisance parameters θ , which encode the effect of systematic uncertainties.

The probability density function for bin b in region r is modelled as a Poisson distribution, $\text{Pois}(n_{rb} | \nu_{rb}(\psi, \theta))$, where n_{rb} is the observed number of events and $\nu_{rb}(\psi, \theta)$ is the predicted event yield. To account for systematic uncertainties, additional constraint terms are introduced, which control the allowed deviations of the nuisance parameters from their nominal values. These constraints are interpreted as auxiliary measurements, with associated global observables \mathbf{a} , such that the full set of observations is denoted by $\mathbf{x} = (\mathbf{n}, \mathbf{a})$, where $\mathbf{n} = n_{rb}$ represents the set of observed yields across all bins and regions. The full likelihood function is then constructed as the product of the Poisson likelihoods for each bin and region and the constraint terms for each nuisance parameter:

$$L(\mathbf{x} | \psi, \theta) = \prod_{r \in \text{regions}} \prod_{b \in \text{bins}} \text{Pois}(n_{rb} | \nu_{rb}(\psi, \theta)) \prod_{\theta \in \theta} f_{\theta}(a_{\theta} | \theta), \quad (1)$$

where $f_\theta(a_\theta | \theta)$ is the constraint term associated with nuisance parameter θ , typically modelled as a Gaussian distribution centred on the nominal value with a width reflecting the corresponding uncertainty.

Different fit configurations are employed to derive the results presented below. All fits are performed independently for each channel and for the validation of the FNP background estimate, and generally also individually for the Run 2 and Run 3 datasets.

The first configuration, referred to as *CR-only fit*, is a background-only fit to the CR-W and CR-Z regions to validate the background estimates by extracting normalisation factors μ_W and μ_Z for the W +jets and Z +jets backgrounds, respectively. In the e + b -jet and μ + b -jet channels, the CR-T-low and CR-T-high regions are additionally included to extract normalisation factors $\mu_{\text{top}}^{\text{low-}m_{\ell j}}$ and $\mu_{\text{top}}^{\text{high-}m_{\ell j}}$ for top backgrounds in the low- and high- $m_{\ell j}$ regimes, respectively. The results of the CR-only fit are extrapolated to the corresponding VRs to compare the post-fit SM predictions with the observed data. For the validation of the FNP estimate, a separate CR-only fit is performed using only the CR-W-fake region to derive predictions in VR-fake, see Section 6 This CR is not included in any other fit.

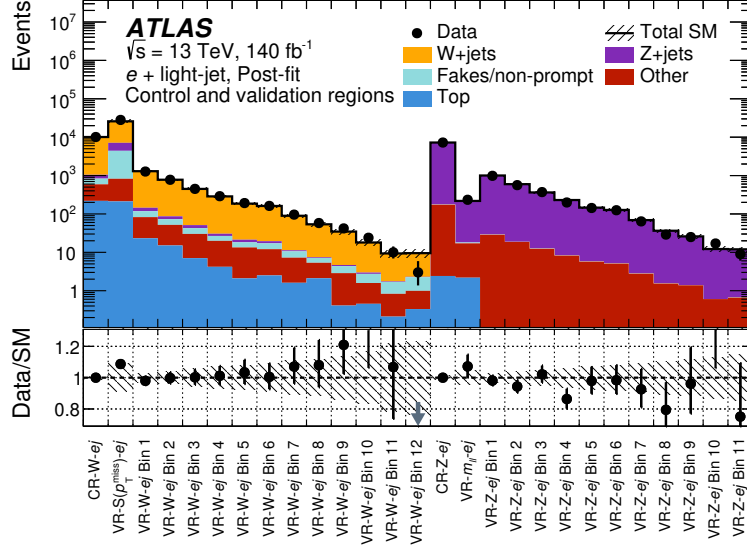
The second configuration, referred to as *CR+SR fit*, simultaneously fits the $m_{\ell j}$ distributions in SR-1L and SR-2L along with the associated CRs. This configuration probes for potential BSM contributions while constraining the background components, and is also used to evaluate the compatibility of the observed data with specific signal hypotheses. The normalisation factors derived in this configuration are found to be compatible with the ones from a CR-only fit.

A third configuration, the *Run 2+3 combination*, maximizes sensitivity to a given signal model by fitting the $m_{\ell j}$ spectra in the SRs of both Run 2 and Run 3 simultaneously. In this configuration, all CRs and SRs from both data-taking periods are included, with independent normalisation factors for the backgrounds in Run 2 and Run 3. All nuisance parameters are treated as uncorrelated between the two data-taking periods, except for most of the JES and JER variations, which are derived from a shared set of in situ calibrations. Treating all nuisance parameters as fully correlated between Run 2 and Run 3 was not found to have a notable impact on the final sensitivity reach of the search.

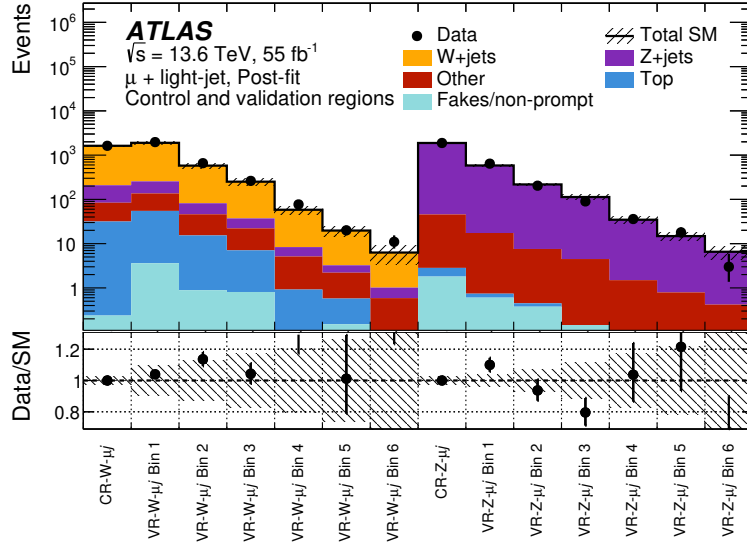
8.1 Results for control and validation regions

The agreement between observed data and SM predictions in the e +light-jet VRs after a fit to CR-W- $e j$ and CR-Z- $e j$ for Run 2 is shown in Figure 8(a). Overall, the data are consistent with the SM predictions within the associated uncertainties. A notable deficit is observed in the last bin of VR-W- $e j$ in Run 2, which is not reproduced in the corresponding Run 3 region and is therefore attributed to a statistical fluctuation. Overall, the observations support the robustness of the W +jets and Z +jets normalisation extrapolation over $m_{\ell j}$.

Similar conclusions are drawn from the CR-only fit results in the VRs of the μ +light-jet, e + b -jet, and μ + b -jet channels. As an example, the Run 3 VR results for the μ +light-jet channel are shown in Figure 8(b), while Figure 9 presents the corresponding VRs for the e + b -jet and μ + b -jet channels. The data generally agree with the SM predictions within uncertainties, and no consistent mis-modelling is observed between Run 2 and Run 3. Table 8 reports the extracted normalisation factors for all channels.

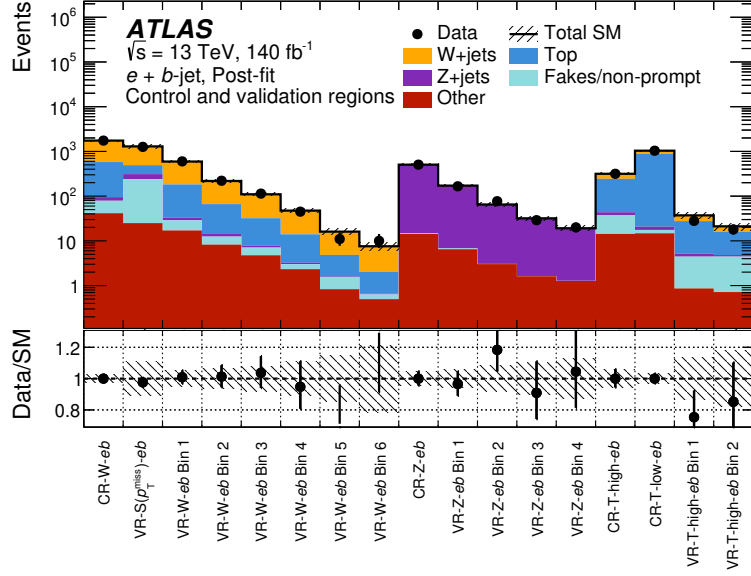


(a)

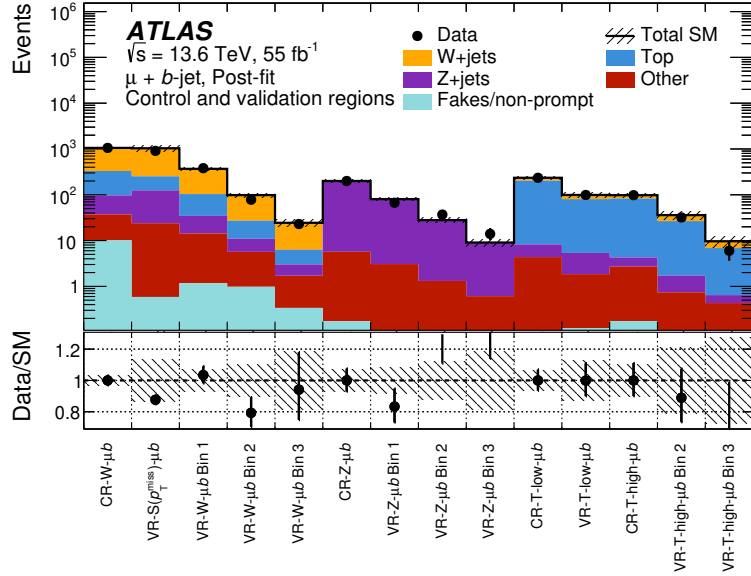


(b)

Figure 8: Data (dots) and post-fit SM predictions (histograms) in the VRs for (a) Run 2 of the $e + \text{light-jet}$ and (b) Run 3 of the $\mu + \text{light-jet}$ channels obtained by a CR-only fit. The lower panel shows the ratio of observed data to the total post-fit SM prediction. Uncertainties in the background estimates include both the statistical and systematic uncertainties, with correlations between uncertainties taken into account. A grey arrow in the lower panel indicates a data point outside the vertical range shown.



(a)



(b)

Figure 9: Data (dots) and post-fit SM predictions (histograms) in the VRs for (a) Run 2 of the $e + b$ -jet and (b) Run 3 of the $\mu + b$ -jet channels obtained by a CR-only fit. The lower panel shows the ratio of observed data to the total post-fit SM prediction. Uncertainties in the background estimates include both the statistical and systematic uncertainties, with correlations between uncertainties taken into account.

Table 8: Normalisation factors μ_W , μ_Z , $\mu_{\text{top}}^{\text{high-}m_{\ell j}}$ and $\mu_{\text{top}}^{\text{low-}m_{\ell j}}$ for the W +jets, Z +jets and top backgrounds, respectively, extracted from CR-only fits using the respective CRs of each channel. The associated uncertainties include all statistical and systematic contributions.

Norm. factor	e + light-jet		μ + light-jet		e + b -jet		μ + b -jet	
	Run 2	Run 3	Run 2	Run 3	Run 2	Run 3	Run 2	Run 3
μ_W	1.08 ± 0.21	1.13 ± 0.25	1.04 ± 0.18	1.05 ± 0.21	1.21 ± 0.28	1.22 ± 0.33	1.24 ± 0.27	1.24 ± 0.31
μ_Z	1.14 ± 0.25	1.20 ± 0.23	1.08 ± 0.20	1.20 ± 0.22	1.24 ± 0.28	1.19 ± 0.26	1.11 ± 0.23	1.31 ± 0.29
$\mu_{\text{top}}^{\text{high-}m_{\ell j}}$	–	–	–	–	0.74 ± 0.17	0.79 ± 0.26	0.55 ± 0.13	0.71 ± 0.27
$\mu_{\text{top}}^{\text{low-}m_{\ell j}}$	–	–	–	–	0.75 ± 0.12	0.77 ± 0.23	0.71 ± 0.12	0.69 ± 0.21

8.2 Results for signal regions

The observed and predicted $m_{\ell j}$ distributions in SR-1L- $e j$ and SR-2L- $e j$ of the e + light-jet channel for Run 2 and Run 3 are shown in Figure 10. The SM predictions agree well with the data within their uncertainties, and no significant excess of events is observed. Among the selections, SR-2L provides the strongest sensitivity to the LQ signals of interest due to its much higher signal to background ratio, as illustrated by the overlaid nominal predictions of two example signal models in Figure 10.

Figure 11 presents the results of SR-1L- μj and SR-2L- μj of the μ + light-jet channel for both Run 2 and Run 3. The data agree well with the SM predictions within uncertainties in the SR-1L- μj regions. Deficits of approximately 50% are observed in the last two bins of SR-2L- μj in Run 2, although compatible with the predictions within uncertainties.

The results of SR-1L- eb and SR-2L- eb of the e + b -jet channel for both data-taking periods are shown in Figure 12, while Figure 13 presents the corresponding SRs, SR-1L- eb and SR-2L- eb , of the μ + b -jet channel. In both channels no significant excesses are observed and the SM predictions generally agree with the data within uncertainties.

To quantitatively probe the observed $m_{\ell j}$ spectra in each channel for a new-physics signal, the p_0 value of the background-only hypothesis is evaluated relative to each signal model and translated into a discovery significance. No deviations above the 1σ level are observed in any channel.

8.3 Interpretations

In the absence of any significant indications for new-physics contributions in the SRs, the observations are interpreted as constraints on minimal LQ production models featuring \tilde{S}_1 with either y_{de} , $y_{s\mu}$, y_{be} , or $y_{b\mu}$ couplings as benchmark scenarios. To evaluate the compatibility of the observed data with a given \tilde{S}_1 model, a combined fit to the Run-2 and Run-3 datasets is performed, effectively fitting the $m_{\ell j}$ spectra from both data-taking periods simultaneously. In these fits, the signal strength is a free parameter and coherently scales the nominal signal predictions across all regions, accounting for the difference of the \tilde{S}_1 production cross-sections between Run 2 and Run 3. The CL_s prescription [98] is used to perform hypothesis tests and set exclusion limits at 95% confidence level (CL), employing the asymptotic approximation [94] for the calculation of the CL_s values. The results were cross-checked using pseudo experiments and found to agree within 10%. In each channel the constraints are dominated by the Run-2 results due to the larger

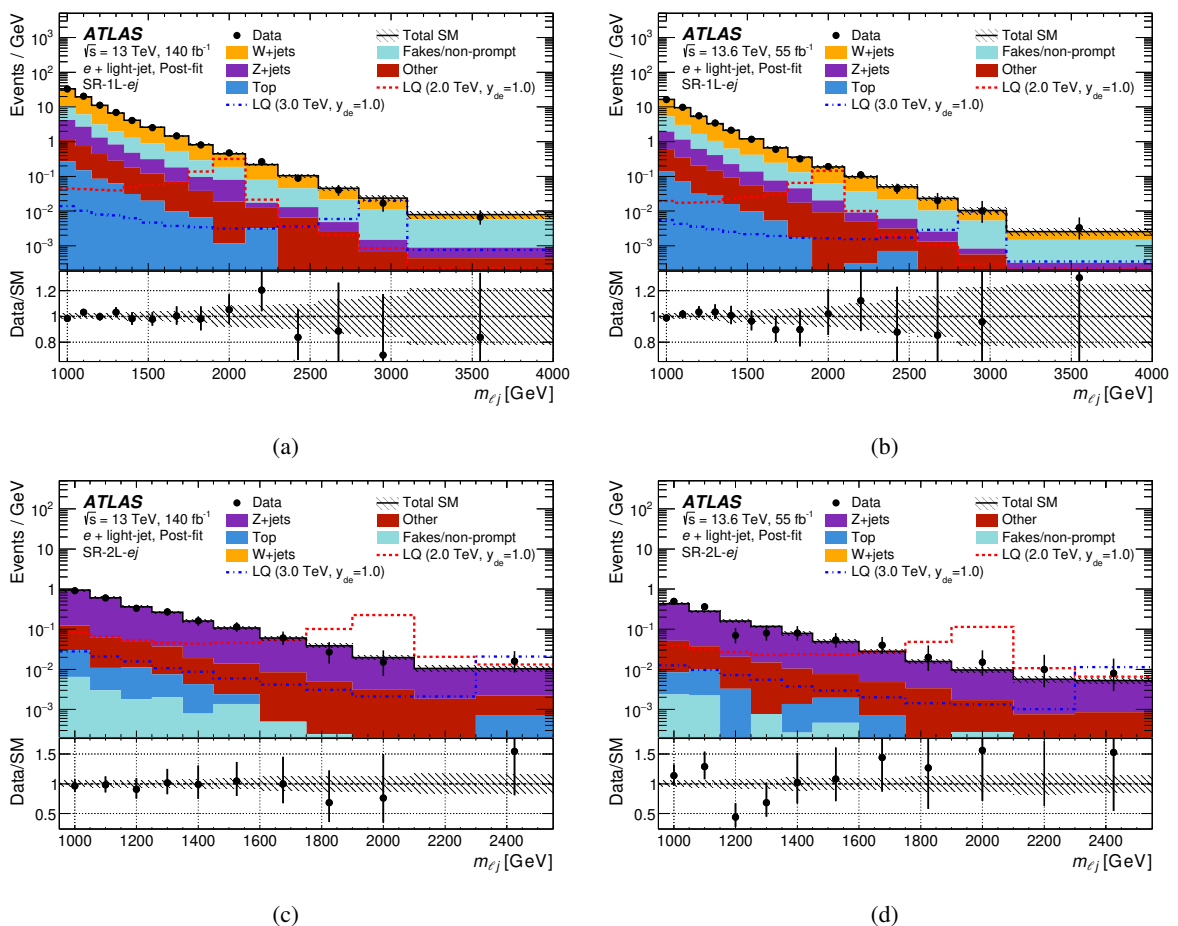


Figure 10: Data (dots) and post-fit SM distribution (histograms) of $m_{\ell j}$ in (a, b) SR-1L- $e j$ and (c, d) SR-2L- $e j$ of the $e + \text{light-jet}$ channel obtained by a CR+SR background-only fit for Run 2 and Run 3, respectively. The lower panel shows the ratio of observed data to the total post-fit SM prediction. The last bin includes the overflow. Uncertainties in the background estimates include both the statistical and systematic uncertainties, with correlations between uncertainties taken into account. The dashed lines show the predicted yields for two benchmark signal models corresponding to $\tilde{S}_1(m, y_{de}) = (2.0 \text{ TeV}, 1.0)$ and $\tilde{S}_1(m, y_{de}) = (3.0 \text{ TeV}, 1.0)$, respectively.

dataset size and the SR-2L regions which are significantly more sensitive to the signal of interest than their respective SR-1L counterparts.

Figure 14 shows the observed and expected exclusion limits for the $e + \text{light-jet}$ channel. The contours are presented in the $m(\tilde{S}_1)$ - y_{de} plane, with couplings ranging from 0.1 to 1.0. In this minimal LQ model, \tilde{S}_1 masses up to approximately 3.4 TeV are excluded for a coupling value of $y_{de} = 1.0$. For couplings larger than roughly 0.25, this search surpasses the limits set by a previous ATLAS search for LQ pair production [13], which are independent of the coupling strength. Strong indirect constraints on y_{de} arise from weak charge measurements of protons and nuclei [10], which impose $y_{de} \leq 0.17 \frac{m(S)}{[\text{TeV}]}$, where $m(S)$ denotes the scalar LQ mass. The results from this search exceed those limits in a small region of parameter space below approximately 2.3 TeV. Although the weak charge constraints dominate across most of the parameter space, they may be relaxed or even vanish in scenarios with more than one LQ present in the mass range of interest [99], rendering the constraints from this search complementary.

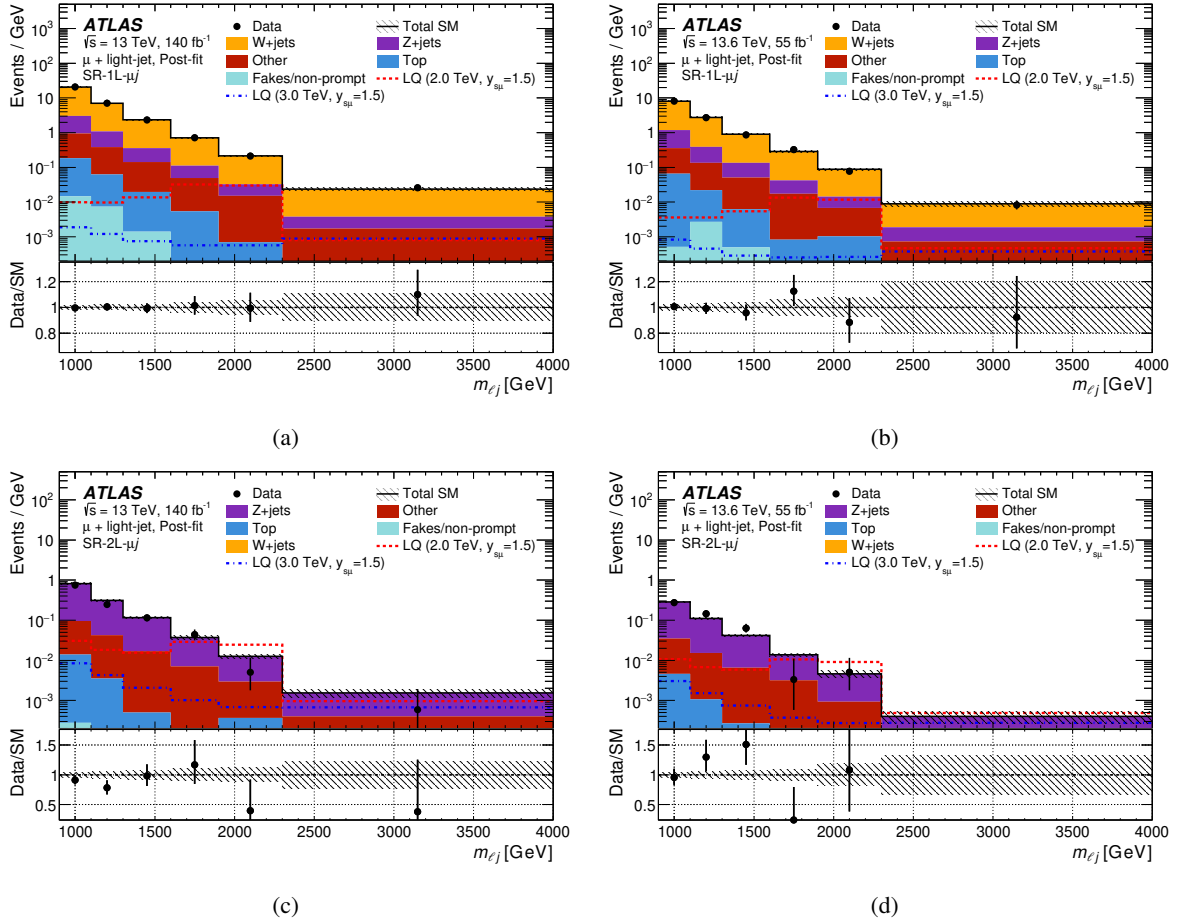


Figure 11: Data (dots) and post-fit SM distribution (histograms) of $m_{\ell j}$ in (a, b) SR-1L- μj and (c, d) SR-2L- μj of the $\mu + \text{light-jet}$ channel obtained by a CR+SR background-only fit for Run 2 and Run 3, respectively. The lower panel shows the ratio of observed data to the total post-fit SM prediction. The last bin includes the overflow. Uncertainties in the background estimates include both the statistical and systematic uncertainties, with correlations between uncertainties taken into account. The dashed lines show the predicted yields for two benchmark signal models corresponding to $\tilde{S}_1(m, y_{S\mu}) = (2.0 \text{ TeV}, 1.5)$ and $\tilde{S}_1(m, y_{S\mu}) = (3.0 \text{ TeV}, 1.5)$, respectively.

The observed and expected exclusion contours for the $\mu + \text{light-jet}$ channel are shown in Figure 15. The deficits observed in the highest $m_{\ell j}$ bins of SR-2L- μj for Run 2 shift the observed limits beyond the 1σ uncertainty band, though they are found to remain well within the 2σ band. \tilde{S}_1 masses up to approximately 4.3 TeV are excluded assuming coupling values of 3.5.

Figure 16 shows the observed and expected exclusion limits for the $e + b\text{-jet}$ channel. The derived constraints on the \tilde{S}_1 mass depend again on the coupling and range up to 3.1 TeV for $y_{be} = 3.5$. The mild excess observed in the third $m_{\ell j}$ bin of SR-2L- eb in Run 2 slightly weakens the observed limit relative to the expected one for masses below approximately 2 TeV.

Exclusion contours for the $\mu + b\text{-jet}$ channel are presented in Figure 17 where constraints on the \tilde{S}_1 mass extend up to 2.8 TeV at couplings of 3.5.

In summary, all channels improve upon existing ATLAS constraints for scalar LQ models at large coupling values—approximately above 0.25 in the $e + \text{light-jet}$ channel, above 0.7 in the $\mu + \text{light-jet}$ channel and

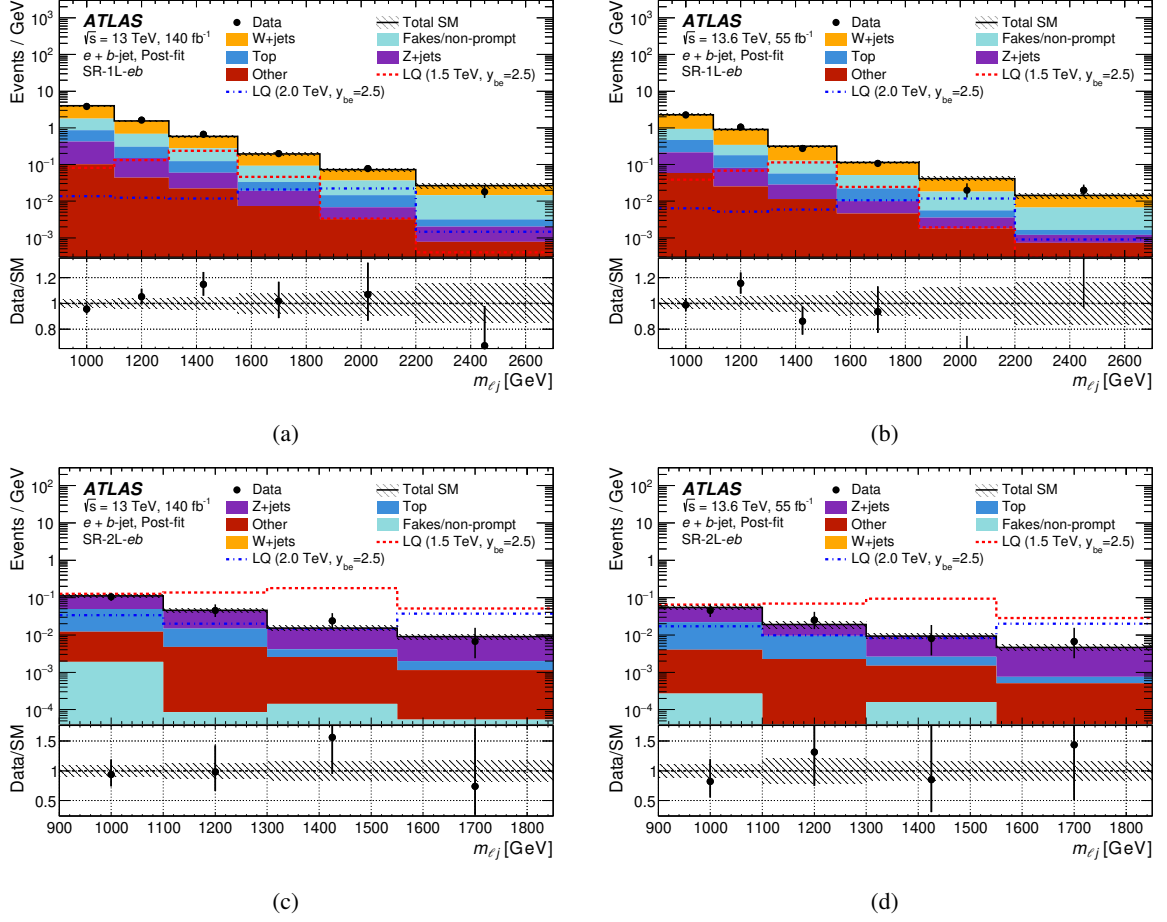


Figure 12: Data (dots) and post-fit SM distribution (histograms) of $m_{\ell j}$ in (a, b) SR-1L- eb and (c, d) SR-2L- eb of the $e + b$ -jet channel obtained by a CR+SR background-only fit for Run 2 and Run 3, respectively. The lower panel shows the ratio of observed data to the total post-fit SM prediction. The last bin includes the overflow. Uncertainties in the background estimates include both the statistical and systematic uncertainties, with correlations between uncertainties taken into account. The dashed lines show the predicted yields for two benchmark signal models corresponding to $\tilde{S}_1(m, y_{be}) = (1.5 \text{ TeV}, 2.5)$ and $\tilde{S}_1(m, y_{be}) = (2.0 \text{ TeV}, 2.5)$, respectively.

above 1.0 in the other channels. At lower couplings, the LQ pair production searches remain more sensitive due to their independence from the LQ coupling strength.

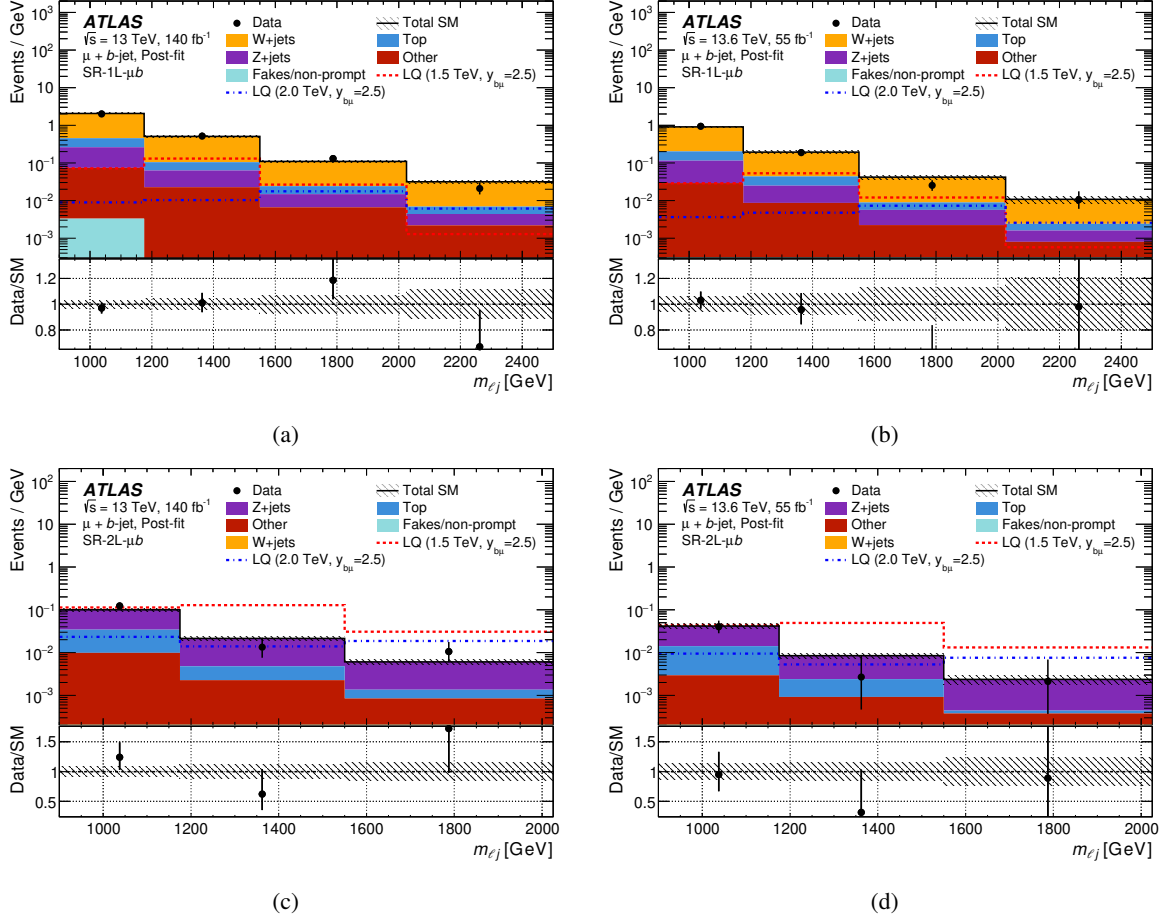


Figure 13: Data (dots) and post-fit SM distribution (histograms) of $m_{\ell j}$ in (a, b) SR-1L- μb and (c, d) SR-2L- μb of the $\mu + b$ -jet channel obtained by a CR+SR background-only fit for Run 2 and Run 3, respectively. The lower panel shows the ratio of observed data to the total post-fit SM prediction. The last bin includes the overflow. Uncertainties in the background estimates include both the statistical and systematic uncertainties, with correlations between uncertainties taken into account. The dashed lines show the predicted yields for two benchmark signal models corresponding to $\tilde{S}_1(m, y_{b\mu}) = (1.5 \text{ TeV}, 1.5)$ and $\tilde{S}_1(m, y_{b\mu}) = (2.0 \text{ TeV}, 1.5)$, respectively.

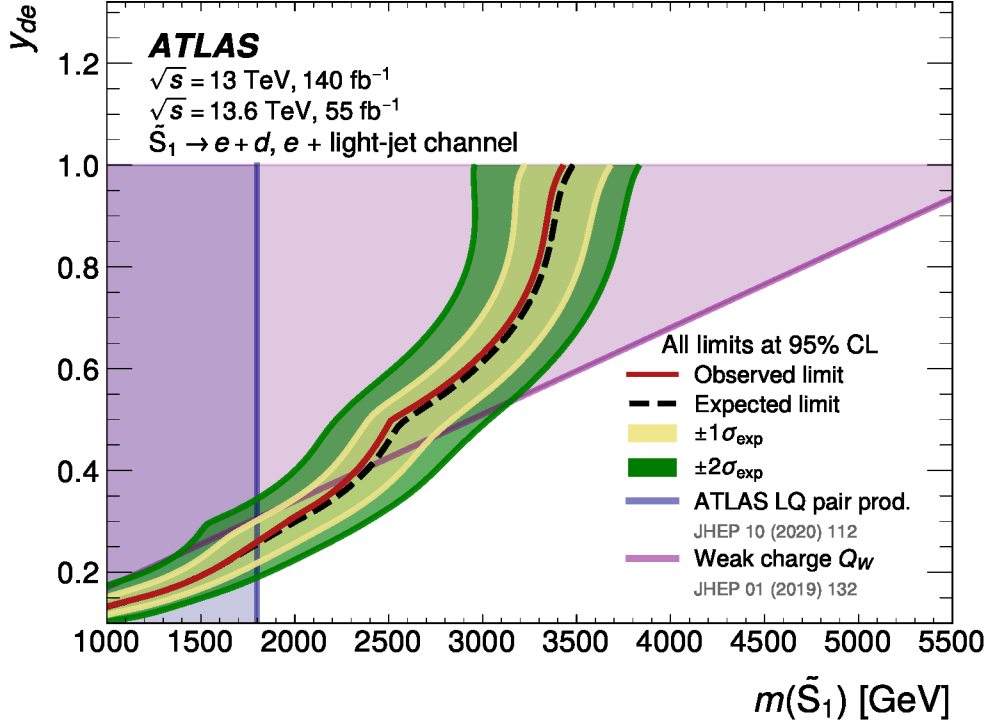


Figure 14: Exclusion limits for minimal models of \tilde{S}_1 production with only y_{de} being non-zero obtained from a simultaneous fit to SR-1L and SR-2L of the $e + \text{light-jet}$ channel combining Run-2 and Run-3 data. All limits are computed at 95% CL and the observed (red solid lines) and expected (black dashed lines) exclusion limits are shown in the $m(\tilde{S}_1) - y_{de}$ plane. The observed exclusion should be interpreted as the region above the red line. The yellow inner (green outer) shaded band around the expected limits corresponds to the $\pm 1\sigma$ ($\pm 2\sigma$) variations of the expected limit, accounting for all uncertainties. The observed limit obtained from ATLAS searches for LQ pair production is also shown as dark blue line [13]. Constraints from weak charge measurements of protons and nuclei on y_{de} couplings derived by Ref. [10] are shown as light magenta line.

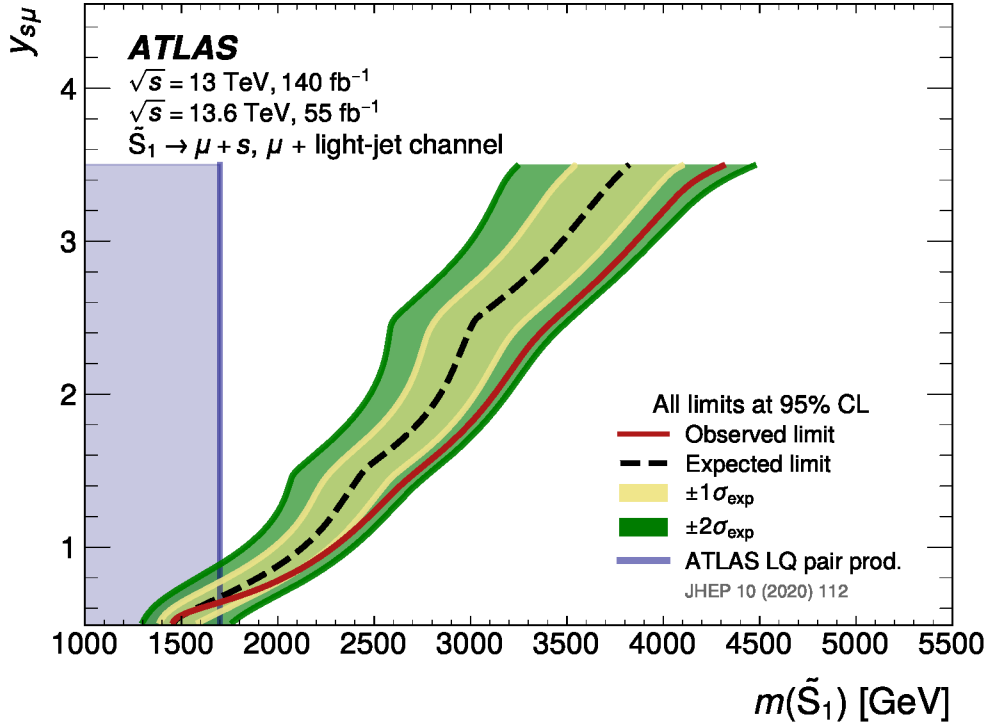


Figure 15: Exclusion limits for minimal models of \tilde{S}_1 production with only $y_{s\mu}$ being non-zero obtained from a simultaneous fit to SR-1L and SR-2L of the $\mu + \text{light-jet}$ channel combining Run-2 and Run-3 data. All limits are computed at 95% CL and the observed (red solid lines) and expected (black dashed lines) exclusion limits are shown in the $m(\tilde{S}_1) - y_{s\mu}$ plane. The observed exclusion should be interpreted as the region above the red line. The yellow inner (green outer) shaded band around the expected limits corresponds to the $\pm 1\sigma$ ($\pm 2\sigma$) variations of the expected limit, accounting for all uncertainties. The observed limit obtained from ATLAS searches for LQ pair production is also shown as dark blue line [13].

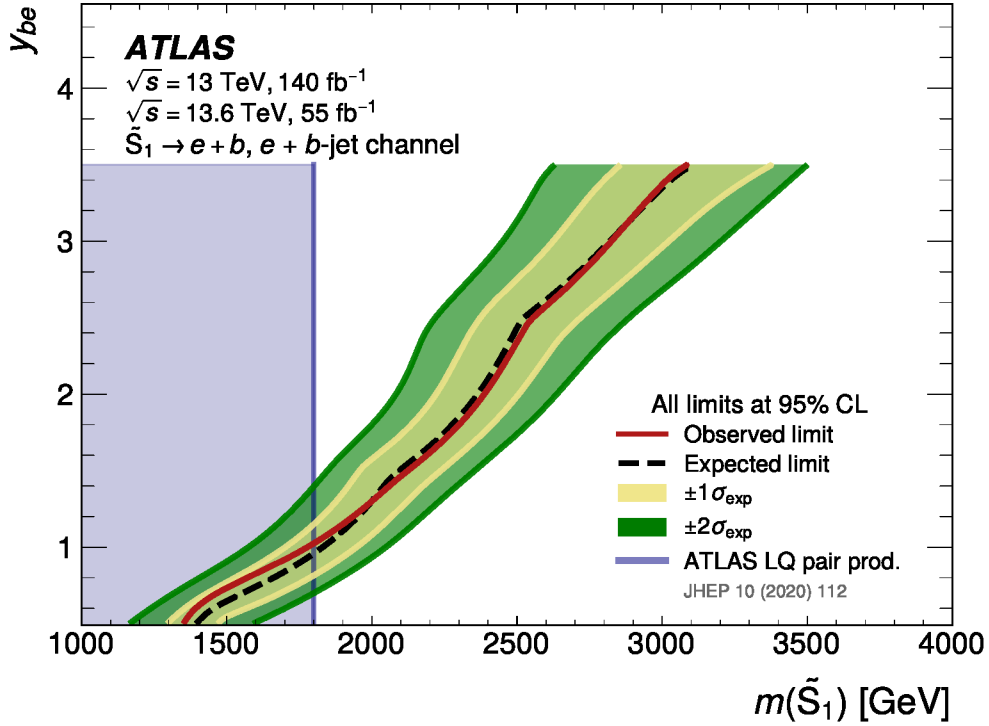


Figure 16: Exclusion limits for minimal models of \tilde{S}_1 production with only y_{be} being non-zero obtained from a simultaneous fit to SR-1L and SR-2L of the $e + b$ -jet channel combining Run-2 and Run-3 data. All limits are computed at 95% CL and the observed (red solid lines) and expected (black dashed lines) exclusion limits are shown in the $m(\tilde{S}_1) - y_{be}$ plane. The observed exclusion should be interpreted as the region above the red line. The yellow inner (green outer) shaded band around the expected limits corresponds to the $\pm 1\sigma$ ($\pm 2\sigma$) variations of the expected limit, accounting for all uncertainties. The observed limit obtained from ATLAS searches for LQ pair production is also shown as dark blue line [13].

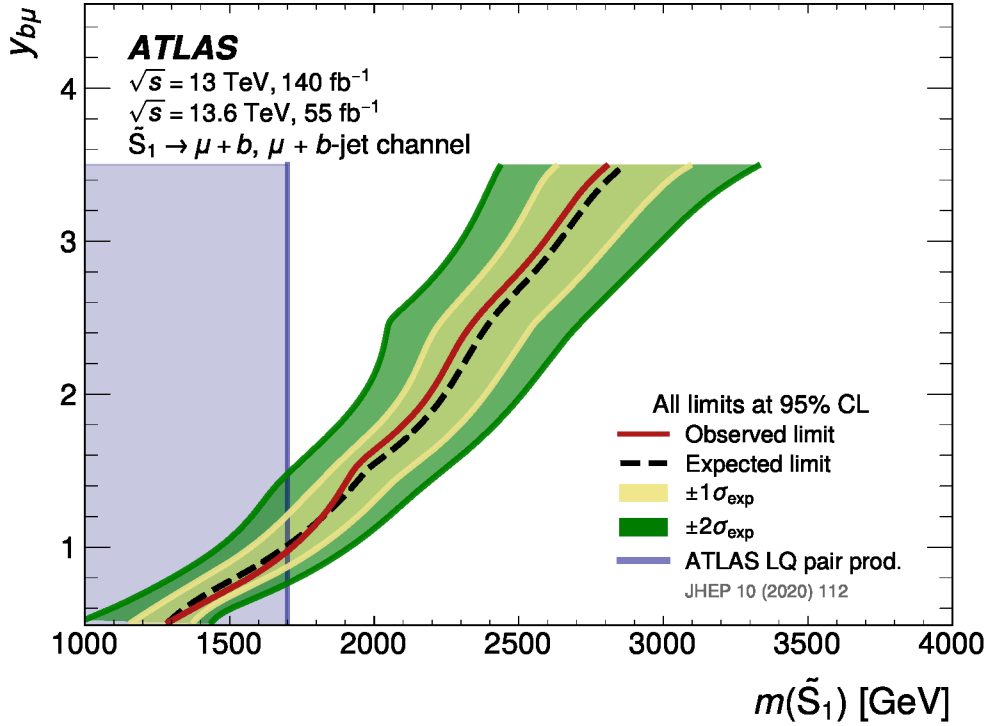


Figure 17: Exclusion limits for minimal models of \tilde{S}_1 production with only $y_{b\mu}$ being non-zero obtained from a simultaneous fit to SR-1L and SR-2L of the $\mu + b$ -jet channel combining Run-2 and Run-3 data. All limits are computed at 95% CL and the observed (red solid lines) and expected (black dashed lines) exclusion limits are shown in the $m(\tilde{S}_1) - y_{b\mu}$ plane. The observed exclusion should be interpreted as the region above the red line. The yellow inner (green outer) shaded band around the expected limits corresponds to the $\pm 1\sigma$ ($\pm 2\sigma$) variations of the expected limit, accounting for all uncertainties. The observed limit obtained from ATLAS searches for LQ pair production is also shown as dark blue line [13].

9 Conclusion

This paper reports a search for resonantly produced LQs using proton–proton collision data from the full Run-2 (2015–2018) and partial Run-3 (2022–2023) datasets at the LHC. The analysis probes the s -channel production of LQs, which exploits the lepton content of the proton to yield a distinctive lepton+jet final state. The signal topology features a narrow $m_{\ell j}$ peak near the LQ mass, and the inclusion of 2-lepton+jet final states—motivated by NLO contributions to resonant LQ production—is crucial for maximizing the analysis sensitivity as it also provides acceptance for additional LQ production modes beyond the lepton- and photon-induced processes.

Four orthogonal channels— e + light-jet, μ + light-jet, e + b -jet, and μ + b -jet—are analysed, each with individually optimised SRs binned in $m_{\ell j}$ to maximize coverage across a broad range of LQ masses. Dominant SM backgrounds, including W +jets and Z +jets, are constrained through dedicated CRs at low $m_{\ell j}$, with extrapolations validated in VRs. For b -jet channels, the top background is further controlled using two CRs spanning distinct kinematic regimes of $m_{\ell j}$, addressing observed dependencies in top processes modelling.

No significant excesses beyond SM predictions are observed in any of the SRs. The results are interpreted within a minimal \tilde{S}_1 -model framework, where only a single LQ coupling is non-zero. Combining Run-2 and partial Run-3 data, the analysis achieves stringent exclusion limits on LQ masses: for electron+jet channels (e + light-jet and e + b -jet), LQ masses below 3.4 TeV (coupling $y_{de} = 1.0$) and 3.1 TeV ($y_{be} = 3.5$) are excluded at 95% CL. For muon+jet channels (μ + light-jet and μ + b -jet), exclusion reaches extend to 4.3 TeV ($y_{s\mu} = 3.5$) and 2.8 TeV ($y_{b\mu} = 3.5$), respectively. These limits surpass those from previous ATLAS searches for LQ pair production for sufficiently large couplings ($y_{de} \gtrsim 0.25, y_{s\mu} \gtrsim 0.7, y_{be, b\mu} \gtrsim 1.0$). By establishing robust exclusion limits for LQ masses and couplings beyond the reach of pair-production searches, this work underscores the critical role of resonant production as a complementary probe of TeV-scale LQ scenarios. The results also highlight the potential of early Run-3 data to constrain exotic physics, paving the way for future high-luminosity LHC analyses to explore uncharted parameter space in LQ models.

Acknowledgements

We thank CERN for the very successful operation of the LHC and its injectors, as well as the support staff at CERN and at our institutions worldwide without whom ATLAS could not be operated efficiently.

The crucial computing support from all WLCG partners is acknowledged gratefully, in particular from CERN, the ATLAS Tier-1 facilities at TRIUMF/SFU (Canada), NDGF (Denmark, Norway, Sweden), CC-IN2P3 (France), KIT/GridKA (Germany), INFN-CNAF (Italy), NL-T1 (Netherlands), PIC (Spain), RAL (UK) and BNL (USA), the Tier-2 facilities worldwide and large non-WLCG resource providers. Major contributors of computing resources are listed in Ref. [100].

We gratefully acknowledge the support of ANPCyT, Argentina; YerPhI, Armenia; ARC, Australia; BMWFW and FWF, Austria; ANAS, Azerbaijan; CNPq and FAPESP, Brazil; NSERC, NRC and CFI, Canada; CERN; ANID, Chile; CAS, MOST and NSFC, China; Minciencias, Colombia; MEYS CR, Czech Republic; DNRf and DNSRC, Denmark; IN2P3-CNRS and CEA-DRF/IRFU, France; SRNSFG, Georgia; BMFTR, HGF and MPG, Germany; GSRI, Greece; RGC and Hong Kong SAR, China; ICHEP and Academy of Sciences and Humanities, Israel; INFN, Italy; MEXT and JSPS, Japan; CNRST, Morocco; NWO, Netherlands;

RCN, Norway; MNiSW, Poland; FCT, Portugal; MNE/IFA, Romania; MSTDI, Serbia; MSSR, Slovakia; ARIS and MVZI, Slovenia; DSI/NRF, South Africa; MICIU/AEI, Spain; SRC and Wallenberg Foundation, Sweden; SERI, SNSF and Cantons of Bern and Geneva, Switzerland; NSTC, Taipei; TENMAK, Türkiye; STFC/UKRI, United Kingdom; DOE and NSF, United States of America.

Individual groups and members have received support from BCKDF, CANARIE, CRC and DRAC, Canada; CERN-CZ, FORTE and PRIMUS, Czech Republic; COST, ERC, ERDF, Horizon 2020, ICSC-NextGenerationEU and Marie Skłodowska-Curie Actions, European Union; Investissements d’Avenir Labex, Investissements d’Avenir Idex and ANR, France; DFG and AvH Foundation, Germany; Herakleitos, Thales and Aristeia programmes co-financed by EU-ESF and the Greek NSRF, Greece; BSF-NSF and MINERVA, Israel; NCN and NAWA, Poland; La Caixa Banking Foundation, CERCA Programme Generalitat de Catalunya and PROMETEO and GenT Programmes Generalitat Valenciana, Spain; Göran Gustafssons Stiftelse, Sweden; The Royal Society and Leverhulme Trust, United Kingdom.

In addition, individual members wish to acknowledge support from CERN: European Organization for Nuclear Research (CERN DOCT); Chile: Agencia Nacional de Investigación y Desarrollo (FONDECYT 1230812, FONDECYT 1240864); China: Chinese Ministry of Science and Technology (MOST-2023YFA1605700, MOST-2023YFA1609300), National Natural Science Foundation of China (NSFC - 12175119, NSFC 12275265); Czech Republic: Czech Science Foundation (GACR - 24-11373S), Ministry of Education Youth and Sports (ERC-CZ-LL2327, FORTE CZ.02.01.01/00/22_008/0004632), PRIMUS Research Programme (PRIMUS/21/SCI/017); EU: H2020 European Research Council (ERC - 101002463); European Union: European Research Council (BARD No. 101116429, ERC - 948254, ERC 101089007), European Regional Development Fund (SMASH COFUND 101081355, SLO ERDF), Horizon 2020 Framework Programme (MUCCA - CHIST-ERA-19-XAI-00), European Union, Future Artificial Intelligence Research (FAIR-NextGenerationEU PE00000013), Italian Center for High Performance Computing, Big Data and Quantum Computing (ICSC, NextGenerationEU); France: Agence Nationale de la Recherche (ANR-21-CE31-0022, ANR-22-EDIR-0002); Germany: Baden-Württemberg Stiftung (BW Stiftung-Postdoc Eliteprogramme), Deutsche Forschungsgemeinschaft (DFG - 469666862, DFG - CR 312/5-2); China: Research Grants Council (GRF); Italy: Istituto Nazionale di Fisica Nucleare (ICSC, NextGenerationEU), Ministero dell’Università e della Ricerca (NextGeneration PRIN I53D23001490006, NextGenEU I53D23000820006 M4C2.1.1, SOE2024_0000023); Japan: Japan Society for the Promotion of Science (JSPS KAKENHI JP22H01227, JSPS KAKENHI JP22H04944, JSPS KAKENHI JP22KK0227, JSPS KAKENHI JP24K23939, JSPS KAKENHI JP24KK0251, JSPS KAKENHI JP25H00650, JSPS KAKENHI JP25H01291, JSPS KAKENHI JP25K01023); Norway: Research Council of Norway (RCN-314472); Poland: Ministry of Science and Higher Education (IDUB AGH, POB8, D4 no 9722), Polish National Science Centre (NCN 2021/42/E/ST2/00350, NCN OPUS 2023/51/B/ST2/02507, NCN OPUS nr 2022/47/B/ST2/03059, NCN UMO-2019/34/E/ST2/00393, UMO-2022/47/O/ST2/00148, UMO-2023/49/B/ST2/04085, UMO-2023/51/B/ST2/00920, UMO-2024/53/N/ST2/00869); Portugal: Foundation for Science and Technology (FCT); Spain: Ministry of Science and Innovation (MCIN & NextGenEU PCI2022-135018-2, MICIN & FEDER PID2021-125273NB, RYC2019-028510-I, RYC2020-030254-I, RYC2021-031273-I, RYC2022-038164-I); Sweden: Carl Trygger Foundation (Carl Trygger Foundation CTS 22:2312), Swedish Research Council (Swedish Research Council 2023-04654, VR 2021-03651, VR 2022-03845, VR 2022-04683, VR 2023-03403, VR 2024-05451), Knut and Alice Wallenberg Foundation (KAW 2018.0458, KAW 2022.0358, KAW 2023.0366); Switzerland: Swiss National Science Foundation (SNSF - PCEFP2_194658); United Kingdom: Royal Society (NIF-R1-231091); United States of America: U.S. Department of Energy (ECA DE-AC02-76SF00515), Neubauer Family Foundation.

References

- [1] ATLAS Collaboration, *Observation of a new particle in the search for the Standard Model Higgs boson with the ATLAS detector at the LHC*, *Phys. Lett. B* **716** (2012) 1, arXiv: [1207.7214 \[hep-ex\]](#).
- [2] CMS Collaboration, *Observation of a new boson at a mass of 125 GeV with the CMS experiment at the LHC*, *Phys. Lett. B* **716** (2012) 30, arXiv: [1207.7235 \[hep-ex\]](#).
- [3] ATLAS Collaboration, *A detailed map of Higgs boson interactions by the ATLAS experiment ten years after the discovery*, *Nature* **607** (2022) 52, arXiv: [2207.00092 \[hep-ex\]](#), Erratum: *Nature* **612** (2022) E24.
- [4] CMS Collaboration, *A portrait of the Higgs boson by the CMS experiment ten years after the discovery*, *Nature* **607** (2022) 60, arXiv: [2207.00043 \[hep-ex\]](#), Erratum: *Nature* **623** (2023) E4.
- [5] L. Evans and P. Bryant, *LHC Machine*, *JINST* **3** (2008) S08001.
- [6] J. C. Pati and A. Salam, *Lepton number as the fourth "color"*, *Phys. Rev. D* **10** (1974) 275.
- [7] W. Buchmüller, R. Rückl and D. Wyler, *Leptoquarks in lepton-quark collisions*, *Phys. Lett. B* **191** (1987) 442.
- [8] I. Doršner, S. Fajfer, A. Greljo, J. F. Kamenik and N. Košnik, *Physics of leptoquarks in precision experiments and at particle colliders*, *Phys. Rept.* **641** (2016) 1, arXiv: [1603.04993 \[hep-ph\]](#).
- [9] B. Diaz, M. Schmaltz and Y.-M. Zhong, *The leptoquark Hunter's guide: Pair production*, *JHEP* **10** (2017) 097, arXiv: [1706.05033 \[hep-ph\]](#).
- [10] M. Schmaltz and Y.-M. Zhong, *The leptoquark Hunter's guide: large coupling*, *JHEP* **01** (2019) 132, arXiv: [1810.10017 \[hep-ph\]](#).
- [11] L. Buonocore, P. Nason, F. Tramontano and G. Zanderighi, *Leptons in the proton*, *JHEP* **08** (2020) 019, arXiv: [2005.06477 \[hep-ph\]](#).
- [12] L. Buonocore, U. Haisch, P. Nason, F. Tramontano and G. Zanderighi, *Lepton-Quark Collisions at the Large Hadron Collider*, *Phys. Rev. Lett.* **125** (2020) 231804, arXiv: [2005.06475 \[hep-ph\]](#).
- [13] ATLAS Collaboration, *Search for pairs of scalar leptoquarks decaying into quarks and electrons or muons in $\sqrt{s} = 13$ TeV pp collisions with the ATLAS detector*, *JHEP* **10** (2020) 112, arXiv: [2006.05872 \[hep-ex\]](#).
- [14] ATLAS Collaboration, *Combination of searches for pair-produced leptoquarks at $\sqrt{s} = 13$ TeV with the ATLAS detector*, *Phys. Lett. B* **854** (2024) 138736, arXiv: [2401.11928 \[hep-ex\]](#).
- [15] CMS Collaboration, *Search for pair production of first-generation scalar leptoquarks at $\sqrt{s} = 13$ TeV*, *Phys. Rev. D* **99** (2019) 052002, arXiv: [1811.01197 \[hep-ex\]](#).
- [16] CMS Collaboration, *Search for pair production of second-generation leptoquarks at $\sqrt{s} = 13$ TeV*, *Phys. Rev. D* **99** (2019) 032014, arXiv: [1808.05082 \[hep-ex\]](#).

- [17] CMS Collaboration, *Search for pair production of scalar and vector leptoquarks decaying to muons and bottom quarks in proton–proton collisions at $\sqrt{s} = 13$ TeV*, [Phys. Rev. D **109** \(2024\) 112003](#), arXiv: [2402.08668 \[hep-ex\]](#).
- [18] CMS Collaboration, *Search for t -channel scalar and vector leptoquark exchange in the high-mass dimuon and dielectron spectra in proton–proton collisions at $\sqrt{s} = 13$ TeV*, (2025), arXiv: [2503.20023 \[hep-ex\]](#).
- [19] CMS Collaboration, *Search for Scalar Leptoquarks Produced via τ -Lepton–Quark Scattering in pp Collisions at $\sqrt{s} = 13$ TeV*, [Phys. Rev. Lett. **132** \(2024\) 061801](#), arXiv: [2308.06143 \[hep-ex\]](#).
- [20] ATLAS Collaboration, *The ATLAS Experiment at the CERN Large Hadron Collider*, [JINST **3** \(2008\) S08003](#).
- [21] ATLAS Collaboration, *The ATLAS experiment at the CERN Large Hadron Collider: a description of the detector configuration for Run 3*, [JINST **19** \(2024\) P05063](#), arXiv: [2305.16623 \[physics.ins-det\]](#).
- [22] ATLAS Collaboration, *Performance of the ATLAS trigger system in 2015*, [Eur. Phys. J. C **77** \(2017\) 317](#), arXiv: [1611.09661 \[hep-ex\]](#).
- [23] ATLAS Collaboration, *The ATLAS trigger system for LHC Run 3 and trigger performance in 2022*, [JINST **19** \(2024\) P06029](#), arXiv: [2401.06630 \[hep-ex\]](#).
- [24] ATLAS Collaboration, *Software and computing for Run 3 of the ATLAS experiment at the LHC*, [Eur. Phys. J. C **85** \(2025\) 234](#), arXiv: [2404.06335 \[hep-ex\]](#).
- [25] ATLAS Collaboration, *Performance of electron and photon triggers in ATLAS during LHC Run 2*, [Eur. Phys. J. C **80** \(2020\) 47](#), arXiv: [1909.00761 \[hep-ex\]](#).
- [26] ATLAS Collaboration, *Performance of the ATLAS muon triggers in Run 2*, [JINST **15** \(2020\) P09015](#), arXiv: [2004.13447 \[physics.ins-det\]](#).
- [27] ATLAS Collaboration, *ATLAS data quality operations and performance for 2015–2018 data-taking*, [JINST **15** \(2020\) P04003](#), arXiv: [1911.04632 \[physics.ins-det\]](#).
- [28] ATLAS Collaboration, *The ATLAS Simulation Infrastructure*, [Eur. Phys. J. C **70** \(2010\) 823](#), arXiv: [1005.4568 \[physics.ins-det\]](#).
- [29] S. Agostinelli et al., *GEANT4 – a simulation toolkit*, [Nucl. Instrum. Meth. A **506** \(2003\) 250](#).
- [30] L. Buonocore et al., *Resonant leptoquark at NLO with POWHEG*, [JHEP **11** \(2022\) 129](#), arXiv: [2209.02599 \[hep-ph\]](#).
- [31] J. Bellm et al., *Herwig 7.2 release note*, [Eur. Phys. J. C **80** \(2020\) 452](#), arXiv: [1912.06509 \[hep-ph\]](#).
- [32] D. J. Lange, *The EvtGen particle decay simulation package*, [Nucl. Instrum. Meth. A **462** \(2001\) 152](#).
- [33] U. Haisch, L. Schnell and S. Schulte, *On Drell-Yan production of scalar leptoquarks coupling to heavy-quark flavours*, [JHEP **11** \(2022\) 106](#), arXiv: [2207.00356 \[hep-ph\]](#).
- [34] R. D. Ball et al., *The PDF4LHC21 combination of global PDF fits for the LHC Run III*, [J. Phys. G **49** \(2022\) 080501](#), arXiv: [2203.05506 \[hep-ph\]](#).

- [35] ATLAS Collaboration, *ATLAS simulation of boson plus jets processes in Run 2*, ATL-PHYS-PUB-2017-006, 2017, URL: <https://cds.cern.ch/record/2261937>.
- [36] ATLAS Collaboration, *Improvements in $t\bar{t}$ modelling using NLO+PS Monte Carlo generators for Run 2*, ATL-PHYS-PUB-2018-009, 2018, URL: <https://cds.cern.ch/record/2630327>.
- [37] ATLAS Collaboration, *Simulation of top-quark production for the ATLAS experiment at $\sqrt{s} = 13$ TeV*, ATL-PHYS-PUB-2016-004, 2016, URL: <https://cds.cern.ch/record/2120417>.
- [38] ATLAS Collaboration, *Multi-Boson Simulation for 13 TeV ATLAS Analyses*, ATL-PHYS-PUB-2017-005, 2017, URL: <https://cds.cern.ch/record/2261933>.
- [39] J. Alwall et al., *The automated computation of tree-level and next-to-leading order differential cross sections, and their matching to parton shower simulations*, *JHEP* **07** (2014) 079, arXiv: [1405.0301](https://arxiv.org/abs/1405.0301) [[hep-ph](#)].
- [40] NNPDF Collaboration, R. D. Ball et al., *Parton distributions with LHC data*, *Nucl. Phys. B* **867** (2013) 244, arXiv: [1207.1303](https://arxiv.org/abs/1207.1303) [[hep-ph](#)].
- [41] E. Bothmann et al., *Event generation with Sherpa 2.2*, *SciPost Phys.* **7** (2019) 034, arXiv: [1905.09127](https://arxiv.org/abs/1905.09127) [[hep-ph](#)].
- [42] T. Gleisberg and S. Höche, *Comix, a new matrix element generator*, *JHEP* **12** (2008) 039, arXiv: [0808.3674](https://arxiv.org/abs/0808.3674) [[hep-ph](#)].
- [43] S. Schumann and F. Krauss, *A parton shower algorithm based on Catani–Seymour dipole factorisation*, *JHEP* **03** (2008) 038, arXiv: [0709.1027](https://arxiv.org/abs/0709.1027) [[hep-ph](#)].
- [44] ATLAS Collaboration, *Inclusive W^\pm and Z^0 cross sections at next-to-next-to leading order QCD for the ATLAS experiment*, ATL-PHYS-PUB-2023-026, 2023, URL: <https://cds.cern.ch/record/2871755>.
- [45] NNPDF Collaboration, R. D. Ball et al., *Parton distributions for the LHC run II*, *JHEP* **04** (2015) 040, arXiv: [1410.8849](https://arxiv.org/abs/1410.8849) [[hep-ph](#)].
- [46] S. Frixione, G. Ridolfi and P. Nason, *A positive-weight next-to-leading-order Monte Carlo for heavy flavour hadroproduction*, *JHEP* **09** (2007) 126, arXiv: [0707.3088](https://arxiv.org/abs/0707.3088) [[hep-ph](#)].
- [47] P. Nason, *A new method for combining NLO QCD with shower Monte Carlo algorithms*, *JHEP* **11** (2004) 040, arXiv: [hep-ph/0409146](https://arxiv.org/abs/hep-ph/0409146).
- [48] S. Frixione, P. Nason and C. Oleari, *Matching NLO QCD computations with parton shower simulations: the POWHEG method*, *JHEP* **11** (2007) 070, arXiv: [0709.2092](https://arxiv.org/abs/0709.2092) [[hep-ph](#)].
- [49] S. Alioli, P. Nason, C. Oleari and E. Re, *A general framework for implementing NLO calculations in shower Monte Carlo programs: the POWHEG BOX*, *JHEP* **06** (2010) 043, arXiv: [1002.2581](https://arxiv.org/abs/1002.2581) [[hep-ph](#)].
- [50] T. Sjöstrand et al., *An introduction to PYTHIA 8.2*, *Comput. Phys. Commun.* **191** (2015) 159, arXiv: [1410.3012](https://arxiv.org/abs/1410.3012) [[hep-ph](#)].

- [51] M. Beneke, P. Falgari, S. Klein and C. Schwinn, *Hadronic top-quark pair production with NNLL threshold resummation*, *Nucl. Phys. B* **855** (2012) 695, arXiv: [1109.1536 \[hep-ph\]](#).
- [52] M. Cacciari, M. Czakon, M. Mangano, A. Mitov and P. Nason, *Top-pair production at hadron colliders with next-to-next-to-leading logarithmic soft-gluon resummation*, *Phys. Lett. B* **710** (2012) 612, arXiv: [1111.5869 \[hep-ph\]](#).
- [53] P. Bärnreuther, M. Czakon and A. Mitov, *Percent-Level-Precision Physics at the Tevatron: Next-to-Next-to-Leading Order QCD Corrections to $q\bar{q} \rightarrow t\bar{t} + X$* , *Phys. Rev. Lett.* **109** (2012) 132001, arXiv: [1204.5201 \[hep-ph\]](#).
- [54] M. Czakon and A. Mitov, *NNLO corrections to top-pair production at hadron colliders: the all-fermionic scattering channels*, *JHEP* **12** (2012) 054, arXiv: [1207.0236 \[hep-ph\]](#).
- [55] M. Czakon and A. Mitov, *NNLO corrections to top pair production at hadron colliders: the quark-gluon reaction*, *JHEP* **01** (2013) 080, arXiv: [1210.6832 \[hep-ph\]](#).
- [56] M. Czakon, P. Fiedler and A. Mitov, *Total Top-Quark Pair-Production Cross Section at Hadron Colliders Through $O(\alpha_S^4)$* , *Phys. Rev. Lett.* **110** (2013) 252004, arXiv: [1303.6254 \[hep-ph\]](#).
- [57] M. Czakon and A. Mitov, *Top++: A program for the calculation of the top-pair cross-section at hadron colliders*, *Comput. Phys. Commun.* **185** (2014) 2930, arXiv: [1112.5675 \[hep-ph\]](#).
- [58] ATLAS Collaboration, *ATLAS Pythia 8 tunes to 7 TeV data*, ATL-PHYS-PUB-2014-021, 2014, URL: <https://cds.cern.ch/record/1966419>.
- [59] E. Re, *Single-top Wt -channel production matched with parton showers using the POWHEG method*, *Eur. Phys. J. C* **71** (2011) 1547, arXiv: [1009.2450 \[hep-ph\]](#).
- [60] N. Kidonakis, *Two-loop soft anomalous dimensions for single top quark associated production with a W^- or H^-* , *Phys. Rev. D* **82** (2010) 054018, arXiv: [1005.4451 \[hep-ph\]](#).
- [61] S. Höche, F. Krauss, M. Schönherr and F. Siegert, *A critical appraisal of NLO+PS matching methods*, *JHEP* **09** (2012) 049, arXiv: [1111.1220 \[hep-ph\]](#).
- [62] S. Höche, F. Krauss, M. Schönherr and F. Siegert, *QCD matrix elements + parton showers. The NLO case*, *JHEP* **04** (2013) 027, arXiv: [1207.5030 \[hep-ph\]](#).
- [63] S. Catani, F. Krauss, B. R. Webber and R. Kuhn, *QCD Matrix Elements + Parton Showers*, *JHEP* **11** (2001) 063, arXiv: [hep-ph/0109231](#).
- [64] S. Höche, F. Krauss, S. Schumann and F. Siegert, *QCD matrix elements and truncated showers*, *JHEP* **05** (2009) 053, arXiv: [0903.1219 \[hep-ph\]](#).
- [65] R. Frederix et al., *The automation of next-to-leading order electroweak calculations*, *JHEP* **07** (2018) 185, arXiv: [1804.10017 \[hep-ph\]](#), Erratum: *JHEP* **11** (2021) 085.
- [66] ATLAS Collaboration, *Multijet simulation for 13 TeV ATLAS Analyses*, ATL-PHYS-PUB-2019-017, 2019, URL: <https://cds.cern.ch/record/2672252>.

- [67] ATLAS Collaboration, *Vertex Reconstruction Performance of the ATLAS Detector at $\sqrt{s} = 13$ TeV*, ATL-PHYS-PUB-2015-026, 2015, URL: <https://cds.cern.ch/record/2037717>.
- [68] ATLAS Collaboration, *Selection of jets produced in 13 TeV proton–proton collisions with the ATLAS detector*, ATLAS-CONF-2015-029, 2015, URL: <https://cds.cern.ch/record/2037702>.
- [69] ATLAS Collaboration, *Electron reconstruction and identification in the ATLAS experiment using the 2015 and 2016 LHC proton–proton collision data at $\sqrt{s} = 13$ TeV*, *Eur. Phys. J. C* **79** (2019) 639, arXiv: [1902.04655](https://arxiv.org/abs/1902.04655) [[physics.ins-det](#)].
- [70] ATLAS Collaboration, *Electron and photon efficiencies in LHC Run 2 with the ATLAS experiment*, *JHEP* **05** (2024) 162, arXiv: [2308.13362](https://arxiv.org/abs/2308.13362) [[hep-ex](#)].
- [71] ATLAS Collaboration, *Muon reconstruction and identification efficiency in ATLAS using the full Run 2 pp collision data set at $\sqrt{s} = 13$ TeV*, *Eur. Phys. J. C* **81** (2021) 578, arXiv: [2012.00578](https://arxiv.org/abs/2012.00578) [[hep-ex](#)].
- [72] M. Cacciari, G. P. Salam and G. Soyez, *The anti- k_t jet clustering algorithm*, *JHEP* **04** (2008) 063, arXiv: [0802.1189](https://arxiv.org/abs/0802.1189) [[hep-ph](#)].
- [73] M. Cacciari, G. P. Salam and G. Soyez, *FastJet user manual*, *Eur. Phys. J. C* **72** (2012) 1896, arXiv: [1111.6097](https://arxiv.org/abs/1111.6097) [[hep-ph](#)].
- [74] ATLAS Collaboration, *Jet reconstruction and performance using particle flow with the ATLAS Detector*, *Eur. Phys. J. C* **77** (2017) 466, arXiv: [1703.10485](https://arxiv.org/abs/1703.10485) [[hep-ex](#)].
- [75] ATLAS Collaboration, *Topological cell clustering in the ATLAS calorimeters and its performance in LHC Run 1*, *Eur. Phys. J. C* **77** (2017) 490, arXiv: [1603.02934](https://arxiv.org/abs/1603.02934) [[hep-ex](#)].
- [76] ATLAS Collaboration, *Jet energy scale and resolution measured in proton–proton collisions at $\sqrt{s} = 13$ TeV with the ATLAS detector*, *Eur. Phys. J. C* **81** (2021) 689, arXiv: [2007.02645](https://arxiv.org/abs/2007.02645) [[hep-ex](#)].
- [77] ATLAS Collaboration, *Performance of pile-up mitigation techniques for jets in pp collisions at $\sqrt{s} = 8$ TeV using the ATLAS detector*, *Eur. Phys. J. C* **76** (2016) 581, arXiv: [1510.03823](https://arxiv.org/abs/1510.03823) [[hep-ex](#)].
- [78] ATLAS Collaboration, *Transforming jet flavour tagging at ATLAS*, (2025), arXiv: [2505.19689](https://arxiv.org/abs/2505.19689) [[hep-ex](#)].
- [79] ATLAS Collaboration, *The performance of missing transverse momentum reconstruction and its significance with the ATLAS detector using 140fb^{-1} of $\sqrt{s} = 13$ TeV pp collisions*, *Eur. Phys. J. C* **85** (2025) 606, arXiv: [2402.05858](https://arxiv.org/abs/2402.05858) [[hep-ex](#)].
- [80] M. Cacciari and G. P. Salam, *Pileup subtraction using jet areas*, *Phys. Lett. B* **659** (2008) 119, arXiv: [0707.1378](https://arxiv.org/abs/0707.1378) [[hep-ph](#)].
- [81] ATLAS Collaboration, *Tools for estimating fake/non-prompt lepton backgrounds with the ATLAS detector at the LHC*, *JINST* **18** (2023) T11004, arXiv: [2211.16178](https://arxiv.org/abs/2211.16178) [[hep-ex](#)].
- [82] M. Baak et al., *HistFitter software framework for statistical data analysis*, *Eur. Phys. J. C* **75** (2015) 153, arXiv: [1410.1280](https://arxiv.org/abs/1410.1280) [[hep-ex](#)].

- [83] ATLAS Collaboration, *Electron and photon performance measurements with the ATLAS detector using the 2015–2017 LHC proton–proton collision data*, *JINST* **14** (2019) P12006, arXiv: [1908.00005 \[hep-ex\]](#).
- [84] ATLAS Collaboration, *ATLAS b -jet identification performance and efficiency measurement with $t\bar{t}$ events in pp collisions at $\sqrt{s} = 13$ TeV*, *Eur. Phys. J. C* **79** (2019) 970, arXiv: [1907.05120 \[hep-ex\]](#).
- [85] ATLAS Collaboration, *Measurement of the c -jet mistagging efficiency in $t\bar{t}$ events using pp collision data at $\sqrt{s} = 13$ TeV collected with the ATLAS detector*, *Eur. Phys. J. C* **82** (2022) 95, arXiv: [2109.10627 \[hep-ex\]](#).
- [86] ATLAS Collaboration, *Calibration of the light-flavour jet mistagging efficiency of the b -tagging algorithms with Z +jets events using 139fb^{-1} of ATLAS proton–proton collision data at $\sqrt{s} = 13$ TeV*, *Eur. Phys. J. C* **83** (2023) 728, arXiv: [2301.06319 \[hep-ex\]](#).
- [87] ATLAS Collaboration, *Luminosity determination in pp collisions at $\sqrt{s} = 13$ TeV using the ATLAS detector at the LHC*, *Eur. Phys. J. C* **83** (2023) 982, arXiv: [2212.09379 \[hep-ex\]](#).
- [88] ATLAS Collaboration, *Preliminary analysis of the luminosity calibration of the ATLAS 13.6 TeV data recorded in 2022*, ATL-DAPR-PUB-2023-001, 2023, URL: <https://cds.cern.ch/record/2853525>.
- [89] ATLAS Collaboration, *Preliminary analysis of the luminosity calibration for the ATLAS 13.6 TeV data recorded in 2023*, ATL-DAPR-PUB-2024-001, 2024, URL: <https://cds.cern.ch/record/2900949>.
- [90] G. Avoni et al., *The new LUCID-2 detector for luminosity measurement and monitoring in ATLAS*, *JINST* **13** (2018) P07017.
- [91] S. Kallweit, J. M. Lindert, P. Maierhöfer, S. Pozzorini and M. Schönherr, *NLO electroweak automation and precise predictions for W +multijet production at the LHC*, *JHEP* **04** (2015) 012, arXiv: [1412.5157 \[hep-ph\]](#).
- [92] S. Höche, S. Mrenna, S. Payne, C. T. Preuss and P. Skands, *A Study of QCD Radiation in VBF Higgs Production with Vincia and Pythia*, *SciPost Phys.* **12** (2022) 010, arXiv: [2106.10987 \[hep-ph\]](#).
- [93] S. Frixione, E. Laenen, P. Motylinski, C. White and B. R. Webber, *Single-top hadroproduction in association with a W boson*, *JHEP* **07** (2008) 029, arXiv: [0805.3067 \[hep-ph\]](#).
- [94] G. Cowan, K. Cranmer, E. Gross and O. Vitells, *Asymptotic formulae for likelihood-based tests of new physics*, *Eur. Phys. J. C* **71** (2011) 1554, arXiv: [1007.1727 \[physics.data-an\]](#), Erratum: *Eur. Phys. J. C* **73** (2013) 2501.
- [95] Cranmer, Kyle and Held, Alexander, *Building and steering binned template fits with cabinetry*, *EPJ Web Conf.* **251** (2021) 03067.
- [96] L. Heinrich, M. Feickert, G. Stark and K. Cranmer, *pyhf: pure-Python implementation of HistFactory statistical models*, *JOSS* **6** (2021) 2823.
- [97] ROOT Collaboration, *HistFactory: A tool for creating statistical models for use with RooFit and RooStats*, CERN-OPEN-2012-016 (2012).

- [98] A. L. Read, *Presentation of search results: the CL_s technique*, *J. Phys. G* **28** (2002) 2693.
- [99] I. Doršner, A. Lejlić and S. Saad, *Asymmetric leptoquark pair production at LHC*, *JHEP* **03** (2023) 025, arXiv: 2210.11004 [hep-ph].
- [100] ATLAS Collaboration, *ATLAS Computing Acknowledgements*, ATL-SOFT-PUB-2025-001, 2025, URL: <https://cds.cern.ch/record/2922210>.

The ATLAS Collaboration

G. Aad ¹⁰⁴, E. Aakvaag ¹⁷, B. Abbott ¹²³, S. Abdelhameed ^{119a}, K. Abeling ⁵⁵, N.J. Abicht ⁴⁹, S.H. Abidi ³⁰, M. Aboeela ⁴⁵, A. Aboulhorma ^{36e}, H. Abramowicz ¹⁵⁷, Y. Abulaiti ¹²⁰, B.S. Acharya ^{69a,69b,m}, A. Ackermann ^{63a}, C. Adam Bourdarios ⁴, L. Adamezyk ^{86a}, S.V. Addepalli ¹⁴⁹, M.J. Addison ¹⁰³, J. Adelman ¹¹⁸, A. Adiguzel ^{22c}, T. Adye ¹³⁷, A.A. Affolder ¹³⁹, Y. Afik ⁴⁰, M.N. Agaras ¹³, A. Aggarwal ¹⁰², C. Agheorghiesei ^{28c}, F. Ahmadov ^{39,ad}, S. Ahuja ⁹⁷, X. Ai ^{143b}, G. Aielli ^{76a,76b}, A. Aikot ¹⁶⁹, M. Ait Tamliah ^{36e}, B. Aitbenkikh ^{36a}, M. Akbiyik ¹⁰², T.P.A. Åkesson ¹⁰⁰, A.V. Akimov ¹⁵¹, D. Akiyama ¹⁷⁴, N.N. Akolkar ²⁵, S. Aktas ¹⁷², G.L. Alberghi ^{24b}, J. Albert ¹⁷¹, U. Alberti ²⁰, P. Albicocco ⁵³, G.L. Albouy ⁶⁰, S. Alderweireldt ⁵², Z.L. Alegria ¹²⁴, M. Aleksa ³⁷, I.N. Aleksandrov ³⁹, C. Alexa ^{28b}, T. Alexopoulos ¹⁰, F. Alfonsi ^{24b}, M. Algren ⁵⁶, M. Alhroob ¹⁷³, B. Ali ¹³⁵, H.M.J. Ali ^{93,w}, S. Ali ³², S.W. Alibocus ⁹⁴, M. Aliev ^{34c}, G. Alimonti ^{71a}, W. Alkakh ⁵⁵, C. Allaire ⁶⁶, B.M.M. Allbrooke ¹⁵², J.S. Allen ¹⁰³, J.F. Allen ⁵², P.P. Allport ²¹, A. Aloisio ^{72a,72b}, F. Alonso ⁹², C. Alpigiani ¹⁴², Z.M.K. Alsolami ⁹³, A. Alvarez Fernandez ¹⁰², M. Alves Cardoso ⁵⁶, M.G. Alviggi ^{72a,72b}, M. Aly ¹⁰³, Y. Amaral Coutinho ^{83b}, A. Ambler ¹⁰⁶, C. Amelung ³⁷, M. Amerl ¹⁰³, C.G. Ames ¹¹¹, T. Amezza ¹³⁰, D. Amidei ¹⁰⁸, B. Amini ⁵⁴, K. Amiric ¹⁶¹, A. Amirkhanov ³⁹, S.P. Amor Dos Santos ^{133a}, K.R. Amos ¹⁶⁹, D. Amperiadou ¹⁵⁸, S. An ⁸⁴, C. Anastopoulos ¹⁴⁵, T. Andeen ¹¹, J.K. Anders ⁹⁴, A.C. Anderson ⁵⁹, A. Andreatta ^{71a,71b}, S. Angelidakis ⁹, A. Angerami ⁴², A.V. Anisenkov ³⁹, A. Annovi ^{74a}, C. Antel ³⁷, E. Antipov ¹⁵¹, M. Antonelli ⁵³, F. Anulli ^{75a}, M. Aoki ⁸⁴, T. Aoki ¹⁵⁹, M.A. Aparo ¹⁵², L. Aperio Bella ⁴⁸, M. Apicella ³¹, C. Appelt ¹⁵⁷, A. Apyan ²⁷, M. Arampatzi ¹⁰, S.J. Arbiol Val ⁸⁷, C. Arcangeletti ⁵³, A.T.H. Arce ⁵¹, J-F. Arguin ¹¹⁰, S. Argyropoulos ¹⁵⁸, J.-H. Arling ⁴⁸, O. Arnaez ⁴, H. Arnold ¹⁵¹, G. Artoni ^{75a,75b}, H. Asada ¹¹³, K. Asai ¹²¹, S. Asatryan ¹⁷⁹, N.A. Asbah ³⁷, R.A. Ashby Pickering ¹⁷³, A.M. Aslam ⁹⁷, K. Assamagan ³⁰, R. Astalos ^{29a}, K.S.V. Astrand ¹⁰⁰, S. Atashi ¹⁶⁵, R.J. Atkin ^{34a}, H. Atmani ^{36f}, P.A. Atlasiddha ¹³¹, K. Augsten ¹³⁵, A.D. Auriol ⁴¹, V.A. Austrup ¹⁰³, A.S. Avad ⁹⁶, G. Avolio ³⁷, K. Axiotis ⁵⁶, A. Azzam ¹³, D. Babal ^{29b}, H. Bachacou ¹³⁸, K. Bachas ^{158,q}, A. Bachiu ³⁵, E. Bachmann ⁵⁰, M.J. Backes ^{63a}, A. Badea ⁴⁰, T.M. Baer ¹⁰⁸, P. Bagnaia ^{75a,75b}, M. Bahmani ¹⁹, D. Bahner ⁵⁴, K. Bai ¹²⁶, J.T. Baines ¹³⁷, L. Baines ⁹⁶, O.K. Baker ¹⁷⁸, E. Bakos ¹⁶, D. Bakshi Gupta ⁸, L.E. Balabram Filho ^{83b}, V. Balakrishnan ¹²³, R. Balasubramanian ⁴, E.M. Baldin ³⁸, P. Balek ^{86a}, E. Ballabene ^{24b,24a}, F. Balli ¹³⁸, L.M. Baltes ^{63a}, W.K. Balunas ³³, J. Balz ¹⁰², I. Bamwidhi ^{119b}, E. Banas ⁸⁷, M. Bandieramonte ¹³², A. Bandyopadhyay ²⁵, S. Bansal ²⁵, L. Barak ¹⁵⁷, M. Barakat ⁴⁸, E.L. Barberio ¹⁰⁷, D. Barberis ^{18b}, M. Barbero ¹⁰⁴, M.Z. Barel ¹¹⁷, T. Barillari ¹¹², M-S. Barisits ³⁷, T. Barklow ¹⁴⁹, P. Baron ¹³⁶, D.A. Baron Moreno ¹⁰³, A. Baroncelli ⁶², A.J. Barr ¹²⁹, J.D. Barr ⁹⁸, F. Barreiro ¹⁰¹, J. Barreiro Guimarães da Costa ¹⁴, M.G. Barros Teixeira ^{133a}, S. Barsov ³⁸, F. Bartels ^{63a}, R. Bartoldus ¹⁴⁹, A.E. Barton ⁹³, P. Bartos ^{29a}, M. Baselga ⁴⁹, S. Bashiri ⁸⁷, A. Bassalat ^{66,b}, M.J. Basso ^{162a}, S. Bataju ⁴⁵, R. Bate ¹⁷⁰, R.L. Bates ⁵⁹, S. Batlamous ¹⁰¹, M. Battaglia ¹³⁹, D. Battulga ¹⁹, M. Baucé ^{75a,75b}, M. Bauer ⁷⁹, P. Bauer ²⁵, L.T. Bayer ⁴⁸, L.T. Bazzano Hurrell ³¹, J.B. Beacham ¹¹², T. Beau ¹³⁰, J.Y. Beauchamp ⁹², P.H. Beauchemin ¹⁶⁴, P. Bechtel ²⁵, H.P. Beck ^{20,p}, K. Becker ¹⁷³, A.J. Beddall ⁸², V.A. Bednyakov ³⁹, C.P. Bee ¹⁵¹, L.J. Beemster ¹⁶, M. Begalli ^{83d}, M. Begel ³⁰, J.K. Behr ⁴⁸, J.F. Beirer ³⁷, F. Beisiegel ²⁵, M. Belfkir ^{119b}, G. Bella ¹⁵⁷, L. Bellagamba ^{24b}, A. Bellerive ³⁵, C.D. Bellgraph ⁶⁸, P. Bellos ²¹, K. Beloborodov ³⁸, I. Benaoumeur ²¹, D. Benckroun ^{36a}, F. Bendebba ^{36a}, Y. Benhammou ¹⁵⁷, K.C. Benkendorfer ⁶¹, L. Beresford ⁴⁸,

M. Beretta ⁵³, E. Bergeaas Kuutmann ¹⁶⁷, N. Berger ⁴, B. Bergmann ¹³⁵, J. Beringer ^{18a},
G. Bernardi ⁵, C. Bernius ¹⁴⁹, F.U. Bernlochner ²⁵, A. Berrocal Guardia ¹³, T. Berry ⁹⁷,
P. Berta ¹³⁶, A. Berthold ⁵⁰, A. Berti ^{133a}, R. Bertrand ¹⁰⁴, S. Bethke ¹¹², A. Betti ^{75a,75b},
A.J. Bevan ⁹⁶, L. Bezio ⁵⁶, N.K. Bhalla ⁵⁴, S. Bharthuar ¹¹², S. Bhatta ¹⁵¹, P. Bhattacharai ¹⁴⁹,
Z.M. Bhatti ¹²⁰, K.D. Bhide ⁵⁴, V.S. Bhopatkar ¹²⁴, R.M. Bianchi ¹³², G. Bianco ^{24b,24a},
O. Biebel ¹¹¹, M. Biglietti ^{77a}, C.S. Billingsley ⁴⁵, Y. Bimgdi ^{36f}, M. Bindi ⁵⁵, A. Bingham ¹⁷⁷,
A. Bingul ^{22b}, C. Bini ^{75a,75b}, G.A. Bird ³³, M. Birman ¹⁷⁵, M. Biros ¹³⁶, S. Biryukov ¹⁵²,
T. Bisanz ⁴⁹, E. Bisceglie ^{24b,24a}, J.P. Biswal ¹³⁷, D. Biswas ¹⁴⁷, I. Bloch ⁴⁸, A. Blue ⁵⁹,
U. Blumenschein ⁹⁶, V.S. Bobrovnikov ³⁹, L. Boccardo ^{57b,57a}, M. Boehler ⁵⁴, B. Boehm ¹⁷²,
D. Bogavac ¹³, A.G. Bogdanchikov ³⁸, L.S. Boggia ¹³⁰, V. Boisvert ⁹⁷, P. Bokan ³⁷, T. Bold ^{86a},
M. Bomben ⁵, M. Bona ⁹⁶, M. Boonekamp ¹³⁸, A.G. Borbély ⁵⁹, I.S. Bordulev ³⁸,
G. Borissov ⁹³, D. Bortoletto ¹²⁹, D. Boscherini ^{24b}, M. Bosman ¹³, K. Bouaouda ^{36a},
N. Bouchhar ¹⁶⁹, L. Boudet ⁴, J. Boudreau ¹³², E.V. Bouhova-Thacker ⁹³, D. Boumediene ⁴¹,
R. Bouquet ^{57b,57a}, A. Boveia ¹²², J. Boyd ³⁷, D. Boye ³⁰, I.R. Boyko ³⁹, L. Bozianu ⁵⁶,
J. Bracinik ²¹, N. Brahimi ⁴, G. Brandt ¹⁷⁷, O. Brandt ³³, B. Brau ¹⁰⁵, J.E. Brau ¹²⁶,
R. Brenner ¹⁷⁵, L. Brenner ¹¹⁷, R. Brenner ¹⁶⁷, S. Bressler ¹⁷⁵, G. Brianti ^{78a,78b}, D. Britton ⁵⁹,
D. Britzger ¹¹², I. Brock ²⁵, R. Brock ¹⁰⁹, G. Brooijmans ⁴², A.J. Brooks ⁶⁸, E.M. Brooks ^{162b},
E. Brost ³⁰, L.M. Brown ^{171,162a}, L.E. Bruce ⁶¹, T.L. Bruckler ¹²⁹, P.A. Bruckman de Renstrom ⁸⁷,
B. Brüers ⁴⁸, A. Bruni ^{24b}, G. Bruni ^{24b}, D. Brunner ^{47a,47b}, M. Bruschi ^{24b}, N. Bruscinò ^{75a,75b},
T. Buanes ¹⁷, Q. Buat ¹⁴², D. Buchin ¹¹², A.G. Buckley ⁵⁹, O. Bulekov ⁸², B.A. Bullard ¹⁴⁹,
S. Burdin ⁹⁴, C.D. Burgard ⁴⁹, A.M. Burger ⁹¹, B. Burghgrave ⁸, O. Burlayenko ⁵⁴,
J. Burleson ¹⁶⁸, J.C. Burzynski ¹⁴⁸, E.L. Busch ⁴², V. Büscher ¹⁰², P.J. Bussey ⁵⁹,
J.M. Butler ²⁶, C.M. Buttar ⁵⁹, J.M. Butterworth ⁹⁸, W. Buttinger ¹³⁷, C.J. Buxo Vazquez ¹⁰⁹,
A.R. Buzykaev ³⁹, S. Cabrera Urbán ¹⁶⁹, L. Cadamuro ⁶⁶, H. Cai ³⁷, Y. Cai ^{24b,114c,24a},
Y. Cai ^{114a}, V.M.M. Cairo ³⁷, O. Cakir ^{3a}, N. Calace ³⁷, P. Calafiura ^{18a}, G. Calderini ¹³⁰,
P. Calfayan ³⁵, L. Calic ¹⁰⁰, G. Callea ⁵⁹, L.P. Caloba ^{83b}, D. Calvet ⁴¹, S. Calvet ⁴¹,
R. Camacho Toro ¹³⁰, S. Camarda ³⁷, D. Camarero Munoz ²⁷, P. Camarri ^{76a,76b},
C. Camincher ¹⁷¹, M. Campanelli ⁹⁸, A. Camplani ⁴³, V. Canale ^{72a,72b}, A.C. Canbay ^{3a},
E. Canonero ⁹⁷, J. Cantero ¹⁶⁹, Y. Cao ¹⁶⁸, F. Capocasa ²⁷, M. Capua ^{44b,44a}, A. Carbone ^{71a,71b},
R. Cardarelli ^{76a}, J.C.J. Cardenas ⁸, M.P. Cardiff ²⁷, G. Carducci ^{44b,44a}, T. Carli ³⁷,
G. Carlino ^{72a}, J.I. Carlotto ¹³, B.T. Carlson ^{132,r}, E.M. Carlson ¹⁷¹, J. Carmignani ⁹⁴,
L. Carminati ^{71a,71b}, A. Carnelli ⁴, M. Carnesale ³⁷, S. Caron ¹¹⁶, E. Carquin ^{140g}, I.B. Carr ¹⁰⁷,
S. Carrá ^{73a,73b}, G. Carratta ^{24b,24a}, C. Carrion Martinez ¹⁶⁹, A.M. Carroll ¹²⁶, M.P. Casado ^{13,h},
P. Casolaro ^{72a,72b}, M. Caspar ⁴⁸, F.L. Castillo ⁴, L. Castillo Garcia ¹³, V. Castillo Gimenez ¹⁶⁹,
N.F. Castro ^{133a,133e}, A. Catinaccio ³⁷, J.R. Catmore ¹²⁸, T. Cavaliere ⁴, V. Cavaliere ³⁰,
L.J. Caviedes Betancourt ^{23b}, E. Celebi ⁸², S. Cella ³⁷, V. Cepaitis ⁵⁶, K. Cerny ¹²⁵,
A.S. Cerqueira ^{83a}, A. Cerri ^{74a,74b,am}, L. Cerrito ^{76a,76b}, F. Cerutti ^{18a}, B. Cervato ^{71a,71b},
A. Cervelli ^{24b}, G. Cesarini ⁵³, S.A. Cetin ⁸², P.M. Chabrilat ¹³⁰, R. Chakkappai ⁶⁶,
S. Chakraborty ¹⁷³, J. Chan ^{18a}, W.Y. Chan ¹⁵⁹, J.D. Chapman ³³, E. Chapon ¹³⁸,
B. Chargeishvili ^{155b}, D.G. Charlton ²¹, C. Chauhan ¹³⁶, Y. Che ^{114a}, S. Chekanov ⁶,
S.V. Chekulaev ^{162a}, G.A. Chelkov ^{39,a}, B. Chen ¹⁵⁷, B. Chen ¹⁷¹, H. Chen ^{114a}, H. Chen ³⁰,
J. Chen ^{144a}, J. Chen ¹⁴⁸, M. Chen ¹²⁹, S. Chen ⁸⁹, S.J. Chen ^{114a}, X. Chen ^{144a}, X. Chen ^{15,ah},
Z. Chen ⁶², C.L. Cheng ¹⁷⁶, H.C. Cheng ^{64a}, S. Cheong ¹⁴⁹, A. Cheplakov ³⁹,
E. Cherepanova ¹¹⁷, R. Cherkaoui El Moursli ^{36e}, E. Cheu ⁷, K. Cheung ⁶⁵, L. Chevalier ¹³⁸,
V. Chiarella ⁵³, G. Chiarelli ^{74a}, G. Chiodini ^{70a}, A.S. Chisholm ²¹, A. Chitan ^{28b},
M. Chitishvili ¹⁶⁹, M.V. Chizhov ^{39,s}, K. Choi ¹¹, Y. Chou ¹⁴², E.Y.S. Chow ¹¹⁶, K.L. Chu ¹⁷⁵,
M.C. Chu ^{64a}, X. Chu ^{14,114c}, Z. Chubinidze ⁵³, J. Chudoba ¹³⁴, J.J. Chwastowski ⁸⁷,

D. Cieri [id112](#), K.M. Ciesla [id86a](#), V. Cindro [id95](#), A. Ciocio [id18a](#), F. Cirotto [id72a,72b](#), Z.H. Citron [id175](#),
 M. Citterio [id71a](#), D.A. Ciubotaru [id28b](#), A. Clark [id56](#), P.J. Clark [id52](#), N. Clarke Hall [id98](#), C. Clarry [id161](#),
 S.E. Clawson [id48](#), C. Clement [id47a,47b](#), Y. Coadou [id104](#), M. Cobal [id69a,69c](#), A. Coccaro [id57b](#),
 R.F. Coelho Barrue [id133a](#), R. Coelho Lopes De Sa [id105](#), S. Coelli [id71a](#), L.S. Colangeli [id161](#), B. Cole [id42](#),
 P. Collado Soto [id101](#), J. Collot [id60](#), R. Coluccia [id70a,70b](#), P. Conde Muiño [id133a,133g](#), M.P. Connell [id34c](#),
 S.H. Connell [id34c](#), E.I. Conroy [id129](#), M. Contreras Cossio [id11](#), F. Conventi [id72a,aj](#),
 A.M. Cooper-Sarkar [id129](#), L. Corazzina [id75a,75b](#), F.A. Corchia [id24b,24a](#), A. Cordeiro Oudot Choi [id142](#),
 L.D. Corpe [id41](#), M. Corradi [id75a,75b](#), F. Corriveau [id106,ab](#), A. Cortes-Gonzalez [id159](#), M.J. Costa [id169](#),
 F. Costanza [id4](#), D. Costanzo [id145](#), J. Couthures [id4](#), G. Cowan [id97](#), K. Cranmer [id176](#), L. Cremer [id49](#),
 D. Cremonini [id24b,24a](#), S. Crépe-Renaudin [id60](#), F. Crescioli [id130](#), T. Cresta [id73a,73b](#), M. Cristinziani [id147](#),
 M. Cristoforetti [id78a,78b](#), V. Croft [id117](#), G. Crosetti [id44b,44a](#), A. Cueto [id101](#), H. Cui [id98](#), Z. Cui [id7](#),
 B.M. Cunnett [id152](#), W.R. Cunningham [id59](#), F. Curcio [id169](#), J.R. Curran [id52](#),
 M.J. Da Cunha Sargedas De Sousa [id57b,57a](#), J.V. Da Fonseca Pinto [id83b](#), C. Da Via [id103](#),
 W. Dabrowski [id86a](#), T. Dado [id37](#), S. Dahbi [id154](#), T. Dai [id108](#), D. Dal Santo [id20](#), C. Dallapiccola [id105](#),
 M. Dam [id43](#), G. D'amen [id30](#), V. D'Amico [id111](#), J. Damp [id102](#), J.R. Dandoy [id35](#), M. D'andrea [id57b,57a](#),
 D. Dannheim [id37](#), G. D'anniballe [id74a,74b](#), M. Danninger [id148](#), V. Dao [id151](#), G. Darbo [id57b](#),
 S.J. Das [id30](#), F. Dattola [id48](#), S. D'Auria [id71a,71b](#), A. D'Avanzo [id72a,72b](#), T. Davidek [id136](#),
 J. Davidson [id173](#), I. Dawson [id96](#), K. De [id8](#), C. De Almeida Rossi [id161](#), R. De Asmundis [id72a](#),
 N. De Biase [id48](#), S. De Castro [id24b,24a](#), N. De Groot [id116](#), P. de Jong [id117](#), H. De la Torre [id118](#),
 A. De Maria [id114a](#), A. De Salvo [id75a](#), U. De Sanctis [id76a,76b](#), F. De Santis [id70a,70b](#), A. De Santo [id152](#),
 J.B. De Vivie De Regie [id60](#), J. Debevc [id95](#), D.V. Dedovich [id39](#), J. Degens [id94](#), A.M. Deiana [id45](#),
 J. Del Peso [id101](#), L. Delagrangé [id130](#), F. Deliot [id138](#), C.M. Delitzsch [id49](#), M. Della Pietra [id72a,72b](#),
 D. Della Volpe [id56](#), A. Dell'Acqua [id37](#), L. Dell'Asta [id71a,71b](#), M. Delmastro [id4](#), C.C. Delogu [id102](#),
 P.A. Delsart [id60](#), S. Demers [id178](#), M. Demichev [id39](#), S.P. Denisov [id38](#), H. Denizli [id22a,1](#),
 L. D'Eramo [id41](#), D. Derendarz [id87](#), F. Derue [id130](#), P. Dervan [id94](#), A.M. Desai [id1](#), K. Desch [id25](#),
 F.A. Di Bello [id57b,57a](#), A. Di Ciaccio [id76a,76b](#), L. Di Ciaccio [id4](#), A. Di Domenico [id75a,75b](#),
 C. Di Donato [id72a,72b](#), A. Di Girolamo [id37](#), G. Di Gregorio [id37](#), A. Di Luca [id78a,78b](#),
 B. Di Micco [id77a,77b](#), R. Di Nardo [id77a,77b](#), K.F. Di Petrillo [id40](#), M. Diamantopoulou [id35](#), F.A. Dias [id117](#),
 M.A. Diaz [id140a,140b](#), A.R. Didenko [id39](#), M. Didenko [id169](#), S.D. Diefenbacher [id18a](#), E.B. Diehl [id108](#),
 S. Díez Cornell [id48](#), C. Díez Pardos [id147](#), C. Dimitriadi [id150](#), A. Dimitrievska [id21](#), A. Dimri [id151](#),
 Y. Ding [id62](#), J. Dingfelder [id25](#), T. Dingley [id129](#), I-M. Dinu [id28b](#), S.J. Dittmeier [id63b](#), F. Dittus [id37](#),
 M. Divisek [id136](#), B. Dixit [id94](#), F. Djama [id104](#), T. Djobava [id155b](#), C. Doglioni [id103,100](#),
 A. Dohnalova [id29a](#), Z. Dolezal [id136](#), K. Domijan [id86a](#), K.M. Dona [id40](#), M. Donadelli [id83d](#),
 B. Dong [id109](#), J. Donini [id41](#), A. D'Onofrio [id72a,72b](#), M. D'Onofrio [id94](#), J. Dopke [id137](#), A. Doria [id72a](#),
 N. Dos Santos Fernandes [id133a](#), I.A. Dos Santos Luz [id83e](#), P. Dougan [id103](#), M.T. Dova [id92](#),
 A.T. Doyle [id59](#), M.P. Drescher [id55](#), E. Dreyer [id175](#), I. Drivas-koulouris [id10](#), M. Drnevich [id120](#),
 D. Du [id62](#), T.A. du Pree [id117](#), Z. Duan [id114a](#), M. Dubau [id4](#), F. Dubinin [id39](#), M. Dubovsky [id29a](#),
 E. Duchovni [id175](#), G. Duckeck [id111](#), P.K. Duckett [id98](#), O.A. Ducu [id28b](#), D. Duda [id52](#), A. Dudarev [id37](#),
 M.M. Dudek [id87](#), E.R. Duden [id27](#), M. D'uffizi [id103](#), L. Duflost [id66](#), M. Dührssen [id37](#), I. Duminica [id28g](#),
 A.E. Dumitriu [id28b](#), M. Dunford [id63a](#), K. Dunne [id47a,47b](#), A. Duperrin [id104](#), H. Duran Yildiz [id3a](#),
 A. Durglishvili [id155b](#), G.I. Dyckes [id18a](#), M. Dyndal [id86a](#), B.S. Dziedzic [id37](#), Z.O. Earnshaw [id152](#),
 G.H. Eberwein [id129](#), B. Eckerova [id29a](#), S. Eggebrecht [id55](#), E. Egidio Purcino De Souza [id83e](#),
 G. Eigen [id17](#), K. Einsweiler [id18a](#), T. Ekelof [id167](#), P.A. Ekman [id100](#), S. El Farkh [id36b](#), Y. El Ghazali [id62](#),
 H. El Jarrari [id37](#), A. El Moussaouy [id36a](#), D. Elitez [id37](#), M. Ellert [id167](#), F. Ellinghaus [id177](#),
 T.A. Elliot [id97](#), N. Ellis [id37](#), J. Elmsheuser [id30](#), M. Elsayy [id119a](#), M. Elsing [id37](#), D. Emeliyanov [id137](#),
 Y. Enari [id84](#), C. Engel [id102](#), S. Epari [id110](#), D. Ernani Martins Neto [id87](#), F. Ernst [id37](#), M. Errenst [id177](#),
 M. Escalier [id66](#), C. Escobar [id169](#), E. Etzion [id157](#), G. Evans [id133a,133b](#), H. Evans [id68](#), L.S. Evans [id48](#),

A. Ezhilov ^{id}38, S. Ezzarqtouni ^{id}36a, F. Fabbri ^{id}24b,24a, L. Fabbri ^{id}24b,24a, G. Facini ^{id}98, V. Fadeyev ^{id}139, R.M. Fakhrutdinov ^{id}38, D. Fakoudis ^{id}102, S. Falciano ^{id}75a, L.F. Falda Ulhoa Coelho ^{id}133a, F. Fallavollita ^{id}112, G. Falsetti ^{id}44b,44a, J. Faltova ^{id}136, C. Fan ^{id}168, K.Y. Fan ^{id}64b, Y. Fan ^{id}14, Y. Fang ^{id}14,114c, M. Fanti ^{id}71a,71b, M. Faraj ^{id}69a,69b, Z. Farazpay ^{id}99, A. Farbin ^{id}8, A. Farilla ^{id}77a, K. Farman ^{id}154, T. Farooque ^{id}109, J.N. Farr ^{id}178, S.M. Farrington ^{id}137,52, F. Fassi ^{id}36e, D. Fassouliotis ^{id}9, L. Fayard ^{id}66, P. Federic ^{id}136, P. Federicova ^{id}134, O.L. Fedin ^{id}38,a, M. Feickert ^{id}176, L. Feligioni ^{id}104, D.E. Fellers ^{id}18a, C. Feng ^{id}143a, Y. Feng ^{id}14, Z. Feng ^{id}117, M.J. Fenton ^{id}165, L. Ferencz ^{id}48, B. Fernandez Barbadillo ^{id}93, P. Fernandez Martinez ^{id}67, M.J.V. Fernoux ^{id}104, J. Ferrando ^{id}93, A. Ferrari ^{id}167, P. Ferrari ^{id}117,116, R. Ferrari ^{id}73a, D. Ferrere ^{id}56, C. Ferretti ^{id}108, M.P. Fewell ^{id}1, D. Fiacco ^{id}75a,75b, F. Fiedler ^{id}102, P. Fiedler ^{id}135, S. Filimonov ^{id}39, M.S. Filip ^{id}28b,t, A. Filipčič ^{id}95, E.K. Filmer ^{id}162a, F. Filthaut ^{id}116, M.C.N. Fiolhais ^{id}133a,133c,c, L. Fiorini ^{id}169, W.C. Fisher ^{id}109, T. Fitschen ^{id}103, P.M. Fitzhugh ^{id}138, I. Fleck ^{id}147, P. Fleischmann ^{id}108, T. Flick ^{id}177, M. Flores ^{id}34d,ag, L.R. Flores Castillo ^{id}64a, L. Flores Sanz De Acedo ^{id}37, F.M. Follega ^{id}78a,78b, N. Fomin ^{id}33, J.H. Foo ^{id}161, A. Formica ^{id}138, A.C. Forti ^{id}103, E. Fortin ^{id}37, A.W. Fortman ^{id}18a, L. Foster ^{id}18a, L. Fountas ^{id}9,i, D. Fournier ^{id}66, H. Fox ^{id}93, P. Francavilla ^{id}74a,74b, S. Francescato ^{id}61, S. Franchellucci ^{id}56, M. Franchini ^{id}24b,24a, S. Franchino ^{id}63a, D. Francis ^{id}37, L. Franco ^{id}116, L. Franconi ^{id}48, M. Franklin ^{id}61, G. Frattari ^{id}27, Y.Y. Frid ^{id}157, J. Friend ^{id}59, N. Fritzsche ^{id}37, A. Froch ^{id}56, D. Froidevaux ^{id}37, J.A. Frost ^{id}129, Y. Fu ^{id}109, S. Fuenzalida Garrido ^{id}140g, M. Fujimoto ^{id}151, K.Y. Fung ^{id}64a, E. Furtado De Simas Filho ^{id}83e, M. Furukawa ^{id}159, J. Fuster ^{id}169, A. Gaa ^{id}55, A. Gabrielli ^{id}24b,24a, A. Gabrielli ^{id}161, P. Gadow ^{id}37, G. Gagliardi ^{id}57b,57a, L.G. Gagnon ^{id}18a, S. Gaid ^{id}88b, S. Galantzan ^{id}157, J. Gallagher ^{id}1, E.J. Gallas ^{id}129, A.L. Gallen ^{id}167, B.J. Gallop ^{id}137, K.K. Gan ^{id}122, S. Ganguly ^{id}159, Y. Gao ^{id}52, A. Garabaglu ^{id}142, F.M. Garay Walls ^{id}140a,140b, C. García ^{id}169, A. Garcia Alonso ^{id}117, A.G. Garcia Caffaro ^{id}178, J.E. García Navarro ^{id}169, M.A. Garcia Ruiz ^{id}23b, M. Garcia-Sciveres ^{id}18a, G.L. Gardner ^{id}131, R.W. Gardner ^{id}40, N. Garelli ^{id}164, R.B. Garg ^{id}149, J.M. Gargan ^{id}33, C.A. Garner ^{id}161, C.M. Garvey ^{id}34a, V.K. Gassmann ^{id}164, G. Gaudio ^{id}73a, V. Gautam ^{id}13, P. Gauzzi ^{id}75a,75b, J. Gavranovic ^{id}95, I.L. Gavrilenko ^{id}133a, A. Gavrilyuk ^{id}38, C. Gay ^{id}170, G. Gaycken ^{id}126, E.N. Gazis ^{id}10, A. Gekow ^{id}122, C. Gemme ^{id}57b, M.H. Genest ^{id}60, A.D. Gentry ^{id}115, S. George ^{id}97, T. Geralis ^{id}46, A.A. Gerwin ^{id}123, P. Gessinger-Befurt ^{id}37, M.E. Geyik ^{id}177, M. Ghani ^{id}173, K. Ghorbanian ^{id}96, A. Ghosal ^{id}147, A. Ghosh ^{id}165, A. Ghosh ^{id}7, B. Giacobbe ^{id}24b, S. Giagu ^{id}75a,75b, T. Giani ^{id}117, A. Giannini ^{id}62, S.M. Gibson ^{id}97, M. Gignac ^{id}139, D.T. Gil ^{id}86b, A.K. Gilbert ^{id}86a, B.J. Gilbert ^{id}42, D. Gillberg ^{id}35, G. Gilles ^{id}117, D.M. Gingrich ^{id}2,ai, M.P. Giordani ^{id}69a,69c, P.F. Giraud ^{id}138, G. Giugliarelli ^{id}69a,69c, D. Giugni ^{id}71a, F. Giuli ^{id}76a,76b, I. Gkialas ^{id}9,i, L.K. Gladilin ^{id}38, C. Glasman ^{id}101, M. Glazewska ^{id}20, R.M. Gleason ^{id}165, G. Glemža ^{id}48, M. Glisic ^{id}126, I. Gnesi ^{id}44b, Y. Go ^{id}30, M. Goblirsch-Kolb ^{id}37, B. Gocke ^{id}49, D. Godin ^{id}110, B. Gokturk ^{id}22a, S. Goldfarb ^{id}107, T. Golling ^{id}56, M.G.D. Gololo ^{id}34c, D. Golubkov ^{id}38, J.P. Gombas ^{id}109, A. Gomes ^{id}133a,133b, G. Gomes Da Silva ^{id}147, A.J. Gomez Delegido ^{id}37, R. Gonçalves ^{id}133a, L. Gonella ^{id}21, A. Gongadze ^{id}155c, F. Gonnella ^{id}21, J.L. Gonski ^{id}149, R.Y. González Andana ^{id}52, S. González de la Hoz ^{id}169, M.V. Gonzalez Rodrigues ^{id}48, R. Gonzalez Suarez ^{id}167, S. Gonzalez-Sevilla ^{id}56, L. Goossens ^{id}37, B. Gorini ^{id}37, E. Gorini ^{id}70a,70b, A. Gorišek ^{id}95, T.C. Gosart ^{id}131, A.T. Goshaw ^{id}51, M.I. Gostkin ^{id}39, S. Goswami ^{id}124, C.A. Gottardo ^{id}37, S.A. Gotz ^{id}111, M. Goughri ^{id}36b, A.G. Goussiou ^{id}142, N. Govender ^{id}34c, R.P. Grabarczyk ^{id}129, I. Grabowska-Bold ^{id}86a, K. Graham ^{id}35, E. Gramstad ^{id}128, S. Grancagnolo ^{id}70a,70b, C.M. Grant ^{id}1, P.M. Gravila ^{id}28f, F.G. Gravili ^{id}70a,70b, H.M. Gray ^{id}18a, M. Greco ^{id}112, M.J. Green ^{id}1, C. Grefe ^{id}25, A.S. Grefsrud ^{id}17, I.M. Gregor ^{id}48, K.T. Greif ^{id}165, P. Grenier ^{id}149, S.G. Grewe ^{id}112, A.A. Grillo ^{id}139, K. Grimm ^{id}32, S. Grinstein ^{id}13,x, J.-F. Grivaz ^{id}66, E. Gross ^{id}175, J. Grosse-Knetter ^{id}55, L. Guan ^{id}108, G. Guerrieri ^{id}37, R. Guevara ^{id}128, R. Gugel ^{id}102, J.A.M. Guhit ^{id}108, A. Guida ^{id}19, E. Guilloton ^{id}173, S. Guindon ^{id}37, F. Guo ^{id}14,114c, J. Guo ^{id}144a,

L. Guo ⁴⁸, L. Guo ^{114b,v}, Y. Guo ¹⁰⁸, A. Gupta ⁴⁹, R. Gupta ¹³², S. Gupta ²⁷, S. Gurbuz ²⁵,
 S.S. Gurdasani ⁴⁸, G. Gustavino ^{75a,75b}, P. Gutierrez ¹²³, L.F. Gutierrez Zagazeta ¹³¹,
 M. Gutsche ⁵⁰, C. Gutschow ⁹⁸, C. Gwenlan ¹²⁹, C.B. Gwilliam ⁹⁴, E.S. Haaland ¹²⁸,
 A. Haas ¹²⁰, M. Habedank ⁵⁹, C. Haber ^{18a}, H.K. Hadavand ⁸, A. Haddad ⁴¹, A. Hadeif ⁵⁰,
 A.I. Hagan ⁹³, J.J. Hahn ¹⁴⁷, E.H. Haines ⁹⁸, M. Haleem ¹⁷², J. Haley ¹²⁴, G.D. Hallewell ¹⁰⁴,
 K. Hamano ¹⁷¹, H. Hamdaoui ¹⁶⁷, M. Hamer ²⁵, S.E.D. Hammoud ⁶⁶, E.J. Hampshire ⁹⁷,
 J. Han ^{143a}, L. Han ^{114a}, L. Han ⁶², S. Han ¹⁴, K. Hanagaki ⁸⁴, M. Hance ¹³⁹, D.A. Hangal ⁴²,
 H. Hanif ¹⁴⁸, M.D. Hank ¹³¹, J.B. Hansen ⁴³, P.H. Hansen ⁴³, D. Harada ⁵⁶, T. Harenberg ¹⁷⁷,
 S. Harkusha ¹⁷⁹, M.L. Harris ¹⁰⁵, Y.T. Harris ²⁵, J. Harrison ¹³, N.M. Harrison ¹²²,
 P.F. Harrison ¹⁷³, M.L.E. Hart ⁹⁸, N.M. Hartman ¹¹², N.M. Hartmann ¹¹¹, R.Z. Hasan ^{97,137},
 Y. Hasegawa ¹⁴⁶, F. Haslbeck ¹²⁹, S. Hassan ¹⁷, R. Hauser ¹⁰⁹, M. Haviernik ¹³⁶,
 C.M. Hawkes ²¹, R.J. Hawkings ³⁷, Y. Hayashi ¹⁵⁹, D. Hayden ¹⁰⁹, C. Hayes ¹⁰⁸,
 R.L. Hayes ¹¹⁷, C.P. Hays ¹²⁹, J.M. Hays ⁹⁶, H.S. Hayward ⁹⁴, M. He ^{14,114c}, Y. He ⁴⁸,
 Y. He ⁹⁸, N.B. Heatley ⁹⁶, V. Hedberg ¹⁰⁰, C. Heidegger ⁵⁴, K.K. Heidegger ⁵⁴, J. Heilman ³⁵,
 S. Heim ⁴⁸, T. Heim ^{18a}, J.J. Heinrich ¹²⁶, L. Heinrich ¹¹², J. Hejbal ¹³⁴, M. Helbig ⁵⁰,
 A. Held ¹⁷⁶, S. Hellesund ¹⁷, C.M. Helling ¹⁷⁰, S. Hellman ^{47a,47b}, A.M. Henriques Correia ³⁷,
 H. Herde ¹⁰⁰, Y. Hernández Jiménez ¹⁵¹, L.M. Herrmann ²⁵, T. Herrmann ⁵⁰, G. Herten ⁵⁴,
 R. Hertenberger ¹¹¹, L. Hervas ³⁷, M.E. Hesping ¹⁰², N.P. Hessey ^{162a}, J. Hessler ¹¹²,
 M. Hidaoui ^{36b}, N. Hidic ¹³⁶, E. Hill ¹⁶¹, T.S. Hillersoy ¹⁷, S.J. Hillier ²¹, J.R. Hinds ¹⁰⁹,
 F. Hinterkeuser ²⁵, M. Hirose ¹²⁷, S. Hirose ¹⁶³, D. Hirschbuehl ¹⁷⁷, T.G. Hitchings ¹⁰³,
 B. Hiti ⁹⁵, J. Hobbs ¹⁵¹, R. Hobincu ^{28e}, N. Hod ¹⁷⁵, A.M. Hodges ¹⁶⁸, M.C. Hodgkinson ¹⁴⁵,
 B.H. Hodgkinson ¹²⁹, A. Hoecker ³⁷, D.D. Hofer ¹⁰⁸, J. Hofer ¹⁶⁹, J. Hofner ¹⁰², M. Holzbock ³⁷,
 L.B.A.H. Hommels ³³, V. Homsak ¹²⁹, B.P. Honan ¹⁰³, J.J. Hong ⁶⁸, T.M. Hong ¹³²,
 B.H. Hooberman ¹⁶⁸, W.H. Hopkins ⁶, M.C. Hoppesch ¹⁶⁸, Y. Horii ¹¹³, M.E. Horstmann ¹¹²,
 S. Hou ¹⁵⁴, M.R. Housenga ¹⁶⁸, J. Howarth ⁵⁹, J. Hoya ⁶, M. Hrabovsky ¹²⁵, T. Hryn'ova ⁴,
 P.J. Hsu ⁶⁵, S.-C. Hsu ¹⁴², T. Hsu ⁶⁶, M. Hu ^{18a}, Q. Hu ⁶², S. Huang ³³, X. Huang ^{14,114c},
 Y. Huang ¹³⁶, Y. Huang ^{114b}, Y. Huang ¹⁴, Z. Huang ⁶⁶, Z. Hubacek ¹³⁵, F. Huegging ²⁵,
 T.B. Huffman ¹²⁹, M. Hufnagel Maranha De Faria ^{83a}, C.A. Hugli ⁴⁸, M. Huhtinen ³⁷,
 S.K. Huiberts ¹⁷, R. Hulsken ¹⁰⁶, C.E. Hultquist ^{18a}, D.L. Humphreys ¹⁰⁵, N. Huseynov ¹²,
 J. Huston ¹⁰⁹, J. Huth ⁶¹, L. Huth ⁴⁸, R. Hyneman ⁷, G. Iacobucci ⁵⁶, G. Iakovidis ³⁰,
 L. Iconomidou-Fayard ⁶⁶, J.P. Iddon ³⁷, P. Iengo ^{72a,72b}, R. Iguchi ¹⁵⁹, Y. Iiyama ¹⁵⁹,
 T. Iizawa ¹⁵⁹, Y. Ikegami ⁸⁴, D. Iliadis ¹⁵⁸, N. Ilic ¹⁶¹, H. Imam ^{36a}, G. Inacio Goncalves ^{83d},
 S.A. Infante Cabanas ^{140c}, T. Ingebretsen Carlson ^{47a,47b}, J.M. Inglis ⁹⁶, G. Introzzi ^{73a,73b},
 M. Iodice ^{77a}, V. Ippolito ^{75a,75b}, R.K. Irwin ⁹⁴, M. Ishino ¹⁵⁹, W. Islam ¹⁷⁶, C. Issever ¹⁹,
 S. Istin ^{22a,ao}, K. Itabashi ⁸⁴, H. Ito ¹⁷⁴, R. Iuppa ^{78a,78b}, A. Ivina ¹⁷⁵, V. Izzo ^{72a}, P. Jacka ¹³⁵,
 P. Jackson ¹, P. Jain ⁴⁸, K. Jakobs ⁵⁴, T. Jakoubek ¹⁷⁵, J. Jamieson ⁵⁹, W. Jang ¹⁵⁹,
 S. Jankovych ¹³⁶, M. Javurkova ¹⁰⁵, P. Jawahar ¹⁰³, L. Jeanty ¹²⁶, J. Jejelava ^{155a,ae}, P. Jenni ^{54,f},
 C.E. Jessiman ³⁵, C. Jia ^{143a}, H. Jia ¹⁷⁰, J. Jia ¹⁵¹, X. Jia ^{112,114c}, Z. Jia ^{114a}, C. Jiang ⁵²,
 Q. Jiang ^{64b}, S. Jiggins ⁴⁸, M. Jimenez Ortega ¹⁶⁹, J. Jimenez Pena ¹³, S. Jin ^{114a}, A. Jinaru ^{28b},
 O. Jinnouchi ¹⁴¹, P. Johansson ¹⁴⁵, K.A. Johns ⁷, J.W. Johnson ¹³⁹, F.A. Jolly ⁴⁸,
 D.M. Jones ¹⁵², E. Jones ⁴⁸, K.S. Jones ⁸, P. Jones ³³, R.W.L. Jones ⁹³, T.J. Jones ⁹⁴,
 H.L. Joos ⁵⁵, R. Joshi ¹²², J. Jovicevic ¹⁶, X. Ju ^{18a}, J.J. Junggeburth ³⁷, T. Junkermann ^{63a},
 A. Juste Rozas ^{13,x}, M.K. Juzek ⁸⁷, S. Kabana ^{140f}, A. Kaczmarska ⁸⁷, S.A. Kadir ¹⁴⁹,
 M. Kado ¹¹², H. Kagan ¹²², M. Kagan ¹⁴⁹, A. Kahn ¹³¹, C. Kahra ¹⁰², T. Kaji ¹⁵⁹,
 E. Kajomovitz ¹⁵⁶, N. Kakati ¹⁷⁵, N. Kakoty ¹³, I. Kalaitzidou ⁵⁴, S. Kandel ⁸, N.J. Kang ¹³⁹,
 D. Kar ^{34h}, E. Karentzos ²⁵, K. Karki ⁸, O. Karkout ¹¹⁷, S.N. Karpov ³⁹, Z.M. Karpova ³⁹,
 V. Kartvelishvili ⁹³, A.N. Karyukhin ³⁸, E. Kasimi ¹⁵⁸, J. Katzy ⁴⁸, S. Kaur ³⁵, K. Kawade ¹⁴⁶,

M.P. Kawale [id123](#), C. Kawamoto [id89](#), T. Kawamoto [id62](#), E.F. Kay [id37](#), F.I. Kaya [id164](#), S. Kazakos [id109](#),
V.F. Kazanin [id38](#), J.M. Keaveney [id34a](#), R. Keeler [id171](#), G.V. Kehris [id61](#), J.S. Keller [id35](#), J.M. Kelly [id171](#),
J.J. Kempster [id152](#), O. Kepka [id134](#), J. Kerr [id162b](#), B.P. Kerridge [id137](#), B.P. Kerševan [id95](#),
L. Keszeghova [id29a](#), R.A. Khan [id132](#), A. Khanov [id124](#), A.G. Kharlamov [id38](#), T. Kharlamova [id38](#),
E.E. Khoda [id142](#), M. Kholodenko [id133a](#), T.J. Khoo [id19](#), G. Khorauli [id172](#), Y. Khoulaki [id36a](#),
J. Khubua [id155b,*](#), Y.A.R. Khwairia [id130](#), B. Kibirige^{34h}, D. Kim [id6](#), D.W. Kim [id47a,47b](#), Y.K. Kim [id40](#),
N. Kimura [id98](#), M.K. Kingston [id55](#), A. Kirchhoff [id55](#), C. Kirfel [id25](#), F. Kirfel [id25](#), J. Kirk [id137](#),
A.E. Kiryunin [id112](#), S. Kita [id163](#), O. Kivernyk [id25](#), M. Klassen [id164](#), C. Klein [id35](#), L. Klein [id172](#),
M.H. Klein [id45](#), S.B. Klein [id56](#), U. Klein [id94](#), A. Klimentov [id30](#), T. Klioutchnikova [id37](#), P. Kluit [id117](#),
S. Kluth [id112](#), E. Kneringer [id79](#), T.M. Knight [id161](#), A. Knue [id49](#), M. Kobel [id50](#), D. Kobylanski [id175](#),
S.F. Koch [id129](#), M. Kocian [id149](#), P. Kodyš [id136](#), D.M. Koeck [id126](#), T. Koffas [id35](#), O. Kolay [id50](#),
I. Koletsou [id4](#), T. Komarek [id87](#), K. Köneke [id55](#), A.X.Y. Kong [id1](#), T. Kono [id121](#), N. Konstantinidis [id98](#),
P. Kontaxakis [id56](#), B. Konya [id100](#), R. Kopeliansky [id42](#), S. Koperny [id86a](#), K. Korcyl [id87](#),
K. Kordas [id158,d](#), A. Korn [id98](#), S. Korn [id55](#), I. Korolkov [id13](#), N. Korotkova [id38](#), B. Kortman [id117](#),
O. Kortner [id112](#), S. Kortner [id112](#), W.H. Kostecka [id118](#), M. Kostov [id29a](#), V.V. Kostyukhin [id147](#),
A. Kotsokechagia [id37](#), A. Kotwal [id51](#), A. Koulouris [id37](#), A. Kourkoumeli-Charalampidi [id73a,73b](#),
C. Kourkoumelis [id9](#), E. Kourlitis [id112](#), O. Kovanda [id126](#), R. Kowalewski [id171](#), W. Kozanecki [id126](#),
A.S. Kozhin [id38](#), V.A. Kramarenko [id38](#), G. Kramberger [id95](#), P. Kramer [id25](#), M.W. Krasny [id130](#),
A. Krasznahorkay [id105](#), A.C. Kraus [id118](#), J.W. Kraus [id177](#), J.A. Kremer [id48](#), N.B. Krenzel [id147](#),
T. Kresse [id50](#), L. Kretschmann [id177](#), J. Kretzschmar [id94](#), P. Krieger [id161](#), K. Krizka [id21](#),
K. Kroeninger [id49](#), H. Kroha [id112](#), J. Kroll [id134](#), J. Kroll [id131](#), K.S. Krowpman [id109](#), U. Kruchonak [id39](#),
H. Krüger [id25](#), N. Krumnack⁸¹, M.C. Kruse [id51](#), O. Kuchinskaia [id39](#), S. Kuday [id3a](#), S. Kuehn [id37](#),
R. Kuesters [id54](#), T. Kuhl [id48](#), V. Kukhtin [id39](#), Y. Kulchitsky [id39](#), S. Kuleshov [id140d,140b](#), J. Kull [id1](#),
E.V. Kumar [id111](#), M. Kumar [id34h](#), N. Kumari [id48](#), P. Kumari [id162b](#), A. Kupco [id134](#), A. Kupich [id38](#),
O. Kuprash [id54](#), H. Kurashige [id85](#), L.L. Kurchaninov [id162a](#), O. Kurdysh [id4](#), Y.A. Kurochkin [id38](#),
A. Kurova [id38](#), M. Kuze [id141](#), A.K. Kvam [id105](#), J. Kvita [id125](#), N.G. Kyriacou [id142](#), C. Lacasta [id169](#),
F. Lacava [id75a,75b](#), H. Lacker [id19](#), D. Lacour [id130](#), N.N. Lad [id98](#), E. Ladygin [id39](#), A. Lafarge [id41](#),
B. Laforge [id130](#), T. Lagouri [id178](#), F.Z. Lahbabi [id36a](#), S. Lai [id55,37](#), W.S. Lai [id98](#), J.E. Lambert [id171](#),
S. Lammers [id68](#), W. Lampl [id7](#), C. Lampoudis [id158,d](#), G. Lamprinoudis [id102](#), A.N. Lancaster [id118](#),
E. Lançon [id30](#), U. Landgraf [id54](#), M.P.J. Landon [id96](#), V.S. Lang [id54](#), O.K.B. Langrekken [id128](#),
A.J. Lankford [id165](#), F. Lanni [id37](#), K. Lantzsch [id25](#), A. Lanza [id73a](#), M. Lanzac Berrocal [id169](#),
J.F. Laporte [id138](#), T. Lari [id71a](#), D. Larsen [id17](#), L. Larson [id11](#), F. Lasagni Manghi [id24b](#), M. Lassnig [id37](#),
S.D. Lawlor [id145](#), R. Lazaridou¹⁶⁵, M. Lazzaroni [id71a,71b](#), E.T.T. Le¹⁶⁵, H.D.M. Le [id109](#),
E.M. Le Boulicaut [id178](#), L.T. Le Pottier [id18a](#), B. Leban [id24b,24a](#), F. Ledroit-Guillon [id60](#), T.F. Lee [id162b](#),
L.L. Leeuw [id34c](#), M. Lefebvre [id171](#), C. Leggett [id18a](#), G. Lehmann Miotto [id37](#), M. Leigh [id56](#),
W.A. Leight [id105](#), W. Leinonen [id116](#), A. Leisos [id158,u](#), M.A.L. Leite [id83c](#), C.E. Leitgeb [id19](#),
R. Leitner [id136](#), K.J.C. Leney [id45](#), T. Lenz [id25](#), S. Leone [id74a](#), C. Leonidopoulos [id52](#), A. Leopold [id150](#),
J.H. Lepage Bourbonnais [id35](#), R. Les [id109](#), C.G. Lester [id33](#), M. Levchenko [id38](#), J. Levêque [id4](#),
L.J. Levinson [id175](#), G. Levrini [id24b,24a](#), M.P. Lewicki [id87](#), C. Lewis [id142](#), D.J. Lewis [id4](#), L. Lewitt [id145](#),
A. Li [id30](#), B. Li [id143a](#), C. Li¹⁰⁸, C-Q. Li [id112](#), H. Li [id143a](#), H. Li [id103](#), H. Li [id15](#), H. Li⁶², H. Li [id143a](#),
J. Li [id144a](#), K. Li [id14](#), L. Li [id144a](#), R. Li [id178](#), S. Li [id14,114c](#), S. Li [id144b,144a](#), T. Li [id5](#), X. Li [id106](#), Y. Li¹⁴,
Z. Li [id159](#), Z. Li [id14,114c](#), Z. Li [id62](#), S. Liang [id14,114c](#), Z. Liang [id14](#), M. Liberatore [id138](#), B. Liberti [id76a](#),
G.B. Libotte [id83d](#), K. Lie [id64c](#), J. Lieber Marin [id83e](#), H. Lien [id68](#), H. Lin [id108](#), S.F. Lin [id151](#),
L. Linden [id111](#), R.E. Lindley [id7](#), J.H. Lindon [id37](#), J. Ling [id61](#), E. Lipeles [id131](#), A. Lipniacka [id17](#),
A. Lister [id170](#), J.D. Little [id68](#), B. Liu [id14](#), B.X. Liu [id114b](#), D. Liu [id144b,144a](#), D. Liu [id139](#),
E.H.L. Liu [id21](#), J.K.K. Liu [id120](#), K. Liu [id144b](#), K. Liu [id144b,144a](#), M. Liu [id62](#), M.Y. Liu [id62](#), P. Liu [id14](#),
Q. Liu [id144b,142,144a](#), S. Liu [id151](#), X. Liu [id62](#), X. Liu [id143a](#), Y. Liu [id114b,114c](#), Y. Liu [id168](#), Y.L. Liu [id143a](#),










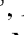
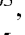
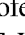


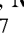
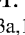
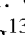


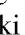



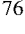



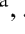

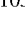


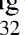
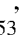
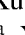

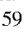



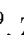
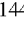
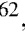
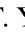





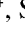


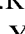


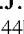
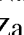
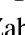
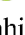
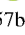






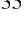
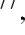
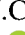
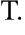

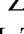
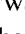

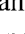


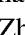

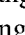





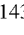

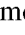
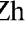
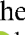
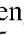


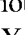

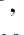





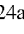



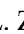






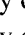















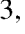




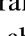


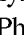





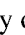
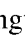



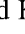
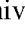
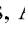




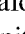
Y.W. Liu ⁶², Z. Liu ^{66,k}, S.L. Lloyd ⁹⁶, E.M. Lobodzinska ⁴⁸, P. Loch ⁷, E. Lodhi ¹⁶¹,
 K. Lohwasser ¹⁴⁵, E. Loiacono ⁴⁸, J.D. Lomas ²¹, J.D. Long ⁴², I. Longarini ¹⁶⁵, R. Longo ¹⁶⁸,
 A. Lopez Solis ¹³, N.A. Lopez-canelas ⁷, N. Lorenzo Martinez ⁴, A.M. Lory ¹¹¹, M. Losada ^{119a},
 G. Löschcke Centeno ⁴, X. Lou ^{47a,47b}, X. Lou ^{14,114c}, A. Lounis ⁶⁶, P.A. Love ⁹³, M. Lu ⁶⁶,
 S. Lu ¹³¹, Y.J. Lu ¹⁵⁴, H.J. Lubatti ¹⁴², C. Luci ^{75a,75b}, F.L. Lucio Alves ^{114a}, F. Luehring ⁶⁸,
 B.S. Lunday ¹³¹, O. Lundberg ¹⁵⁰, J. Lunde ³⁷, N.A. Luongo ⁶, M.S. Lutz ³⁷, A.B. Lux ²⁶,
 D. Lynn ³⁰, R. Lysak ¹³⁴, V. Lysenko ¹³⁵, E. Lytken ¹⁰⁰, V. Lyubushkin ³⁹, T. Lyubushkina ³⁹,
 M.M. Lyukova ¹⁵¹, M.Firdaus M. Soberi ⁵², H. Ma ³⁰, K. Ma ⁶², L.L. Ma ^{143a}, W. Ma ⁶²,
 Y. Ma ¹²⁴, J.C. MacDonald ¹⁰², P.C. Machado De Abreu Farias ^{83e}, D. Macina ³⁷, R. Madar ⁴¹,
 T. Madula ⁹⁸, J. Maeda ⁸⁵, T. Maeno ³⁰, P.T. Mafa ^{34c,j}, H. Maguire ¹⁴⁵, M. Maheshwari ³³,
 V. Maiboroda ⁶⁶, A. Maio ^{133a,133b,133d}, K. Maj ^{86a}, O. Majersky ⁴⁸, S. Majewski ¹²⁶,
 R. Makhmanazarov ³⁸, N. Makovec ⁶⁶, V. Maksimovic ¹⁶, B. Malaescu ¹³⁰, J. Malamant ¹²⁸,
 Pa. Malecki ⁸⁷, V.P. Maleev ³⁸, F. Malek ^{60,o}, M. Mali ⁹⁵, D. Malito ⁹⁷, U. Mallik ^{80,*},
 A. Maloizel ⁵, S. Maltezos ¹⁰, A. Malvezzi Lopes ^{83d}, S. Malyukov ³⁹, J. Mamuzic ⁹⁵, G. Mancini ⁵³,
 M.N. Mancini ²⁷, G. Manco ^{73a,73b}, J.P. Mandalia ⁹⁶, S.S. Mandarry ¹⁵², I. Mandić ⁹⁵,
 L. Manhaes de Andrade Filho ^{83a}, I.M. Maniatis ¹⁷⁵, J. Manjarres Ramos ⁹¹, D.C. Mankad ¹⁷⁵,
 A. Mann ¹¹¹, T. Manoussos ³⁷, M.N. Mantinan ⁴⁰, S. Manzoni ³⁷, L. Mao ^{144a},
 X. Mapekula ^{34c}, A. Marantis ¹⁵⁸, R.R. Marcelo Gregorio ⁹⁶, G. Marchiori ⁵, C. Marcon ^{71a},
 E. Maricic ¹⁶, M. Marinescu ⁴⁸, S. Marium ⁴⁸, M. Marjanovic ¹²³, A. Markhoos ⁵⁴,
 M. Markovitch ⁶⁶, M.K. Maroun ¹⁰⁵, M.C. Marr ¹⁴⁸, G.T. Marsden ¹⁰³, E.J. Marshall ⁹³,
 Z. Marshall ^{18a}, S. Marti-Garcia ¹⁶⁹, J. Martin ⁹⁸, T.A. Martin ¹³⁷, V.J. Martin ⁵²,
 B. Martin dit Latour ¹⁷, L. Martinelli ^{75a,75b}, M. Martinez ^{13,x}, P. Martinez Agullo ¹⁶⁹,
 V.I. Martinez Outschoorn ¹⁰⁵, P. Martinez Suarez ³⁷, S. Martin-Haugh ¹³⁷, G. Martinovicova ¹³⁶,
 V.S. Martoiu ^{28b}, A.C. Martyniuk ⁹⁸, A. Marzin ³⁷, D. Mascione ^{78a,78b}, L. Masetti ¹⁰²,
 J. Masik ¹⁰³, A.L. Maslennikov ³⁹, S.L. Mason ⁴², P. Massarotti ^{72a,72b}, P. Mastrandrea ^{74a,74b},
 A. Mastroberardino ^{44b,44a}, T. Masubuchi ¹²⁷, T.T. Mathew ¹²⁶, J. Matousek ¹³⁶, D.M. Mattern ⁴⁹,
 J. Maurer ^{28b}, T. Maurin ⁵⁹, A.J. Maury ⁶⁶, B. Maček ⁹⁵, C. Mavungu Tsava ¹⁰⁴,
 D.A. Maximov ³⁸, A.E. May ¹⁰³, E. Mayer ⁴¹, R. Mazini ^{34h}, I. Maznas ¹¹⁸, S.M. Mazza ¹³⁹,
 E. Mazzeo ³⁷, J.P. Mc Gowan ¹⁷¹, S.P. Mc Kee ¹⁰⁸, C.A. Mc Lean ⁶, C.C. McCracken ¹⁷⁰,
 E.F. McDonald ¹⁰⁷, A.E. McDougall ¹¹⁷, L.F. Mcelhinney ⁹³, J.A. Mcfayden ¹⁵²,
 R.P. McGovern ¹³¹, R.P. Mckenzie ^{34h}, T.C. McLachlan ⁴⁸, D.J. McLaughlin ⁹⁸, S.J. McMahon ¹³⁷,
 C.M. Mcpartland ⁹⁴, R.A. McPherson ^{171,ab}, S. Mehlhase ¹¹¹, A. Mehta ⁹⁴, D. Melini ¹⁶⁹,
 B.R. Mellado Garcia ^{34h}, A.H. Melo ⁵⁵, F. Meloni ⁴⁸, A.M. Mendes Jacques Da Costa ¹⁰³,
 L. Meng ⁹³, S. Menke ¹¹², M. Mentink ³⁷, E. Meoni ^{44b,44a}, G. Mercado ¹¹⁸, S. Merianos ¹⁵⁸,
 C. Merlassino ^{69a,69c}, C. Meroni ^{71a,71b}, J. Metcalfe ⁶, A.S. Mete ⁶, E. Meuser ¹⁰², C. Meyer ⁶⁸,
 J-P. Meyer ¹³⁸, Y. Miao ^{114a}, R.P. Middleton ¹³⁷, M. Mihovilovic ⁶⁶, L. Mijović ⁵²,
 G. Mikenberg ¹⁷⁵, M. Mikestikova ¹³⁴, M. Mikuž ⁹⁵, H. Mildner ¹⁰², A. Milic ³⁷,
 D.W. Miller ⁴⁰, E.H. Miller ¹⁴⁹, A. Milov ¹⁷⁵, D.A. Milstead ^{47a,47b}, T. Min ^{114a}, A.A. Minaenko ³⁸,
 I.A. Minashvili ^{155b}, A.I. Mincer ¹²⁰, B. Mindur ^{86a}, M. Mineev ³⁹, Y. Mino ⁸⁹, L.M. Mir ¹³,
 M. Miralles Lopez ⁵⁹, M. Mironova ^{18a}, M.C. Missio ⁴¹, A. Mitra ¹⁷³, V.A. Mitsou ¹⁶⁹,
 Y. Mitsumori ¹¹³, O. Miu ¹⁶¹, P.S. Miyagawa ⁹⁶, T. Mkrtchyan ³⁷, M. Mlinarevic ⁹⁸,
 T. Mlinarevic ⁹⁸, M. Mlynarikova ¹³⁶, L. Mlynarska ^{86a}, C. Mo ^{144a}, S. Mobius ²⁰,
 M.H. Mohamed Farook ¹¹⁵, S. Mohapatra ⁴², S. Mohiuddin ¹²⁴, G. Mokgatitswane ^{34h},
 L. Moleri ¹⁷⁵, U. Molinatti ¹²⁹, L.G. Mollier ²⁰, B. Mondal ¹³⁴, S. Mondal ¹³⁵, K. Mönig ⁴⁸,
 E. Monnier ¹⁰⁴, L. Monsonis Romero ¹⁶⁹, J. Montejo Berlingen ¹³, A. Montella ^{47a,47b},
 M. Montella ¹²², F. Montekali ^{77a,77b}, F. Monticelli ⁹², S. Monzani ^{69a,69c}, A. Morancho Tarda ⁴³,
 N. Morange ⁶⁶, A.L. Moreira De Carvalho ⁴⁸, M. Moreno Llácer ¹⁶⁹, C. Moreno Martinez ⁵⁶,

J.M. Moreno Perez^{23b}, P. Morettini^{57b}, S. Morgenstern³⁷, M. Morii⁶¹, M. Morinaga¹⁵⁹, M. Moritsu⁹⁰, F. Morodei^{75a,75b}, P. Moschovakos³⁷, B. Moser⁵⁴, M. Mosidze^{155b}, T. Moskalets⁴⁵, P. Moskvitina¹¹⁶, J. Moss³², P. Moszkowicz^{86a}, A. Moussa^{36d}, Y. Moyal¹⁷⁵, H. Moyano Gomez¹³, E.J.W. Moyse¹⁰⁵, T.G. Mroz⁸⁷, O. Mtintsilana^{34h}, S. Muanza¹⁰⁴, M. Mucha²⁵, J. Mueller¹³², R. Müller³⁷, G.A. Mullier¹⁶⁷, A.J. Mullin³³, J.J. Mullin⁵¹, A.C. Mullins⁴⁵, A.E. Mulski⁶¹, D.P. Mungo¹⁶¹, D. Munoz Perez¹⁶⁹, F.J. Munoz Sanchez¹⁰³, W.J. Murray^{173,137}, M. Muškinja⁹⁵, C. Mwewa⁴⁸, A.G. Myagkov^{38,a}, A.J. Myers⁸, G. Myers¹⁰⁸, M. Myska¹³⁵, B.P. Nachman¹⁴⁹, K. Nagai¹²⁹, K. Nagano⁸⁴, R. Nagasaka¹⁵⁹, J.L. Nagle^{30,al}, E. Nagy¹⁰⁴, A.M. Nairz³⁷, Y. Nakahama⁸⁴, K. Nakamura⁸⁴, K. Nakkalil⁵, A. Nandi^{63b}, H. Nanjo¹²⁷, E.A. Narayanan⁴⁵, Y. Narukawa¹⁵⁹, I. Naryshkin³⁸, L. Nasella^{71a,71b}, S. Nasri^{119b}, C. Nass²⁵, G. Navarro^{23a}, A. Nayaz¹⁹, P.Y. Nechaeva³⁸, S. Nechaeva^{24b,24a}, F. Nechansky¹³⁴, L. Nedic¹²⁹, T.J. Neep²¹, A. Negri^{73a,73b}, M. Negrini^{24b}, C. Nellist¹¹⁷, C. Nelson¹⁰⁶, K. Nelson¹⁰⁸, S. Nemecek¹³⁴, M. Nessi^{37,g}, M.S. Neubauer¹⁶⁸, J. Newell⁹⁴, P.R. Newman²¹, Y.W.Y. Ng¹⁶⁸, B. Ngair^{119a}, H.D.N. Nguyen¹¹⁰, J.D. Nichols¹²³, R.B. Nickerson¹²⁹, R. Nicolaidou¹³⁸, J. Nielsen¹³⁹, M. Niemeyer⁵⁵, J. Niermann³⁷, N. Nikiforou³⁷, V. Nikolaenko^{38,a}, I. Nikolic-Audit¹³⁰, P. Nilsson³⁰, I. Ninca⁴⁸, G. Ninio¹⁵⁷, A. Nisati^{75a}, R. Nisius¹¹², N. Nitika¹⁷⁵, J-E. Nitschke⁵⁰, E.K. Nkadimeng^{34b}, T. Nobe¹⁵⁹, D. Noll^{18a}, T. Nommensen¹⁵³, M.B. Norfolk¹⁴⁵, B.J. Norman³⁵, M. Noury^{36a}, J. Novak⁹⁵, T. Novak⁹⁵, R. Novotny¹³⁵, L. Nozka¹²⁵, K. Ntekas¹⁶⁵, N.M.J. Nunes De Moura Junior^{83b}, J. Ocariz¹³⁰, I. Ochoa^{133a}, S. Oerdek^{48,y}, J.T. Offermann⁴⁰, A. Ogrodnik⁸⁷, A. Oh¹⁰³, C.C. Ohm¹⁵⁰, H. Oide⁸⁴, M.L. Ojeda³⁷, Y. Okumura¹⁵⁹, L.F. Oleiro Seabra^{133a}, I. Oleksiyuk⁵⁶, G. Oliveira Correa¹³, D. Oliveira Damazio³⁰, J.L. Oliver¹⁶⁵, R. Omar⁶⁸, Ö.O. Öncel⁵⁴, A.P. O'Neill²⁰, A. Onofre^{133a,133e,e}, P.U.E. Onyisi¹¹, M.J. Oreglia⁴⁰, D. Orestano^{77a,77b}, R. Orlandini^{77a,77b}, R.S. Orr¹⁶¹, L.M. Osojnak⁴², Y. Osumi¹¹³, G. Otero y Garzon³¹, H. Otono⁹⁰, M. Ouchrif^{36d}, F. Ould-Saada¹²⁸, T. Ovsianikova¹⁴², M. Owen⁵⁹, R.E. Owen¹³⁷, V.E. Ozcan^{22a}, F. Ozturk⁸⁷, N. Ozturk⁸, S. Ozturk⁸², H.A. Pacey¹²⁹, K. Pachal^{162a}, A. Pacheco Pages¹³, C. Padilla Aranda¹³, G. Padovano^{75a,75b}, S. Pagan Griso^{18a}, G. Palacino⁶⁸, A. Palazzo^{70a,70b}, J. Pampel²⁵, J. Pan¹⁷⁸, T. Pan^{64a}, D.K. Panchal¹¹, C.E. Pandini⁶⁰, J.G. Panduro Vazquez¹³⁷, H.D. Pandya¹, H. Pang¹³⁸, P. Pani⁴⁸, G. Panizzo^{69a,69c}, L. Panwar¹³⁰, L. Paolozzi⁵⁶, S. Parajuli¹⁶⁸, A. Paramonov⁶, C. Paraskevopoulos⁵³, D. Paredes Hernandez^{64b}, A. Pareti^{73a,73b}, K.R. Park⁴², T.H. Park¹¹², F. Parodi^{57b,57a}, J.A. Parsons⁴², U. Parzefall⁵⁴, B. Pascual Dias⁴¹, L. Pascual Dominguez¹⁰¹, E. Pasqualucci^{75a}, S. Passaggio^{57b}, F. Pastore⁹⁷, P. Patel⁸⁷, U.M. Patel⁵¹, J.R. Pater¹⁰³, T. Pauly³⁷, F. Pauwels¹³⁶, C.I. Pazos¹⁶⁴, M. Pedersen¹²⁸, R. Pedro^{133a}, S.V. Peleganchuk³⁸, O. Penc¹³⁴, S. Peng¹⁵, G.D. Penn¹⁷⁸, K.E. Pensi¹¹¹, M. Penzin³⁸, B.S. Peralva^{83d}, A.P. Pereira Peixoto¹⁴², L. Pereira Sanchez¹⁴⁹, D.V. Perepelitsa^{30,al}, G. Perera¹⁰⁵, E. Perez Codina³⁷, M. Perganti¹⁰, H. Pernegger³⁷, S. Perrella^{75a,75b}, K. Peters⁴⁸, R.F.Y. Peters¹⁰³, B.A. Petersen³⁷, T.C. Petersen⁴³, E. Petit¹⁰⁴, V. Petousis¹³⁵, A.R. Petri^{71a,71b}, C. Petridou^{158,d}, T. Petru¹³⁶, A. Petrukhin¹⁴⁷, M. Pettee^{18a}, A. Petukhov⁸², K. Petukhova³⁷, R. Pezoa^{140g}, L. Pezzotti^{24b,24a}, G. Pezzullo¹⁷⁸, L. Pfaffenbichler³⁷, A.J. Pflieger⁷⁹, T.M. Pham¹⁷⁶, T. Pham¹⁰⁷, P.W. Phillips¹³⁷, G. Piacquadio¹⁵¹, E. Pianori^{18a}, F. Piazza¹²⁶, R. Piegaia³¹, D. Pietreanu^{28b}, A.D. Pilkington¹⁰³, M. Pinamonti^{69a,69c}, J.L. Pinfeld², B.C. Pinheiro Pereira^{133a}, J. Pinol Bel¹³, A.E. Pinto Pinoargote¹³⁰, L. Pintucci^{69a,69c}, K.M. Piper¹⁵², A. Pirttikoski⁵⁶, D.A. Pizzi³⁵, L. Pizzimento^{64b}, A. Plebani³³, M.-A. Pleier³⁰, V. Pleskot¹³⁶, E. Plotnikova³⁹, G. Poddar⁹⁶, R. Poettgen¹⁰⁰, L. Poggioli¹³⁰, S. Polacek¹³⁶, G. Polesello^{73a}, A. Poley¹⁴⁸, A. Polini^{24b}, C.S. Pollard¹⁷³, Z.B. Pollock¹²², E. Pompa Pacchi¹²³, N.I. Pond⁹⁸,

D. Ponomarenko ⁶⁸, L. Pontecorvo ³⁷, S. Popa ^{28a}, G.A. Popeneciu ^{28d}, A. Poreba ³⁷,
 D.M. Portillo Quintero ^{162a}, S. Pospisil ¹³⁵, M.A. Postill ¹⁴⁵, P. Postolache ^{28c}, K. Potamianos ¹⁷³,
 P.A. Potepa ^{86a}, I.N. Potrap ³⁹, C.J. Potter ³³, H. Potti ¹⁵³, J. Poveda ¹⁶⁹,
 M.E. Pozo Astigarraga ³⁷, R. Pozzi ³⁷, A. Prades Ibanez ^{76a,76b}, S.R. Pradhan ¹⁴⁵, J. Pretel ¹⁷¹,
 D. Price ¹⁰³, M. Primavera ^{70a}, L. Primomo ^{69a,69c}, M.A. Principe Martin ¹⁰¹, R. Privara ¹²⁵,
 T. Procter ^{86b}, M.L. Proffitt ¹⁴², N. Proklova ¹³¹, K. Prokofiev ^{64c}, G. Proto ¹¹², J. Proudfoot ⁶,
 M. Przybycien ^{86a}, W.W. Przygoda ^{86b}, A. Psallidas ⁴⁶, J.E. Puddefoot ¹⁴⁵, D. Pudzha ⁵³,
 H.I. Purnell ¹, D. Pyatiizbyantseva ¹¹⁶, J. Qian ¹⁰⁸, R. Qian ¹⁰⁹, D. Qichen ¹²⁹, Y. Qin ¹³,
 T. Qiu ⁵², A. Quadt ⁵⁵, M. Queitsch-Maitland ¹⁰³, G. Quetant ⁵⁶, R.P. Quinn ¹⁷⁰,
 G. Rabanal Bolanos ⁶¹, D. Rafanoharana ¹¹², F. Raffaelli ^{76a,76b}, F. Ragusa ^{71a,71b},
 J.L. Rainbolt ⁴⁰, S. Rajagopalan ³⁰, E. Ramakoti ³⁹, L. Rambelli ^{57b,57a}, I.A. Ramirez-Berend ³⁵,
 K. Ran ^{48,114c}, D.S. Rankin ¹³¹, N.P. Rapheeha ^{34h}, H. Rasheed ^{28b}, D.F. Rassloff ^{63a},
 A. Rastogi ^{18a}, S. Rave ¹⁰², S. Ravera ^{57b,57a}, B. Ravina ³⁷, I. Ravinovich ¹⁷⁵, M. Raymond ³⁷,
 A.L. Read ¹²⁸, N.P. Readioff ¹⁴⁵, D.M. Rebutzi ^{73a,73b}, A.S. Reed ⁵⁹, K. Reeves ²⁷,
 J.A. Reidelsturz ¹⁷⁷, D. Reikher ³⁷, A. Rej ⁴⁹, C. Rembser ³⁷, H. Ren ⁶², M. Renda ^{28b},
 F. Renner ⁴⁸, A.G. Rennie ⁵⁹, A.L. Rescia ^{57b,57a}, S. Resconi ^{71a}, M. Ressegotti ^{57b,57a},
 S. Rettie ¹¹⁷, W.F. Rettie ³⁵, M.M. Revering ³³, E. Reynolds ^{18a}, O.L. Rezanova ³⁹,
 P. Reznicek ¹³⁶, H. Riani ^{36d}, N. Ribaric ⁵¹, B. Ricci ^{69a,69c}, E. Ricci ^{78a,78b}, R. Richter ¹¹²,
 S. Richter ^{47a,47b}, E. Richter-Was ^{86b}, M. Ridel ¹³⁰, S. Ridouani ^{36d}, P. Rieck ¹²⁰, P. Riedler ³⁷,
 E.M. Riefel ^{47a,47b}, J.O. Rieger ¹¹⁷, M. Rijssenbeek ¹⁵¹, M. Rimoldi ³⁷, L. Rinaldi ^{24b,24a},
 P. Rincke ^{167,55}, G. Ripellino ¹⁶⁷, I. Riu ¹³, J.C. Rivera Vergara ¹⁷¹, F. Rizatdinova ¹²⁴,
 E. Rizvi ⁹⁶, B.R. Roberts ^{18a}, S.S. Roberts ¹³⁹, D. Robinson ³³, M. Robles Manzano ¹⁰²,
 A. Robson ⁵⁹, A. Rocchi ^{76a,76b}, C. Roda ^{74a,74b}, S. Rodriguez Bosca ³⁷, Y. Rodriguez Garcia ^{23a},
 A.M. Rodríguez Vera ¹¹⁸, S. Roe ³⁷, J.T. Roemer ³⁷, O. Røhne ¹²⁸, R.A. Rojas ³⁷,
 C.P.A. Roland ¹³⁰, A. Romaniouk ⁷⁹, E. Romano ^{73a,73b}, M. Romano ^{24b},
 A.C. Romero Hernandez ¹⁶⁸, N. Rompotis ⁹⁴, L. Roos ¹³⁰, S. Rosati ^{75a}, B.J. Rosser ⁴⁰,
 E. Rossi ¹²⁹, E. Rossi ^{72a,72b}, L.P. Rossi ⁶¹, L. Rossini ⁵⁴, R. Rosten ¹²², M. Rotaru ^{28b},
 B. Rottler ⁵⁴, D. Rousseau ⁶⁶, D. Rousso ⁴⁸, S. Roy-Garand ¹⁶¹, A. Rozanov ¹⁰⁴,
 Z.M.A. Rozario ⁵⁹, Y. Rozen ¹⁵⁶, A. Rubio Jimenez ¹⁶⁹, V.H. Ruelas Rivera ¹⁹, T.A. Ruggeri ¹,
 A. Ruggiero ¹²⁹, A. Ruiz-Martinez ¹⁶⁹, A. Rummler ³⁷, Z. Rurikova ⁵⁴, N.A. Rusakovich ³⁹,
 S. Ruscelli ⁴⁹, H.L. Russell ¹⁷¹, G. Russo ^{75a,75b}, J.P. Rutherford ⁷, S. Rutherford Colmenares ³³,
 M. Rybar ¹³⁶, P. Rybczynski ^{86a}, A. Ryzhov ⁴⁵, J.A. Sabater Iglesias ⁵⁶, H.F.W. Sadrozinski ¹³⁹,
 F. Safai Tehrani ^{75a}, S. Saha ¹, M. Sahinsoy ⁸², B. Sahoo ¹⁷⁵, A. Saibel ¹⁶⁹, B.T. Saifuddin ¹²³,
 M. Saimpert ¹³⁸, G.T. Saito ^{83c}, M. Saito ¹⁵⁹, T. Saito ¹⁵⁹, A. Sala ^{71a,71b}, A. Salnikov ¹⁴⁹,
 J. Salt ¹⁶⁹, A. Salvador Salas ¹⁵⁷, F. Salvatore ¹⁵², A. Salzburger ³⁷, D. Sammel ⁵⁴,
 E. Sampson ⁹³, D. Sampsonidis ^{158,d}, D. Sampsonidou ¹²⁶, M.A.A. Samy ⁵⁹, J. Sánchez ¹⁶⁹,
 V. Sanchez Sebastian ¹⁶⁹, H. Sandaker ¹²⁸, C.O. Sander ⁴⁸, J.A. Sandesara ¹⁷⁶, M. Sandhoff ¹⁷⁷,
 C. Sandoval ^{23b}, L. Sanfilippo ^{63a}, D.P.C. Sankey ¹³⁷, T. Sano ⁸⁹, A. Sansoni ⁵³,
 M. Santana Queiroz ^{18b}, L. Santi ³⁷, C. Santoni ⁴¹, H. Santos ^{133a,133b}, A. Santra ¹⁷⁵,
 E. Sanzani ^{24b,24a}, K.A. Saoucha ^{88b}, J.G. Saraiva ^{133a,133d}, J. Sardain ⁷, O. Sasaki ⁸⁴,
 K. Sato ¹⁶³, C. Sauer ³⁷, E. Sauvan ⁴, P. Savard ^{161,ai}, R. Sawada ¹⁵⁹, C. Sawyer ¹³⁷,
 L. Sawyer ⁹⁹, C. Sbarra ^{24b}, A. Sbrizzi ^{24b,24a}, T. Scanlon ⁹⁸, J. Schaarschmidt ¹⁴²,
 U. Schäfer ¹⁰², A.C. Schaffer ^{66,45}, D. Schaile ¹¹¹, R.D. Schamberger ¹⁵¹, C. Scharf ¹⁹,
 M.M. Schefer ²⁰, V.A. Schegelsky ³⁸, D. Scheirich ¹³⁶, M. Schernau ^{140f}, C. Scheulen ⁵⁶,
 C. Schiavi ^{57b,57a}, M. Schioppa ^{44b,44a}, B. Schlag ¹⁴⁹, S. Schlenker ³⁷, J. Schmeing ¹⁷⁷,
 E. Schmidt ¹¹², M.A. Schmidt ¹⁷⁷, K. Schmieden ¹⁰², C. Schmitt ¹⁰², N. Schmitt ¹⁰²,
 S. Schmitt ⁴⁸, N.A. Schneider ¹¹¹, L. Schoeffel ¹³⁸, A. Schoening ^{63b}, P.G. Scholer ³⁵,

E. Schopf ¹⁴⁷, M. Schott ²⁵, S. Schramm ⁵⁶, T. Schroer ⁵⁶, H-C. Schultz-Coulon ^{63a},
 M. Schumacher ⁵⁴, B.A. Schumm ¹³⁹, Ph. Schune ¹³⁸, H.R. Schwartz ⁷, A. Schwartzman ¹⁴⁹,
 T.A. Schwarz ¹⁰⁸, Ph. Schwemling ¹³⁸, R. Schwienhorst ¹⁰⁹, F.G. Sciacca ²⁰, A. Sciandra ³⁰,
 G. Sciolla ²⁷, F. Scuri ^{74a}, C.D. Sebastiani ³⁷, K. Sedlaczek ¹¹⁸, S.C. Seidel ¹¹⁵, A. Seiden ¹³⁹,
 B.D. Seidlitz ⁴², C. Seitz ⁴⁸, J.M. Seixas ^{83b}, G. Sekhniaidze ^{72a}, L. Selem ⁶⁰,
 N. Semprini-Cesari ^{24b,24a}, A. Semushin ¹⁷⁹, D. Sengupta ⁵⁶, V. Senthilkumar ¹⁶⁹, L. Serin ⁶⁶,
 M. Sessa ^{72a,72b}, H. Severini ¹²³, F. Sforza ^{57b,57a}, A. Sfyrta ⁵⁶, Q. Sha ¹⁴, E. Shabalina ⁵⁵,
 H. Shaddix ¹¹⁸, A.H. Shah ³³, R. Shaheen ¹⁵⁰, J.D. Shahinian ¹³¹, M. Shamim ³⁷, L.Y. Shan ¹⁴,
 M. Shapiro ^{18a}, A. Sharma ³⁷, A.S. Sharma ¹⁷⁰, P. Sharma ³⁰, P.B. Shatalov ³⁸, K. Shaw ¹⁵²,
 S.M. Shaw ¹⁰³, Q. Shen ^{144a}, D.J. Sheppard ¹⁴⁸, P. Sherwood ⁹⁸, L. Shi ⁹⁸, X. Shi ¹⁴,
 S. Shimizu ⁸⁴, C.O. Shimmin ¹⁷⁸, I.P.J. Shipsey ^{129,*}, S. Shirabe ⁹⁰, M. Shiyakova ^{39,z},
 M.J. Shochet ⁴⁰, D.R. Shope ¹²⁸, B. Shrestha ¹²³, S. Shrestha ^{122,an}, I. Shreyber ³⁹,
 M.J. Shroff ¹⁷¹, P. Sicho ¹³⁴, A.M. Sickles ¹⁶⁸, E. Sideras Haddad ^{34h,166}, A.C. Sidley ¹¹⁷,
 A. Sidoti ^{24b}, F. Siegert ⁵⁰, Dj. Sijacki ¹⁶, F. Sili ⁹², J.M. Silva ⁵², I. Silva Ferreira ^{83b},
 M.V. Silva Oliveira ³⁰, S.B. Silverstein ^{47a}, S. Simion ⁶⁶, R. Simoniello ³⁷, E.L. Simpson ¹⁰³,
 H. Simpson ¹⁵², L.R. Simpson ⁶, S. Simsek ⁸², S. Sindhu ⁵⁵, P. Sinervo ¹⁶¹, S.N. Singh ²⁷,
 S. Singh ³⁰, S. Sinha ⁴⁸, S. Sinha ¹⁰³, M. Sioli ^{24b,24a}, K. Sioulas ⁹, I. Siral ³⁷, E. Sitnikova ⁴⁸,
 J. Sjölin ^{47a,47b}, A. Skaf ⁵⁵, E. Skorda ²¹, P. Skubic ¹²³, M. Slawinska ⁸⁷, I. Slazyk ¹⁷,
 I. Sliusar ¹²⁸, V. Smakhtin ¹⁷⁵, B.H. Smart ¹³⁷, S.Yu. Smirnov ^{140b}, Y. Smirnov ⁸²,
 L.N. Smirnova ^{38,a}, O. Smirnova ¹⁰⁰, A.C. Smith ⁴², D.R. Smith ¹⁶⁵, J.L. Smith ¹⁰³,
 M.B. Smith ³⁵, R. Smith ¹⁴⁹, H. Smitmanns ¹⁰², M. Smizanska ⁹³, K. Smolek ¹³⁵,
 P. Smolyanskiy ¹³⁵, A.A. Snesev ³⁹, H.L. Snoek ¹¹⁷, S. Snyder ³⁰, R. Sobie ^{171,ab},
 A. Soffer ¹⁵⁷, C.A. Solans Sanchez ³⁷, E.Yu. Soldatov ³⁹, U. Soldevila ¹⁶⁹, A.A. Solodkov ^{34h},
 S. Solomon ²⁷, A. Soloshenko ³⁹, K. Solovieva ⁵⁴, O.V. Solovyanov ⁴¹, P. Sommer ⁵⁰,
 A. Sonay ¹³, A. Sopczak ¹³⁵, A.L. Sopio ⁵², F. Sopkova ^{29b}, J.D. Sorenson ¹¹⁵,
 I.R. Sotarriva Alvarez ¹⁴¹, V. Sothilingam ^{63a}, O.J. Soto Sandoval ^{140c,140b}, S. Sottocornola ⁶⁸,
 R. Soualah ^{88a}, Z. Soumami ^{36e}, D. South ⁴⁸, N. Soybelman ¹⁷⁵, S. Spagnolo ^{70a,70b},
 M. Spalla ¹¹², D. Sperlich ⁵⁴, B. Spisso ^{72a,72b}, D.P. Spiteri ⁵⁹, L. Splendori ¹⁰⁴, M. Spousta ¹³⁶,
 E.J. Staats ³⁵, R. Stamen ^{63a}, E. Stanecka ⁸⁷, W. Stanek-Maslouska ⁴⁸, M.V. Stange ⁵⁰,
 B. Stanislaus ^{18a}, M.M. Stanitzki ⁴⁸, B. Stapf ⁴⁸, E.A. Starchenko ³⁸, G.H. Stark ¹³⁹, J. Stark ⁹¹,
 P. Staroba ¹³⁴, P. Starovoitov ^{88b}, R. Staszewski ⁸⁷, C. Stauch ¹¹¹, G. Stavropoulos ⁴⁶,
 A. Stefl ³⁷, A. Stein ¹⁰², P. Steinberg ³⁰, B. Stelzer ^{148,162a}, H.J. Stelzer ¹³²,
 O. Stelzer-Chilton ^{162a}, H. Stenzel ⁵⁸, T.J. Stevenson ¹⁵², G.A. Stewart ³⁷, J.R. Stewart ¹²⁴,
 G. Stoicea ^{28b}, M. Stolarski ^{133a}, S. Stonjek ¹¹², A. Straessner ⁵⁰, J. Strandberg ¹⁵⁰,
 S. Strandberg ^{47a,47b}, M. Stratmann ¹⁷⁷, M. Strauss ¹²³, T. Streblner ¹⁰⁴, P. Strizened ^{29b},
 R. Ströhmer ¹⁷², D.M. Strom ¹²⁶, R. Stroynowski ⁴⁵, A. Strubig ^{47a,47b}, S.A. Stucci ³⁰,
 B. Stugu ¹⁷, J. Stupak ¹²³, N.A. Styles ⁴⁸, D. Su ¹⁴⁹, S. Su ⁶², X. Su ⁶², D. Suchy ^{29a},
 A.D. Sudhakar Ponnu ⁵⁵, K. Sugizaki ¹³¹, V.V. Sulin ³⁸, D.M.S. Sultan ¹²⁹, L. Sultanaliyeva ²⁵,
 S. Sultansoy ^{3b}, S. Sun ¹⁷⁶, W. Sun ¹⁴, N. Sur ¹⁰⁰, M.R. Sutton ¹⁵², M. Svatos ¹³⁴,
 P.N. Swallow ³³, M. Swiatlowski ^{162a}, T. Swirski ¹⁷², A. Swoboda ³⁷, I. Sykora ^{29a},
 M. Sykora ¹³⁶, T. Sykora ¹³⁶, D. Ta ¹⁰², K. Tackmann ^{48,y}, A. Taffard ¹⁶⁵, R. Tafirout ^{162a},
 Y. Takubo ⁸⁴, M. Talby ¹⁰⁴, A.A. Talyshev ³⁸, K.C. Tam ^{64b}, N.M. Tamir ¹⁵⁷, A. Tanaka ¹⁵⁹,
 J. Tanaka ¹⁵⁹, R. Tanaka ⁶⁶, M. Tanasini ¹⁵¹, Z. Tao ¹⁷⁰, S. Tapia Araya ^{140g}, S. Tapprogge ¹⁰²,
 A. Tarek Abouelfadl Mohamed ³⁷, S. Tarem ¹⁵⁶, K. Tariq ¹⁴, G. Tarna ³⁷, G.F. Tartarelli ^{71a},
 M.J. Tartarin ⁹¹, P. Tas ¹³⁶, M. Tasevsky ¹³⁴, E. Tassi ^{44b,44a}, A.C. Tate ¹⁶⁸, Y. Tayalati ^{36e,aa},
 G.N. Taylor ¹⁰⁷, W. Taylor ^{162b}, R.J. Taylor Vara ¹⁶⁹, A.S. Tegetmeier ⁹¹, P. Teixeira-Dias ⁹⁷,
 J.J. Teoh ¹⁶¹, K. Terashi ¹⁵⁹, J. Terron ¹⁰¹, S. Terzo ¹³, M. Testa ⁵³, R.J. Teuscher ^{161,ab},

A. Thaler ⁷⁹, O. Theiner ⁵⁶, T. Theveneaux-Pelzer ¹⁰⁴, D.W. Thomas ⁹⁷, J.P. Thomas ²¹,
 E.A. Thompson ^{18a}, P.D. Thompson ²¹, E. Thomson ¹³¹, R.E. Thornberry ⁴⁵, C. Tian ⁶²,
 Y. Tian ⁵⁶, V. Tikhomirov ⁸², Yu.A. Tikhonov ³⁹, S. Timoshenko ³⁸, D. Timoshyn ¹³⁶,
 E.X.L. Ting ¹, P. Tipton ¹⁷⁸, A. Tishelman-Charny ³⁰, K. Todome ¹⁴¹, S. Todorova-Nova ¹³⁶,
 L. Toffolin ^{69a,69c}, M. Togawa ⁸⁴, J. Tojo ⁹⁰, S. Tokár ^{29a}, O. Toldaiev ⁶⁸, G. Tolkachev ¹⁰⁴,
 M. Tomoto ⁸⁴, L. Tompkins ^{149,n}, E. Torrence ¹²⁶, H. Torres ⁹¹, D.I. Torres Arza ^{140g},
 E. Torró Pastor ¹⁶⁹, M. Toscani ³¹, C. Toscirci ⁴⁰, M. Tost ¹¹, D.R. Tovey ¹⁴⁵, T. Trefzger ¹⁷²,
 P.M. Tricarico ¹³, A. Tricoli ³⁰, I.M. Trigger ^{162a}, S. Trincasz-Duvoid ¹³⁰, D.A. Trischuk ²⁷,
 A. Tropina ³⁹, L. Truong ^{34c}, M. Trzebinski ⁸⁷, A. Trzupiek ⁸⁷, F. Tsai ¹⁵¹, M. Tsai ¹⁰⁸,
 A. Tsiamis ¹⁵⁸, P.V. Tsiareshka ³⁹, S. Tsigaridas ^{162a}, A. Tsigotis ^{158,u}, V. Tsiskaridze ^{155a},
 E.G. Tskhadadze ^{155a}, Y. Tsujikawa ⁸⁹, I.I. Tsukerman ³⁸, V. Tsulaia ^{18a}, S. Tsuno ⁸⁴,
 K. Tsuru ¹²¹, D. Tsybychev ¹⁵¹, Y. Tu ^{64b}, A. Tudorache ^{28b}, V. Tudorache ^{28b}, S.B. Tuncay ¹²⁹,
 S. Turchikhin ^{57b,57a}, I. Turk Cakir ^{3a}, R. Turra ^{71a}, T. Turtuvshin ^{39,ac}, P.M. Tuts ⁴²,
 S. Tzamarias ^{158,d}, Y. Uematsu ⁸⁴, F. Ukegawa ¹⁶³, P.A. Ulloa Poblete ^{140c,140b}, E.N. Umaka ³⁰,
 G. Unal ³⁷, A. Undrus ³⁰, G. Unel ¹⁶⁵, J. Urban ^{29b}, P. Urrejola ^{140e}, G. Usai ⁸,
 R. Ushioda ¹⁶⁰, M. Usman ¹¹⁰, F. Ustuner ⁵², Z. Uysal ⁸², V. Vacek ¹³⁵, B. Vachon ¹⁰⁶,
 T. Vafeiadis ³⁷, A. Vaitkus ⁹⁸, C. Valderanis ¹¹¹, E. Valdes Santurio ^{47a,47b}, M. Valente ³⁷,
 S. Valentinetti ^{24b,24a}, A. Valero ¹⁶⁹, E. Valiente Moreno ¹⁶⁹, A. Vallier ⁹¹, J.A. Valls Ferrer ¹⁶⁹,
 D.R. Van Arneman ¹¹⁷, A. Van Der Graaf ⁴⁹, H.Z. Van Der Schyf ^{34h}, P. Van Gemmeren ⁶,
 M. Van Rijnbach ³⁷, S. Van Stroud ⁹⁸, I. Van Vulpen ¹¹⁷, P. Vana ¹³⁶, M. Vanadia ^{76a,76b},
 U.M. Vande Voorde ¹⁵⁰, W. Vandelli ³⁷, E.R. Vandewall ¹²⁴, D. Vannicola ¹⁵⁷, L. Vannoli ⁵³,
 R. Vari ^{75a}, M. Varma ¹⁷⁸, E.W. Varnes ⁷, C. Varni ¹¹⁸, D. Varouchas ⁶⁶, L. Varriale ¹⁶⁹,
 K.E. Varvell ¹⁵³, M.E. Vasile ^{28b}, L. Vaslin ⁸⁴, M.D. Vassilev ¹⁴⁹, A. Vasyukov ³⁹,
 L.M. Vaughan ¹²⁴, R. Vavricka ¹³⁶, T. Vazquez Schroeder ¹³, J. Veatch ³², V. Vecchio ¹⁰³,
 M.J. Veen ¹⁰⁵, I. Veliscek ³⁰, I. Velkovska ⁹⁵, L.M. Veloce ¹⁶¹, F. Veloso ^{133a,133c},
 S. Veneziano ^{75a}, A. Ventura ^{70a,70b}, A. Verbytskyi ¹¹², M. Verducci ^{74a,74b}, C. Vergis ⁹⁶,
 M. Verissimo De Araujo ^{83b}, W. Verkerke ¹¹⁷, J.C. Vermeulen ¹¹⁷, C. Vernieri ¹⁴⁹,
 M. Vessella ¹⁶⁵, M.C. Vetterli ^{148,ai}, A. Vgenopoulos ¹⁰², N. Viaux Maira ^{140g,af}, T. Vickey ¹⁴⁵,
 O.E. Vickey Boeriu ¹⁴⁵, G.H.A. Viehhauser ¹²⁹, L. Vigani ^{63b}, M. Vigl ¹¹², M. Villa ^{24b,24a},
 M. Villaplana Perez ¹⁶⁹, E.M. Villhauer ⁴⁰, E. Vilucchi ⁵³, M. Vincent ¹⁶⁹, M.G. Vinciter ³⁵,
 A. Visibile ¹¹⁷, A. Visive ¹¹⁷, C. Vittori ³⁷, I. Vivarelli ^{24b,24a}, M.I. Vivas Albornoz ⁴⁸,
 E. Voevodina ¹¹², F. Vogel ¹¹¹, J.C. Voigt ⁵⁰, P. Vokac ¹³⁵, Yu. Volkotrub ^{86b}, L. Vomberg ²⁵,
 E. Von Toerne ²⁵, B. Vormwald ³⁷, K. Vorobev ⁵¹, M. Vos ¹⁶⁹, K. Voss ¹⁴⁷, M. Vozak ³⁷,
 L. Vozdecky ¹²³, N. Vranjes ¹⁶, M. Vranjes Milosavljevic ¹⁶, M. Vreeswijk ¹¹⁷, N.K. Vu ^{144b,144a},
 R. Vuillermet ³⁷, O. Vujinovic ¹⁰², I. Vukotic ⁴⁰, I.K. Vyas ³⁵, J.F. Wack ³³, S. Wada ¹⁶³,
 C. Wagner ¹⁴⁹, J.M. Wagner ^{18a}, W. Wagner ¹⁷⁷, S. Wahdan ¹⁷⁷, H. Wahlberg ⁹², C.H. Waits ¹²³,
 J. Walder ¹³⁷, R. Walker ¹¹¹, K. Walkingshaw Pass ⁵⁹, W. Walkowiak ¹⁴⁷, A. Wall ¹³¹,
 E.J. Wallin ¹⁰⁰, T. Wamorkar ^{18a}, K. Wandall-Christensen ¹⁶⁹, A. Wang ⁶², A.Z. Wang ¹³⁹,
 C. Wang ¹⁰², C. Wang ¹¹, H. Wang ^{18a}, J. Wang ^{64c}, P. Wang ¹⁰³, P. Wang ⁹⁸, R. Wang ⁶¹,
 R. Wang ⁶, S.M. Wang ¹⁵⁴, S. Wang ¹⁴, T. Wang ¹¹⁶, T. Wang ⁶², W.T. Wang ¹²⁹, W. Wang ¹⁴,
 X. Wang ¹⁶⁸, X. Wang ^{144a}, X. Wang ⁴⁸, Y. Wang ^{114a}, Y. Wang ⁶², Z. Wang ¹⁰⁸, Z. Wang ^{144b},
 Z. Wang ¹⁰⁸, C. Wanotayaroj ⁸⁴, A. Warburton ¹⁰⁶, A.L. Warnerbring ¹⁴⁷, S. Waterhouse ⁹⁷,
 A.T. Watson ²¹, H. Watson ⁵², M.F. Watson ²¹, E. Watton ³⁷, G. Watts ¹⁴², B.M. Waugh ⁹⁸,
 J.M. Webb ⁵⁴, C. Weber ³⁰, H.A. Weber ¹⁹, M.S. Weber ²⁰, S.M. Weber ^{63a}, C. Wei ⁶²,
 Y. Wei ⁵⁴, A.R. Weidberg ¹²⁹, E.J. Weik ¹²⁰, J. Weingarten ⁴⁹, C. Weiser ⁵⁴, C.J. Wells ⁴⁸,
 T. Wenaus ³⁰, T. Wengler ³⁷, N.S. Wenke ¹¹², N. Wermes ²⁵, M. Wessels ^{63a}, A.M. Wharton ⁹³,
 A.S. White ⁶¹, A. White ⁸, M.J. White ¹, D. Whiteson ¹⁶⁵, L. Wickremasinghe ¹²⁷,

W. Wiedenmann ¹⁷⁶, M. Wielers ¹³⁷, R. Wierda ¹⁵⁰, C. Wigglesworth ⁴³, H.G. Wilkens ³⁷, J.J.H. Wilkinson ³³, D.M. Williams ⁴², H.H. Williams ¹³¹, S. Williams ³³, S. Willocq ¹⁰⁵, B.J. Wilson ¹⁰³, D.J. Wilson ¹⁰³, P.J. Windischhofer ⁴⁰, F.I. Winkel ³¹, F. Winklmeier ¹²⁶, B.T. Winter ⁵⁴, M. Wittgen ¹⁴⁹, M. Wobisch ⁹⁹, T. Wojtkowski⁶⁰, Z. Wolffs ¹¹⁷, J. Wollrath³⁷, M.W. Wolter ⁸⁷, H. Wolters ^{133a,133c}, M.C. Wong¹³⁹, E.L. Woodward ⁴², S.D. Worm ⁴⁸, B.K. Wosiek ⁸⁷, K.W. Woźniak ⁸⁷, S. Wozniowski ⁵⁵, K. Wraight ⁵⁹, C. Wu ¹⁶¹, C. Wu ²¹, J. Wu ¹⁵⁹, M. Wu ^{114b}, M. Wu ¹¹⁶, S.L. Wu ¹⁷⁶, S. Wu ^{14,ak}, X. Wu ⁶², Y.Q. Wu ¹⁶¹, Y. Wu ⁶², Z. Wu ⁴, Z. Wu ^{114a}, J. Wuerzinger ¹¹², T.R. Wyatt ¹⁰³, B.M. Wynne ⁵², S. Xella ⁴³, L. Xia ^{114a}, M. Xie ⁶², A. Xiong ¹²⁶, D. Xu ¹⁴, H. Xu ⁶², L. Xu ⁶², R. Xu ¹³¹, T. Xu ¹⁰⁸, Y. Xu ¹⁴², Z. Xu ⁵², R. Xue ¹³², B. Yabsley ¹⁵³, S. Yacoob ^{34a}, Y. Yamaguchi ⁸⁴, E. Yamashita ¹⁵⁹, H. Yamauchi ¹⁶³, T. Yamazaki ^{18a}, Y. Yamazaki ⁸⁵, S. Yan ⁵⁹, Z. Yan ¹⁰⁵, H.J. Yang ^{144a,144b}, H.T. Yang ⁶², S. Yang ⁶², T. Yang ^{64c}, X. Yang ³⁷, X. Yang ¹⁴, Y. Yang ¹⁵⁹, Y. Yang⁶², W.-M. Yao ^{18a}, C.L. Yardley ¹⁵², J. Ye ¹⁴, S. Ye ³⁰, X. Ye ⁶², Y. Yeh ⁹⁸, I. Yeletsikh ³⁹, B. Yeo ^{18b}, M.R. Yexley ⁹⁸, T.P. Yildirim ¹²⁹, K. Yorita ¹⁷⁴, C.J.S. Young ³⁷, C. Young ¹⁴⁹, N.D. Young¹²⁶, Y. Yu ⁶², J. Yuan ^{14,114c}, M. Yuan ¹⁰⁸, R. Yuan ^{144b,144a}, L. Yue ⁹⁸, M. Zaazoua ⁶², B. Zabinski ⁸⁷, I. Zahir ^{36a}, A. Zaio^{57b,57a}, Z.K. Zak ⁸⁷, T. Zakareishvili ¹⁶⁹, S. Zambito ⁵⁶, J.A. Zamora Saa ^{140d}, J. Zang ¹⁵⁹, R. Zanzottera ^{71a,71b}, O. Zaplatilek ¹³⁵, C. Zeitnitz ¹⁷⁷, H. Zeng ¹⁴, J.C. Zeng ¹⁶⁸, D.T. Zenger Jr ²⁷, O. Zenin ³⁸, T. Ženiš ^{29a}, S. Zenz ⁹⁶, D. Zerwas ⁶⁶, M. Zhai ^{14,114c}, D.F. Zhang ¹⁴⁵, G. Zhang ^{14,ak}, J. Zhang ^{143a}, J. Zhang ⁶, K. Zhang ^{14,114c}, L. Zhang ⁶², L. Zhang ^{114a}, P. Zhang ^{14,114c}, R. Zhang ^{114a}, S. Zhang ⁹¹, T. Zhang ¹⁵⁹, Y. Zhang ¹⁴², Y. Zhang ⁹⁸, Y. Zhang ⁶², Y. Zhang ^{114a}, Z. Zhang ^{18a}, Z. Zhang ^{143a}, Z. Zhang ⁶⁶, H. Zhao ¹⁴², T. Zhao ^{143a}, Y. Zhao ³⁵, Z. Zhao ⁶², Z. Zhao ⁶², A. Zhemchugov ³⁹, J. Zheng ^{114a}, K. Zheng ¹⁶⁸, X. Zheng ⁶², Z. Zheng ¹⁴⁹, D. Zhong ¹⁶⁸, B. Zhou ¹⁰⁸, H. Zhou ⁷, N. Zhou ^{144a}, Y. Zhou ¹⁵, Y. Zhou ^{114a}, Y. Zhou⁷, C.G. Zhu ^{143a}, J. Zhu ¹⁰⁸, X. Zhu^{144b}, Y. Zhu ^{144a}, Y. Zhu ⁶², X. Zhuang ¹⁴, K. Zhukov ⁶⁸, N.I. Zimine ³⁹, J. Zinsser ^{63b}, M. Ziolkowski ¹⁴⁷, L. Živković ¹⁶, A. Zoccoli ^{24b,24a}, K. Zoch ⁶¹, A. Zografos ³⁷, T.G. Zorbas ¹⁴⁵, O. Zormpa ⁴⁶, L. Zwalinski ³⁷.

¹Department of Physics, University of Adelaide, Adelaide; Australia.

²Department of Physics, University of Alberta, Edmonton AB; Canada.

^{3(a)}Department of Physics, Ankara University, Ankara; ^(b)Division of Physics, TOBB University of Economics and Technology, Ankara; Türkiye.

⁴LAPP, Université Savoie Mont Blanc, CNRS/IN2P3, Annecy; France.

⁵APC, Université Paris Cité, CNRS/IN2P3, Paris; France.

⁶High Energy Physics Division, Argonne National Laboratory, Argonne IL; United States of America.

⁷Department of Physics, University of Arizona, Tucson AZ; United States of America.

⁸Department of Physics, University of Texas at Arlington, Arlington TX; United States of America.

⁹Physics Department, National and Kapodistrian University of Athens, Athens; Greece.

¹⁰Physics Department, National Technical University of Athens, Zografou; Greece.

¹¹Department of Physics, University of Texas at Austin, Austin TX; United States of America.

¹²Institute of Physics, Azerbaijan Academy of Sciences, Baku; Azerbaijan.

¹³Institut de Física d'Altes Energies (IFAE), Barcelona Institute of Science and Technology, Barcelona; Spain.

¹⁴Institute of High Energy Physics, Chinese Academy of Sciences, Beijing; China.

¹⁵Physics Department, Tsinghua University, Beijing; China.

¹⁶Institute of Physics, University of Belgrade, Belgrade; Serbia.

¹⁷Department for Physics and Technology, University of Bergen, Bergen; Norway.

- ^{18(a)}Physics Division, Lawrence Berkeley National Laboratory, Berkeley CA; ^(b)University of California, Berkeley CA; United States of America.
- ¹⁹Institut für Physik, Humboldt Universität zu Berlin, Berlin; Germany.
- ²⁰Albert Einstein Center for Fundamental Physics and Laboratory for High Energy Physics, University of Bern, Bern; Switzerland.
- ²¹School of Physics and Astronomy, University of Birmingham, Birmingham; United Kingdom.
- ^{22(a)}Department of Physics, Bogazici University, Istanbul; ^(b)Department of Physics Engineering, Gaziantep University, Gaziantep; ^(c)Department of Physics, Istanbul University, Istanbul; Türkiye.
- ^{23(a)}Facultad de Ciencias y Centro de Investigaciones, Universidad Antonio Nariño, Bogotá; ^(b)Departamento de Física, Universidad Nacional de Colombia, Bogotá; Colombia.
- ^{24(a)}Dipartimento di Fisica e Astronomia A. Righi, Università di Bologna, Bologna; ^(b)INFN Sezione di Bologna; Italy.
- ²⁵Physikalisches Institut, Universität Bonn, Bonn; Germany.
- ²⁶Department of Physics, Boston University, Boston MA; United States of America.
- ²⁷Department of Physics, Brandeis University, Waltham MA; United States of America.
- ^{28(a)}Transilvania University of Brasov, Brasov; ^(b)Horia Hulubei National Institute of Physics and Nuclear Engineering, Bucharest; ^(c)Department of Physics, Alexandru Ioan Cuza University of Iasi, Iasi; ^(d)National Institute for Research and Development of Isotopic and Molecular Technologies, Physics Department, Cluj-Napoca; ^(e)National University of Science and Technology Politehnica, Bucharest; ^(f)West University in Timisoara, Timisoara; ^(g)Faculty of Physics, University of Bucharest, Bucharest; Romania.
- ^{29(a)}Faculty of Mathematics, Physics and Informatics, Comenius University, Bratislava; ^(b)Department of Subnuclear Physics, Institute of Experimental Physics of the Slovak Academy of Sciences, Kosice; Slovak Republic.
- ³⁰Physics Department, Brookhaven National Laboratory, Upton NY; United States of America.
- ³¹Universidad de Buenos Aires, Facultad de Ciencias Exactas y Naturales, Departamento de Física, y CONICET, Instituto de Física de Buenos Aires (IFIBA), Buenos Aires; Argentina.
- ³²California State University, CA; United States of America.
- ³³Cavendish Laboratory, University of Cambridge, Cambridge; United Kingdom.
- ^{34(a)}Department of Physics, University of Cape Town, Cape Town; ^(b)iThemba Labs, Western Cape; ^(c)Department of Mechanical Engineering Science, University of Johannesburg, Johannesburg; ^(d)National Institute of Physics, University of the Philippines Diliman (Philippines); ^(e)Department of Physics, Stellenbosch University, Matieland; ^(f)University of South Africa, Department of Physics, Pretoria; ^(g)University of Zululand, KwaDlangezwa; ^(h)School of Physics, University of the Witwatersrand, Johannesburg; South Africa.
- ³⁵Department of Physics, Carleton University, Ottawa ON; Canada.
- ^{36(a)}Faculté des Sciences Ain Chock, Université Hassan II de Casablanca; ^(b)Faculté des Sciences, Université Ibn-Tofail, Kénitra; ^(c)Faculté des Sciences Semlalia, Université Cadi Ayyad, LPHEA-Marrakech; ^(d)LPMR, Faculté des Sciences, Université Mohamed Premier, Oujda; ^(e)Faculté des sciences, Université Mohammed V, Rabat; ^(f)Institute of Applied Physics, Mohammed VI Polytechnic University, Ben Guerir; Morocco.
- ³⁷CERN, Geneva; Switzerland.
- ³⁸Affiliated with an institute formerly covered by a cooperation agreement with CERN.
- ³⁹Affiliated with an international laboratory covered by a cooperation agreement with CERN.
- ⁴⁰Enrico Fermi Institute, University of Chicago, Chicago IL; United States of America.
- ⁴¹LPC, Université Clermont Auvergne, CNRS/IN2P3, Clermont-Ferrand; France.
- ⁴²Nevis Laboratory, Columbia University, Irvington NY; United States of America.
- ⁴³Niels Bohr Institute, University of Copenhagen, Copenhagen; Denmark.

- ⁴⁴(*a*) Dipartimento di Fisica, Università della Calabria, Rende; (*b*) INFN Gruppo Collegato di Cosenza, Laboratori Nazionali di Frascati; Italy.
- ⁴⁵Physics Department, Southern Methodist University, Dallas TX; United States of America.
- ⁴⁶National Centre for Scientific Research "Demokritos", Agia Paraskevi; Greece.
- ⁴⁷(*a*) Department of Physics, Stockholm University; (*b*) Oskar Klein Centre, Stockholm; Sweden.
- ⁴⁸Deutsches Elektronen-Synchrotron DESY, Hamburg and Zeuthen; Germany.
- ⁴⁹Fakultät Physik, Technische Universität Dortmund, Dortmund; Germany.
- ⁵⁰Institut für Kern- und Teilchenphysik, Technische Universität Dresden, Dresden; Germany.
- ⁵¹Department of Physics, Duke University, Durham NC; United States of America.
- ⁵²SUPA - School of Physics and Astronomy, University of Edinburgh, Edinburgh; United Kingdom.
- ⁵³INFN e Laboratori Nazionali di Frascati, Frascati; Italy.
- ⁵⁴Physikalisches Institut, Albert-Ludwigs-Universität Freiburg, Freiburg; Germany.
- ⁵⁵II. Physikalisches Institut, Georg-August-Universität Göttingen, Göttingen; Germany.
- ⁵⁶Département de Physique Nucléaire et Corpusculaire, Université de Genève, Genève; Switzerland.
- ⁵⁷(*a*) Dipartimento di Fisica, Università di Genova, Genova; (*b*) INFN Sezione di Genova; Italy.
- ⁵⁸II. Physikalisches Institut, Justus-Liebig-Universität Giessen, Giessen; Germany.
- ⁵⁹SUPA - School of Physics and Astronomy, University of Glasgow, Glasgow; United Kingdom.
- ⁶⁰LPSC, Université Grenoble Alpes, CNRS/IN2P3, Grenoble INP, Grenoble; France.
- ⁶¹Laboratory for Particle Physics and Cosmology, Harvard University, Cambridge MA; United States of America.
- ⁶²Department of Modern Physics and State Key Laboratory of Particle Detection and Electronics, University of Science and Technology of China, Hefei; China.
- ⁶³(*a*) Kirchhoff-Institut für Physik, Ruprecht-Karls-Universität Heidelberg, Heidelberg; (*b*) Physikalisches Institut, Ruprecht-Karls-Universität Heidelberg, Heidelberg; Germany.
- ⁶⁴(*a*) Department of Physics, Chinese University of Hong Kong, Shatin, N.T., Hong Kong; (*b*) Department of Physics, University of Hong Kong, Hong Kong; (*c*) Department of Physics and Institute for Advanced Study, Hong Kong University of Science and Technology, Clear Water Bay, Kowloon, Hong Kong; China.
- ⁶⁵Department of Physics, National Tsing Hua University, Hsinchu; Taiwan.
- ⁶⁶IJCLab, Université Paris-Saclay, CNRS/IN2P3, 91405, Orsay; France.
- ⁶⁷Centro Nacional de Microelectrónica (IMB-CNM-CSIC), Barcelona; Spain.
- ⁶⁸Department of Physics, Indiana University, Bloomington IN; United States of America.
- ⁶⁹(*a*) INFN Gruppo Collegato di Udine, Sezione di Trieste, Udine; (*b*) ICTP, Trieste; (*c*) Dipartimento Politecnico di Ingegneria e Architettura, Università di Udine, Udine; Italy.
- ⁷⁰(*a*) INFN Sezione di Lecce; (*b*) Dipartimento di Matematica e Fisica, Università del Salento, Lecce; Italy.
- ⁷¹(*a*) INFN Sezione di Milano; (*b*) Dipartimento di Fisica, Università di Milano, Milano; Italy.
- ⁷²(*a*) INFN Sezione di Napoli; (*b*) Dipartimento di Fisica, Università di Napoli, Napoli; Italy.
- ⁷³(*a*) INFN Sezione di Pavia; (*b*) Dipartimento di Fisica, Università di Pavia, Pavia; Italy.
- ⁷⁴(*a*) INFN Sezione di Pisa; (*b*) Dipartimento di Fisica E. Fermi, Università di Pisa, Pisa; Italy.
- ⁷⁵(*a*) INFN Sezione di Roma; (*b*) Dipartimento di Fisica, Sapienza Università di Roma, Roma; Italy.
- ⁷⁶(*a*) INFN Sezione di Roma Tor Vergata; (*b*) Dipartimento di Fisica, Università di Roma Tor Vergata, Roma; Italy.
- ⁷⁷(*a*) INFN Sezione di Roma Tre; (*b*) Dipartimento di Matematica e Fisica, Università Roma Tre, Roma; Italy.
- ⁷⁸(*a*) INFN-TIFPA; (*b*) Università degli Studi di Trento, Trento; Italy.
- ⁷⁹Universität Innsbruck, Department of Astro and Particle Physics, Innsbruck; Austria.
- ⁸⁰University of Iowa, Iowa City IA; United States of America.
- ⁸¹Department of Physics and Astronomy, Iowa State University, Ames IA; United States of America.

- ⁸²Istinye University, Sariyer, Istanbul; Türkiye.
- ⁸³(^a)Departamento de Engenharia Elétrica, Universidade Federal de Juiz de Fora (UFJF), Juiz de Fora; (^b)Universidade Federal do Rio De Janeiro COPPE/EE/IF, Rio de Janeiro; (^c)Instituto de Física, Universidade de São Paulo, São Paulo; (^d)Rio de Janeiro State University, Rio de Janeiro; (^e)Federal University of Bahia, Bahia; Brazil.
- ⁸⁴KEK, High Energy Accelerator Research Organization, Tsukuba; Japan.
- ⁸⁵Graduate School of Science, Kobe University, Kobe; Japan.
- ⁸⁶(^a)AGH University of Krakow, Faculty of Physics and Applied Computer Science, Krakow; (^b)Marian Smoluchowski Institute of Physics, Jagiellonian University, Krakow; Poland.
- ⁸⁷Institute of Nuclear Physics Polish Academy of Sciences, Krakow; Poland.
- ⁸⁸(^a)Khalifa University of Science and Technology, Abu Dhabi; (^b)University of Sharjah, Sharjah; United Arab Emirates.
- ⁸⁹Faculty of Science, Kyoto University, Kyoto; Japan.
- ⁹⁰Research Center for Advanced Particle Physics and Department of Physics, Kyushu University, Fukuoka ; Japan.
- ⁹¹L2IT, Université de Toulouse, CNRS/IN2P3, UPS, Toulouse; France.
- ⁹²Instituto de Física La Plata, Universidad Nacional de La Plata and CONICET, La Plata; Argentina.
- ⁹³Physics Department, Lancaster University, Lancaster; United Kingdom.
- ⁹⁴Oliver Lodge Laboratory, University of Liverpool, Liverpool; United Kingdom.
- ⁹⁵Department of Experimental Particle Physics, Jožef Stefan Institute and Department of Physics, University of Ljubljana, Ljubljana; Slovenia.
- ⁹⁶Department of Physics and Astronomy, Queen Mary University of London, London; United Kingdom.
- ⁹⁷Department of Physics, Royal Holloway University of London, Egham; United Kingdom.
- ⁹⁸Department of Physics and Astronomy, University College London, London; United Kingdom.
- ⁹⁹Louisiana Tech University, Ruston LA; United States of America.
- ¹⁰⁰Fysiska institutionen, Lunds universitet, Lund; Sweden.
- ¹⁰¹Departamento de Física Teórica C-15 and CIAFF, Universidad Autónoma de Madrid, Madrid; Spain.
- ¹⁰²Institut für Physik, Universität Mainz, Mainz; Germany.
- ¹⁰³School of Physics and Astronomy, University of Manchester, Manchester; United Kingdom.
- ¹⁰⁴CPPM, Aix-Marseille Université, CNRS/IN2P3, Marseille; France.
- ¹⁰⁵Department of Physics, University of Massachusetts, Amherst MA; United States of America.
- ¹⁰⁶Department of Physics, McGill University, Montreal QC; Canada.
- ¹⁰⁷School of Physics, University of Melbourne, Victoria; Australia.
- ¹⁰⁸Department of Physics, University of Michigan, Ann Arbor MI; United States of America.
- ¹⁰⁹Department of Physics and Astronomy, Michigan State University, East Lansing MI; United States of America.
- ¹¹⁰Group of Particle Physics, University of Montreal, Montreal QC; Canada.
- ¹¹¹Fakultät für Physik, Ludwig-Maximilians-Universität München, München; Germany.
- ¹¹²Max-Planck-Institut für Physik (Werner-Heisenberg-Institut), München; Germany.
- ¹¹³Graduate School of Science and Kobayashi-Maskawa Institute, Nagoya University, Nagoya; Japan.
- ¹¹⁴(^a)Department of Physics, Nanjing University, Nanjing; (^b)School of Science, Shenzhen Campus of Sun Yat-sen University; (^c)University of Chinese Academy of Science (UCAS), Beijing; China.
- ¹¹⁵Department of Physics and Astronomy, University of New Mexico, Albuquerque NM; United States of America.
- ¹¹⁶Institute for Mathematics, Astrophysics and Particle Physics, Radboud University/Nikhef, Nijmegen; Netherlands.
- ¹¹⁷Nikhef National Institute for Subatomic Physics and University of Amsterdam, Amsterdam;

Netherlands.

¹¹⁸Department of Physics, Northern Illinois University, DeKalb IL; United States of America.

¹¹⁹(^a) New York University Abu Dhabi, Abu Dhabi; (^b) United Arab Emirates University, Al Ain; United Arab Emirates.

¹²⁰Department of Physics, New York University, New York NY; United States of America.

¹²¹Ochanomizu University, Otsuka, Bunkyo-ku, Tokyo; Japan.

¹²²Ohio State University, Columbus OH; United States of America.

¹²³Homer L. Dodge Department of Physics and Astronomy, University of Oklahoma, Norman OK; United States of America.

¹²⁴Department of Physics, Oklahoma State University, Stillwater OK; United States of America.

¹²⁵Palacký University, Joint Laboratory of Optics, Olomouc; Czech Republic.

¹²⁶Institute for Fundamental Science, University of Oregon, Eugene, OR; United States of America.

¹²⁷Graduate School of Science, University of Osaka, Osaka; Japan.

¹²⁸Department of Physics, University of Oslo, Oslo; Norway.

¹²⁹Department of Physics, Oxford University, Oxford; United Kingdom.

¹³⁰LPNHE, Sorbonne Université, Université Paris Cité, CNRS/IN2P3, Paris; France.

¹³¹Department of Physics, University of Pennsylvania, Philadelphia PA; United States of America.

¹³²Department of Physics and Astronomy, University of Pittsburgh, Pittsburgh PA; United States of America.

¹³³(^a) Laboratório de Instrumentação e Física Experimental de Partículas - LIP, Lisboa; (^b) Departamento de Física, Faculdade de Ciências, Universidade de Lisboa, Lisboa; (^c) Departamento de Física, Universidade de Coimbra, Coimbra; (^d) Centro de Física Nuclear da Universidade de Lisboa, Lisboa; (^e) Departamento de Física, Escola de Ciências, Universidade do Minho, Braga; (^f) Departamento de Física Teórica y del Cosmos, Universidad de Granada, Granada (Spain); (^g) Departamento de Física, Instituto Superior Técnico, Universidade de Lisboa, Lisboa; Portugal.

¹³⁴Institute of Physics of the Czech Academy of Sciences, Prague; Czech Republic.

¹³⁵Czech Technical University in Prague, Prague; Czech Republic.

¹³⁶Charles University, Faculty of Mathematics and Physics, Prague; Czech Republic.

¹³⁷Particle Physics Department, Rutherford Appleton Laboratory, Didcot; United Kingdom.

¹³⁸IRFU, CEA, Université Paris-Saclay, Gif-sur-Yvette; France.

¹³⁹Santa Cruz Institute for Particle Physics, University of California Santa Cruz, Santa Cruz CA; United States of America.

¹⁴⁰(^a) Departamento de Física, Pontificia Universidad Católica de Chile, Santiago; (^b) Millennium Institute for Subatomic physics at high energy frontier (SAPHIR), Santiago; (^c) Instituto de Investigación Multidisciplinario en Ciencia y Tecnología, y Departamento de Física, Universidad de La Serena; (^d) Universidad Andres Bello, Department of Physics, Santiago; (^e) Universidad San Sebastian, Recoleta; (^f) Instituto de Alta Investigación, Universidad de Tarapacá, Arica; (^g) Departamento de Física, Universidad Técnica Federico Santa María, Valparaíso; Chile.

¹⁴¹Department of Physics, Institute of Science, Tokyo; Japan.

¹⁴²Department of Physics, University of Washington, Seattle WA; United States of America.

¹⁴³(^a) Institute of Frontier and Interdisciplinary Science and Key Laboratory of Particle Physics and Particle Irradiation (MOE), Shandong University, Qingdao; (^b) School of Physics, Zhengzhou University; China.

¹⁴⁴(^a) State Key Laboratory of Dark Matter Physics, School of Physics and Astronomy, Shanghai Jiao Tong University, Key Laboratory for Particle Astrophysics and Cosmology (MOE), SKLPPC, Shanghai; (^b) State Key Laboratory of Dark Matter Physics, Tsung-Dao Lee Institute, Shanghai Jiao Tong University, Shanghai; China.

¹⁴⁵Department of Physics and Astronomy, University of Sheffield, Sheffield; United Kingdom.

- ¹⁴⁶Department of Physics, Shinshu University, Nagano; Japan.
- ¹⁴⁷Department Physik, Universität Siegen, Siegen; Germany.
- ¹⁴⁸Department of Physics, Simon Fraser University, Burnaby BC; Canada.
- ¹⁴⁹SLAC National Accelerator Laboratory, Stanford CA; United States of America.
- ¹⁵⁰Department of Physics, Royal Institute of Technology, Stockholm; Sweden.
- ¹⁵¹Departments of Physics and Astronomy, Stony Brook University, Stony Brook NY; United States of America.
- ¹⁵²Department of Physics and Astronomy, University of Sussex, Brighton; United Kingdom.
- ¹⁵³School of Physics, University of Sydney, Sydney; Australia.
- ¹⁵⁴Institute of Physics, Academia Sinica, Taipei; Taiwan.
- ¹⁵⁵^(a)E. Andronikashvili Institute of Physics, Iv. Javakhishvili Tbilisi State University, Tbilisi; ^(b)High Energy Physics Institute, Tbilisi State University, Tbilisi; ^(c)University of Georgia, Tbilisi; Georgia.
- ¹⁵⁶Department of Physics, Technion, Israel Institute of Technology, Haifa; Israel.
- ¹⁵⁷Raymond and Beverly Sackler School of Physics and Astronomy, Tel Aviv University, Tel Aviv; Israel.
- ¹⁵⁸Department of Physics, Aristotle University of Thessaloniki, Thessaloniki; Greece.
- ¹⁵⁹International Center for Elementary Particle Physics and Department of Physics, University of Tokyo, Tokyo; Japan.
- ¹⁶⁰Graduate School of Science and Technology, Tokyo Metropolitan University, Tokyo; Japan.
- ¹⁶¹Department of Physics, University of Toronto, Toronto ON; Canada.
- ¹⁶²^(a)TRIUMF, Vancouver BC; ^(b)Department of Physics and Astronomy, York University, Toronto ON; Canada.
- ¹⁶³Division of Physics and Tomonaga Center for the History of the Universe, Faculty of Pure and Applied Sciences, University of Tsukuba, Tsukuba; Japan.
- ¹⁶⁴Department of Physics and Astronomy, Tufts University, Medford MA; United States of America.
- ¹⁶⁵Department of Physics and Astronomy, University of California Irvine, Irvine CA; United States of America.
- ¹⁶⁶University of West Attica, Athens; Greece.
- ¹⁶⁷Department of Physics and Astronomy, University of Uppsala, Uppsala; Sweden.
- ¹⁶⁸Department of Physics, University of Illinois, Urbana IL; United States of America.
- ¹⁶⁹Instituto de Física Corpuscular (IFIC), Centro Mixto Universidad de Valencia - CSIC, Valencia; Spain.
- ¹⁷⁰Department of Physics, University of British Columbia, Vancouver BC; Canada.
- ¹⁷¹Department of Physics and Astronomy, University of Victoria, Victoria BC; Canada.
- ¹⁷²Fakultät für Physik und Astronomie, Julius-Maximilians-Universität Würzburg, Würzburg; Germany.
- ¹⁷³Department of Physics, University of Warwick, Coventry; United Kingdom.
- ¹⁷⁴Waseda University, Tokyo; Japan.
- ¹⁷⁵Department of Particle Physics and Astrophysics, Weizmann Institute of Science, Rehovot; Israel.
- ¹⁷⁶Department of Physics, University of Wisconsin, Madison WI; United States of America.
- ¹⁷⁷Fakultät für Mathematik und Naturwissenschaften, Fachgruppe Physik, Bergische Universität Wuppertal, Wuppertal; Germany.
- ¹⁷⁸Department of Physics, Yale University, New Haven CT; United States of America.
- ¹⁷⁹Yerevan Physics Institute, Yerevan; Armenia.
- ^a Also at Affiliated with an institute formerly covered by a cooperation agreement with CERN.
- ^b Also at An-Najah National University, Nablus; Palestine.
- ^c Also at Borough of Manhattan Community College, City University of New York, New York NY; United States of America.
- ^d Also at Center for Interdisciplinary Research and Innovation (CIRI-AUTH), Thessaloniki; Greece.
- ^e Also at Centre of Physics of the Universities of Minho and Porto (CF-UM-UP); Portugal.

- f* Also at CERN, Geneva; Switzerland.
- g* Also at Département de Physique Nucléaire et Corpusculaire, Université de Genève, Genève; Switzerland.
- h* Also at Departament de Física de la Universitat Autònoma de Barcelona, Barcelona; Spain.
- i* Also at Department of Financial and Management Engineering, University of the Aegean, Chios; Greece.
- j* Also at Department of Mathematical Sciences, University of South Africa, Johannesburg; South Africa.
- k* Also at Department of Modern Physics and State Key Laboratory of Particle Detection and Electronics, University of Science and Technology of China, Hefei; China.
- l* Also at Department of Physics, Bolu Abant İzzet Baysal University, Bolu; Türkiye.
- m* Also at Department of Physics, King's College London, London; United Kingdom.
- n* Also at Department of Physics, Stanford University, Stanford CA; United States of America.
- o* Also at Department of Physics, Stellenbosch University; South Africa.
- p* Also at Department of Physics, University of Fribourg, Fribourg; Switzerland.
- q* Also at Department of Physics, University of Thessaly; Greece.
- r* Also at Department of Physics, Westmont College, Santa Barbara; United States of America.
- s* Also at Faculty of Physics, Sofia University, 'St. Kliment Ohridski', Sofia; Bulgaria.
- t* Also at Faculty of Physics, University of Bucharest ; Romania.
- u* Also at Hellenic Open University, Patras; Greece.
- v* Also at Henan University; China.
- w* Also at Imam Mohammad Ibn Saud Islamic University; Saudi Arabia.
- x* Also at Institutio Catalana de Recerca i Estudis Avancats, ICREA, Barcelona; Spain.
- y* Also at Institut für Experimentalphysik, Universität Hamburg, Hamburg; Germany.
- z* Also at Institute for Nuclear Research and Nuclear Energy (INRNE) of the Bulgarian Academy of Sciences, Sofia; Bulgaria.
- aa* Also at Institute of Applied Physics, Mohammed VI Polytechnic University, Ben Guerir; Morocco.
- ab* Also at Institute of Particle Physics (IPP); Canada.
- ac* Also at Institute of Physics and Technology, Mongolian Academy of Sciences, Ulaanbaatar; Mongolia.
- ad* Also at Institute of Physics, Azerbaijan Academy of Sciences, Baku; Azerbaijan.
- ae* Also at Institute of Theoretical Physics, Ilia State University, Tbilisi; Georgia.
- af* Also at Millennium Institute for Subatomic physics at high energy frontier (SAPHIR), Santiago; Chile.
- ag* Also at National Institute of Physics, University of the Philippines Diliman (Philippines); Philippines.
- ah* Also at The Collaborative Innovation Center of Quantum Matter (CICQM), Beijing; China.
- ai* Also at TRIUMF, Vancouver BC; Canada.
- aj* Also at Università di Napoli Parthenope, Napoli; Italy.
- ak* Also at University of Chinese Academy of Sciences (UCAS), Beijing; China.
- al* Also at University of Colorado Boulder, Department of Physics, Colorado; United States of America.
- am* Also at University of Sienna; Italy.
- an* Also at Washington College, Chestertown, MD; United States of America.
- ao* Also at Yeditepe University, Physics Department, Istanbul; Türkiye.
- * Deceased